ELSEVIER

Fusion Engineering and Design 54 (2001) 181–247

Fusion Engineering and Design

www.elsevier.com/locate/fusengdes

On the exploration of innovative concepts for fusion chamber technology

M.A. Abdou [a,*], The APEX TEAM, A. Ying [a], N. Morley [a], K. Gulec [a], S. Smolentsev [a], M. Kotschenreuther [b], S. Malang [c], S. Zinkle [d], T. Rognlien [e], P. Fogarty [d], B. Nelson [d], R. Nygren [f], K. McCarthy [g], M.Z. Youssef [a], N. Ghoniem [a], D. Sze [h], C. Wong [i], M. Sawan [j], H. Khater [j], R. Woolley [k], R. Mattas [h], R. Moir [e], S. Sharafat [a], J. Brooks [h], A. Hassanein [h], D. Petti [g], M. Tillack [l], M. Ulrickson [f], T. Uchimoto [m]

[a] *Mechanical and Aerospace Engineering Department, University of California-Los Angeles, 44–114 Engineering IV, 420 Westwood Plaza, Los Angeles, CA 90095, USA*
[b] *University of Texas, Austin, TX, USA*
[c] *Forschungszentrum Karlsruhe, Karlsruhe, Germany*
[d] *Oak Ridge National Laboratory, Oak Ridge, TN, USA*
[e] *Lawrence Livermore National Laboratory, Livermore, CA, USA*
[f] *Sandia National Laboratory, Albuquerque, NM, USA*
[g] *Idaho National Engineering and Environmental Laboratory, Idaho Falls, ID, USA*
[h] *Argonne National Laboratory, Argonne, IL, USA*
[i] *General Atomics, San Diego, CA, USA*
[j] *University of Wisconsin, Madison, WI, USA*
[k] *Princeton Plasma Physics Laboratory, Princeton, NJ, USA*
[l] *University of California-San Diego, La Jolla, CA, USA*
[m] *University of Tokyo, Tokyo, Japan*

Received 10 March 2000; accepted 7 June 2000

Abstract

This study, called APEX, is exploring novel concepts for fusion chamber technology that can substantially improve the attractiveness of fusion energy systems. The emphasis of the study is on fundamental understanding and advancing the underlying engineering sciences, integration of the physics and engineering requirements, and enhancing innovation for the chamber technology components surrounding the plasma. The chamber technology goals in APEX include: (1) high power density capability with neutron wall load >10 MW/m^2 and surface heat flux >2 MW/m^2, (2) high power conversion efficiency ($>40\%$), (3) high availability, and (4) simple technological and material constraints. Two classes of innovative concepts have emerged that offer great promise and deserve further

* Corresponding author. Tel.: +1-310-2060501; fax: +1-310-8252599.
E-mail address: abdou@fusion.ucla.edu (M.A. Abdou).

PII: S0920-3796(00)00433-6

research and development. The first class seeks to eliminate the solid "bare" first wall by flowing liquids facing the plasma. This liquid wall idea evolved during the APEX study into a number of concepts based on: (a) using liquid metals (Li or Sn–Li) or a molten salt (Flibe) as the working liquid, (b) utilizing electromagnetic, inertial and/or other types of forces to restrain the liquid against a backing wall and control the hydrodynamic flow configurations, and (c) employing a thin (~ 2 cm) or thick (~ 40 cm) liquid layer to remove the surface heat flux and attenuate the neutrons. These liquid wall concepts have some common features but also have widely different issues and merits. Some of the attractive features of liquid walls include the potential for: (1) high power density capability; (2) higher plasma β and stable physics regimes if liquid metals are used; (3) increased disruption survivability; (4) reduced volume of radioactive waste; (5) reduced radiation damage in structural materials; and (6) higher availability. Analyses show that not all of these potential advantages may be realized simultaneously in a single concept. However, the realization of only a subset of these advantages will result in remarkable progress toward attractive fusion energy systems. Of the many scientific and engineering issues for liquid walls, the most important are: (1) plasma–liquid interactions including both plasma–liquid surface and liquid wall–bulk plasma interactions; (2) hydrodynamic flow configuration control in complex geometries including penetrations; and (3) heat transfer at free surface and temperature control. The second class of concepts focuses on ideas for extending the capabilities, particularly the power density and operating temperature limits, of solid first walls. The most promising idea, called EVOLVE, is based on the use of a high-temperature refractory alloy (e.g. W–5% Re) with an innovative cooling scheme based on the use of the heat of vaporization of lithium. Calculations show that an evaporative system with Li at $\sim 1\,200$°C can remove the goal heat loads and result in a high power conversion efficiency. The vapor operating pressure is low, resulting in a very low operating stress in the structure. In addition, the lithium flow rate is about a factor of ten lower than that required for traditional self-cooled first wall/blanket concepts. Therefore, insulator coatings are not required. Key issues for EVOLVE include: (1) two-phase heat transfer and transport including MHD effects; (2) feasibility of fabricating entire blanket segments of W alloys; and (3) the effect of neutron irradiation on W.

Keywords: Chamber technology; First wall; Blanket; Liquid walls; Free surface; Refractory alloys; Two-phase flow; Plasma–material interaction; MHD effects

1. Introduction

A study, called APEX, was initiated in early 1998 as part of the US Fusion Energy Sciences Program initiative to encourage innovation and scientific understanding. The primary objective of APEX is to identify and explore novel, possibly revolutionary, concepts for the chamber technology that can substantially improve the attractiveness of fusion energy systems. The chamber technology includes the components in the immediate exterior of the plasma (i.e. first wall, blanket, divertor, and vacuum vessel) and has a tremendous impact on the economic, safety and environmental attractiveness of fusion energy systems.

The APEX study is being carried out by a multi-disciplinary, multi-institution integrated team. The emphasis of the study has been on fundamental understanding and advancing the underlying engineering sciences, integration of the physics and engineering requirements, and enhancing innovation for the chamber technology.

This paper presents a summary of the technical results from the first phase of the APEX study. A number of promising ideas for new innovative concepts have already emerged from this first phase. While these ideas need extensive research before they can be formulated into mature design concepts, some of them offer great promise for fundamental improvements in the vision for an attractive fusion energy system.

These ideas fall into two categories. The first category seeks to totally eliminate the solid 'bare' first wall. The most promising idea in this category is a flowing liquid wall. The liquid wall idea is 'concept rich'. These concepts vary from 'liquid first walls', where a thin layer of liquid (< 2 cm)

flows on the plasma-side of the first wall, to 'thick liquid walls', where an all-flowing thick liquid (> 40 cm) serves as the liquid wall/liquid blanket. Other variations in the liquid wall concepts include the type of 'restraining force' utilized to 'control' the movement and geometry of the liquid. Candidate liquids range from high conductivity, low Prandtl number liquid metals to low conductivity, high Prandtl number liquids such as the molten salt Flibe. While all concepts in the liquid wall category share some common advantages and issues, each concept has its own unique set of incentives and issues.

The second category of ideas focuses on extending the capabilities, particularly the power density and temperature limits, of solid first walls. A promising example is the use of high temperature refractory alloys (e.g. tungsten) in the first wall together with an innovative heat transfer and heat transport scheme based on vaporization of lithium.

This paper is organized as follows. Section 2 summarizes the study approach. Section 3 provides an introduction to the basic scientific principles of liquid walls. Sections 4 and 5 present the analysis of free-surface hydrodynamics, heat transfer, and MHD effects, as well as tritium breeding, activation, and other considerations for thick and thin liquid walls, respectively. A liquid wall concept based on the utilization of electromagentic forces to restrain the liquid flow movement and geometry is introduced in Section 6. Plasma–liquid interactions are addressed in Sections 7 and 8. Concepts based on using high-temperature refractory solid first walls are analyzed in Section 9 for evaporative lithium cooling and in Section 10 for helium cooling. Section 11 highlights a concept for flowing Li_2O particulates. Structural material and safety considerations for all concepts are investigated in Sections 12 and 13, respectively. A summary of the study is provided in Section 14. It should be noted that because of the depth and breadth of the study, the scope of the presentation in this paper has been limited to the key technical points. Considerable additional details are provided in the study 'report' of ref. [1].

Table 1
Highlights of the APEX study approach

(1) Emphasize innovation
(2) Understand and advance the underlying engineering sciences
(3) Utilize a multidisciplinary, multi-institution integrated TEAM
(4) Provide for open competitive solicitations
(5) Close coupling to the plasma community
(6) Direct participation of material scientists and system design groups
(7) Direct coupling to IFE Chamber Technology community
(8) Encourage international collaboration

2. Study approach

The APEX objective, 'to identify and explore novel, possibly revolutionary, concepts for the Chamber Technology that can substantially improve the attractiveness of future fusion energy systems', represents a challenge that was clearly recognized from the onset of the study. Therefore, careful attention was paid to the study approach. Some of the key elements of the APEX approach are highlighted in Table 1.

Chamber Technology includes the components in the immediate exterior of the plasma (e.g. first wall, blanket, divertor, and vacuum vessel). Concepts for Chamber Technology must satisfy the basic functional requirements shown in Table 2, which include providing a vacuum environment, plasma exhaust, heat removal, and tritium breeding.

A set of primary goals for Chamber Technology was adopted to guide the APEX study. These

Table 2
Functional requirements of chamber technology

Provision of vacuum environment
Exhaust of plasma burn products
Heat removal and power extraction of surface heat loads (from plasma particles and radiation)
Heat removal and power extraction of bulk heating (from energy deposition of neutrons and secondary gamma rays)
Tritium breeding at the rate required to satisfy self-sufficiency
Radiation protection

Table 3
Primary goals for chamber technology[a]

1.	High power density capability (main driver)
	Neutron wall load >10 MW/m^2
	Surface heat flux >2 MW/m^2
2.	High power conversion efficiency ($>40\%$)
3.	High availability
	Lower failure rate (MTBF >43 MTTR)
	Faster maintenance (MTTR <0.023 MTBF)
4.	Simpler technological and material constraints

[a] Goals used to calibrate new ideas and measure progress.

goals, shown in Table 3, have been used as guidelines to calibrate the potential attractiveness of new ideas and to measure progress. These goals provide quantitative targets for key parameters and features related to Chamber Technology that have the highest impact on the attractiveness of fusion energy systems. The rationale for these goals is provided in Ref. [2].

In the early stage of the APEX study, an assessment was conducted to understand the limitations and constraints of traditional concepts (i.e. concepts that were developed over the past 20 years). The results of this assessment [2] are not repeated here. By understanding the limitations and constraints of the traditional concepts, this assessment partially illuminated the path toward extending limits, overcoming constraints, and helped stimulate ideas for potentially more attractive novel concepts.

A diagram illustrating the APEX process for screening and evaluating the scientific bases of new ideas is given in Fig. 1. These ideas went through a 'screening process' which relied on 'expert judgement' by the APEX team. The team tolerated 'high-risk' ideas whenever there was a clear potential for high-payoff. The ideas that passed the screening test proceeded to the stage of 'design idea formulation and analysis using existing tools'. The technical work on those ideas is reported in ref. [1]. However, it should be noted that in the course of this work it became evident that existing models and data were not sufficient. Therefore, substantial effort was devoted to developing new models and exploring new phenomena for the more promising concepts such as liquid walls and high-temperature refractory alloys.

During the work on exploring novel ideas, the team adopted a set of scientific evaluation criteria which are discussed in ref. [1]. These criteria included:

1. Satisfying functional requirements (see Table 2).
2. Demonstrating potential for improved attractiveness, based on: (a) high power density capability; (b) high conversion efficiency; (c) high availability; (d) attractive safety and environmental attributes; (e) simple technological and material constraints, and (f) low cost.

It is important to note that the process flow diagram in Fig. 1 was not intended as a 'rigid' sequence of events. Rather, it was only a 'guide' to measure progress and a tool to focus resources on ideas with better potential. Strong technical judgement by the scientists was the best guidance whenever new, and often surprising, technical results were obtained. Innovation was needed, and has taken place as an ongoing process. For example, when technical results indicated that the temperature of a free-surface liquid wall may be limited by plasma impurity considerations, the following innovative ideas were proposed by team scientists:

1. The use of Sn–Li because it has low vapor pressure at elevated temperatures.
2. Effective schemes to promote controlled surface mixing and wave formation to eliminate the surface thermal boundary layer.
3. Novel ideas for two-stream flows that keep the free-surface temperature low enough for compatibility with plasma operation while the bulk liquid temperature is sufficiently high for attractive energy conversion.

3. Introduction to liquid walls

The idea of flowing liquid walls has emerged as one of the most promising concepts explored so far in APEX. The area of liquid walls appears to be 'concept rich' with many ideas emerging in the past 2 years that have widely different characteristics. Therefore, an introduction to liquid walls is necessary before presenting the technical results of the next five sections.

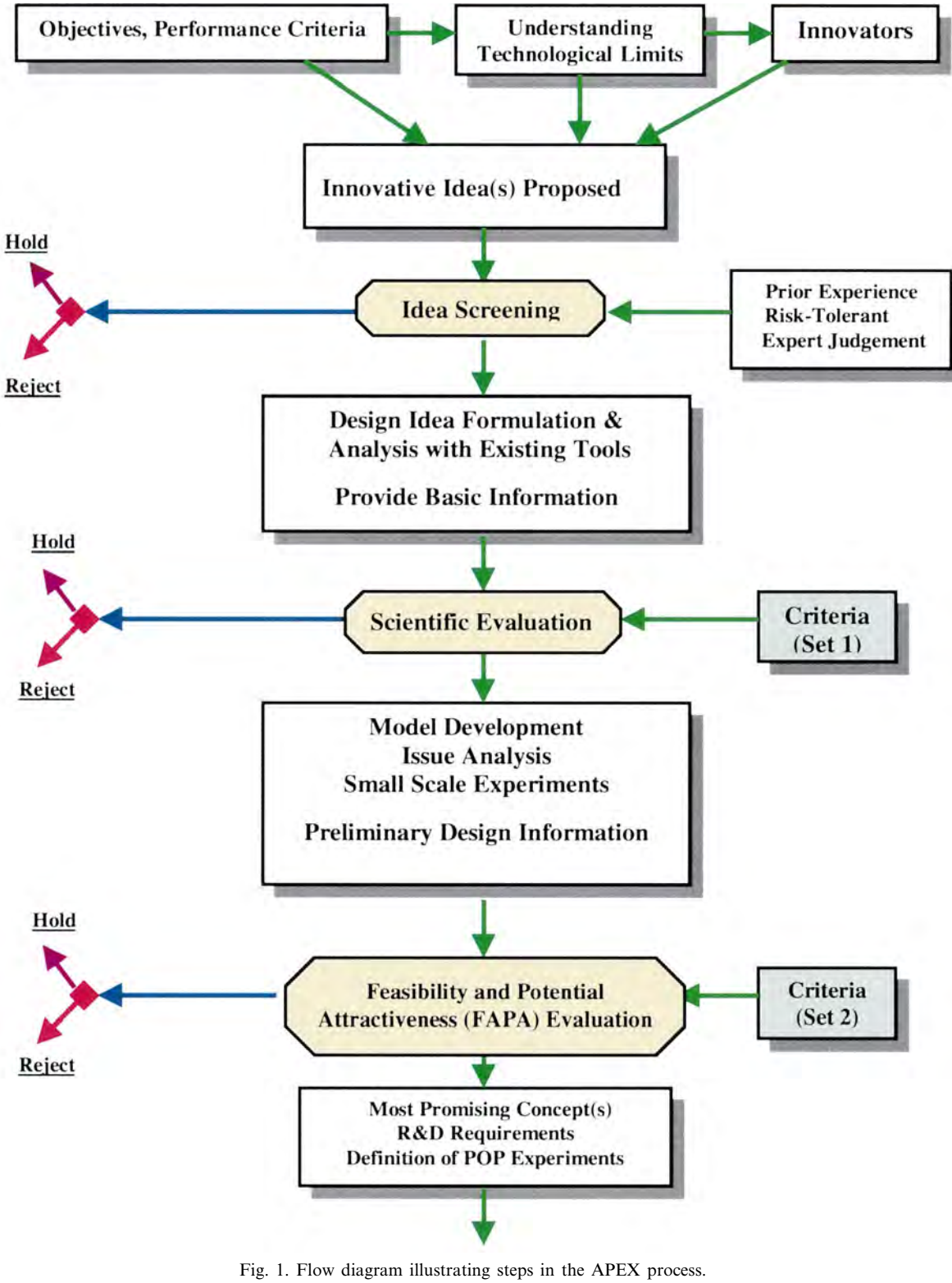

Fig. 1. Flow diagram illustrating steps in the APEX process.

It must be clearly noted here that the concept of liquid walls is an idea that, prior to APEX, has not been subjected to extensive analysis and evaluation. A brief history is in order. The idea of using a liquid blanket in a fusion device was first suggested by Christofilos in 1970 [3] for a field reversed concept (FRC). In this design, the plasma volume was surrounded by a 75 cm thick, free surface lithium blanket flowing at 30 m/s^{-1}. Subsequent uses of the liquid walls for magnetic fusion devices have been documented [4–7].

With regards to inertial fusion reactors, the first published reactor design concept was a liquid wall concept proposed by Fraas of ORNL [8]. This design, called BLASCON, features a cavity formed by a vortex in a rotating liquid-lithium pool. Subsequent liquid wall design concepts include a liquid-lithium waterfall [9], HYLIFE [10], HYLIFE-I [11], and HYLIFE-II [12].

3.1. Liquid wall options

The liquid wall idea evolved during the APEX study into a number of concepts that have some common features but also have widely different issues and merits. These concepts can be classified (as shown in Table 4) according to: (a) thickness of the liquid; (b) type of liquid used; and (c) the type of restraining force used to control the liquid flow (i.e. adhere to a backing wall).

Table 4
Liquid wall options

Thickness	Thin (~2 cm) Moderately thick (~15 cm) Thick (>40 cm)
Working liquid	Lithium Sn–Li Flibe
Hydrodynamic driving/restraining force	Gravity–momentum driven (GMD) GMD with swirl flow Electromagnetically restrained Magnetic propulsion
Liquid structure	Single, contiguous, stream Two streams (fast flowing thin layer on the plasma side and slowly flowing bulk stream)

The working liquid must be a lithium-containing medium in order to provide adequate tritium. The only such practical candidates are the liquid metals lithium and Sn–Li, and the molten salt Flibe. Lead–lithium was eliminated as a candidate early in the study [1,2]. Lithium and Flibe were considered for traditional concepts for many years. Sn–Li was introduced into APEX because it has very low vapor pressure at elevated temperature, which is an important advantage in a plasma-facing flowing liquid. The hydrodynamics and heat transfer related characteristics and issues of high-conductivity, low Prandtl Number liquid metal flows are considerably different from those of the low-conductivity, high Prandtl Number Flibe flows. Flowing liquid metals may require the use of electrical insulators to overcome the MHD drag, while for Flibe free surface flows, MHD effects caused by the interaction with the mean flow are less significant. The effects on plasma stability and confinement also differ based on the electrical conductivity of the working liquid.

The thickness selected for the liquid wall layer flow directly facing the plasma and in front of a solid 'backing wall' leads to different concepts that have some common issues but many unique advantages and challenges. Both thin and thick liquid walls can adequately remove high surface heat flux. A primary difference between thin and thick liquid walls is the magnitude of attenuation of neutrons in the liquid before they reach the backing wall. As seen later, the 'thin' liquid wall concept is easier to attain, but 'thick' liquid wall concepts greatly reduce radiation damage and activation of the structure behind the liquid.

Widely different liquid wall concepts are obtained by applying various forces to drive the liquid flow and restrain it against a backing solid wall. As shown in Table 4, at least four concepts can be considered based on the driving/restraining force scheme. The first is called gravity–momentum driven (GMD). In the

GMD concept, illustrated in Fig. 2, the liquid is injected at the top of the chamber with an angle tangential to the curved backing wall. The fluid adheres to the backing wall by means of centrifugal force and is collected and drained at the bottom of the chamber. The criterion for the continuous attachment of the liquid layer is simply that the centrifugal force pushing the liquid layer towards the wall is greater than the gravitational force.

A GMD with the swirl flow concept is obtained by giving the fluid an azimuthal velocity to produce rotation. The 'swirl flow' results in a substantial increase in the centrifugal acceleration towards the back wall and better adherence to the wall, when the backing wall curvature in the poloidal direction is large and the toroidal curvature is comparable to poloidal curvature. While swirl flow may not be needed for moderate aspect ratio tokamaks, it appears to be necessary in the highly elongated, very low aspect ratio spherical torus (ST).

In APEX, the GMD has been explored for tokamaks. The GMD with the swirl flow concept has been investigated for both the ST and FRC tokamaks. Other plasma confinement schemes will be investigated in the future. The analysis of the GMD and GMD with swirl flow concepts are described in more detail in Sections 4 and 5.

The electromagnetically restrained (EMR) concept, illustrated schematically in Fig. 3, is applicable only to liquid metals. The EMR concept has been explored only for lithium in tokamak configurations. In the EMR, a force field pushing the liquid against the backing wall is generated by injecting current to flow through the liquid lithium in the poloidal direction. The injected poloidal current interacts with the toroidal magnetic field to generate an internal '$J \times B$' body force causing the liquid layer to adhere to the back wall. The EMR concept is explored in Section 6.

Another liquid wall concept not yet explored in APEX is the magnetic propulsion idea proposed by Zakharov [13] and illustrated in Fig. 4. The idea is to create a pressure driving force through the interaction of the toroidal magnetic field with an externally applied longitudinal electrical current in the liquid metal layer. The non-uniformity of the toroidal magnetic field thus generates a non-uniform Lorentz force. The resultant pressure gradient or propulsion effect causes the flow to accelerate from the inboard, where the magnetic field is stronger, to the outboard region. In addition, the Lorentz force provides an active feedback mechanism for stabilizing the flow while its normal component keeps the layer adhered to the structural wall.

3.2. Motivation for liquid wall research

Liquid walls offer many potential advantages that represent an excellent opportunity to substantially enhance the attractiveness of fusion energy systems. Examples of advantages that may be realized if we can develop good liquid wall designs are listed in Table 5. The potential improvements in plasma stability and confinement are analyzed in Section 8. The other potential advantages are discussed in Sections 4–6.

As explained earlier, there are many options for liquid wall concepts. It is not clear yet that all these advantages can be realized simultaneously in a single concept. However, the realization of only a subset of these advantages will result in remarkable progress toward the attractiveness of fusion energy systems.

3.3. Key issues for liquid walls

The scientific and engineering issues for liquid walls are addressed in Sections 4–8. Of all these issues, a number of scientific issues stand out as the highest priority for near-term liquid wall research, which are summarized in Table 6. These include:

1. Plasma–liquid interactions including both plasma–liquid surface and liquid wall–bulk plasma interactions. Plasma stability and transport may be seriously affected and potentially improved through various mechanisms including control field penetration, H/He pumping, passive stabilization, etc.

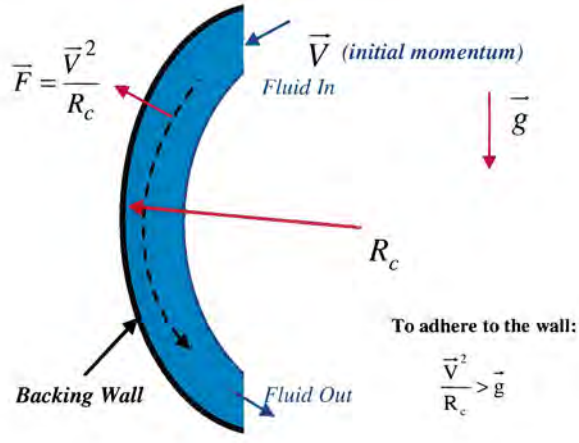

- Liquid adherence to back wall by centrifugal force.
- Applicable to liquid metals or molten salts.

Fig. 2

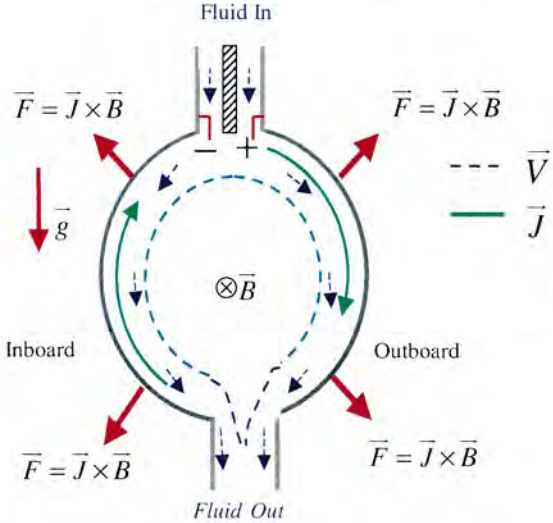

Externally driven current ($\vec{J}$) through the liquid stream.

Liquid adheres to the wall by EM force $\vec{F} = \vec{J} \times \vec{B}$

Fig. 3

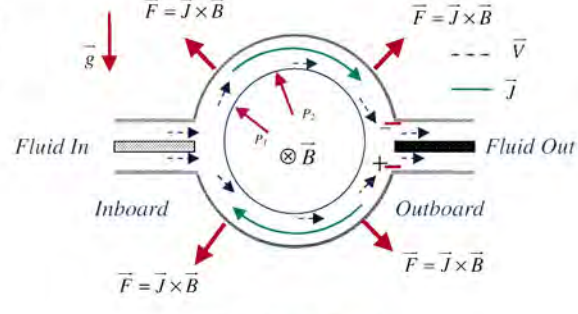

$\vec{V}$ is driven by ΔP

- *Adheres to the wall by $\vec{F} = \vec{J} \times \vec{B}$*
- *Utilizes $1/R$ variation in $\vec{F} = \vec{J} \times \vec{B}$ to drive the liquid metal from inboard to the outboard.*

Fig. 4

Fig. 2. Illustration of principles of gravity–momentum driven (GMD) liquid wall concept ($\vec{V}$ = fluid velocity, $\vec{g}$ = gravitational acceleration, R_c = radius of curvature). Liquid adherence to back wall by centrifugal force. Applicable to liquid metals or molten salts.

Fig. 3. Illustration of principles in electromagnetically restrained (EMR) liquid metal wall concept ($\vec{B}$ = magnetic field, $\vec{J}$ = induced current, $\vec{F}$ = electromagnetic force, $\vec{V}$ = fluid velocity). Externally driven current (J) through the liquid stream. Liquid adheres to the wall by EM force $\vec{F} = \vec{J} \times \vec{B}$.

Fig. 4. Illustration of basic principles of magnetic propulsion liquid metal wall concept ($\vec{B}$ = magnetic field, $\vec{J}$ = induced current, $\vec{F}$ = electromagnetic force, $\vec{V}$ = fluid velocity). Adheres to the wall by $\vec{F} = \vec{J} \times \vec{B}$. Utilizes $1/R$ variation in $\vec{F} = \vec{J} \times \vec{B}$ to drive the liquid metal from inboard to the outboard.

Table 5
Motivation for liquid wall research

What may be realized if we can develop good liquid wall designs:

- Improvements in plasma stability and confinement
  -Enable high β, stable physics regimes if liquid metals are used
- High power density capability
  -Eliminate thermal stress and wall erosion as limiting factors
  -Smaller and lower cost components (chambers, shield, vacuum vessel, magnets)
- Increased potential for disruption survivability
- Reduced volume of radioactive waste
- Reduced radiation damage in structural materials
  -Makes difficult structural material problems more tractable
- Potential for higher availability
  -Increased lifetime and reduced failure rates
  -Faster maintenance (design-dependent)

2. Hydrodynamics flow feasibility in the complex geometry including penetrations needed for plasma maintenance. The issue of establishing a viable hydrodynamic configuration threatens feasibility, while it differs significantly for thick versus thin and for molten salts versus liquid metals. The main issue facing liquid metals is of course that of MHD interaction. Without toroidal axi-symmetry of the flow and field, reliable insulator coatings will be required on all surfaces in contact with the LM layer. Eddy current forces perpendicular to the surface can pull the LM off the surface, even when complete axi-symmetry is assumed in the toroidal direction. Additionally, gradients in toroidal field can exert a significant drag on the free surface flow. For thick liquid walls, the main issue concerns the formation and removal of the liquid flow in the plasma chamber, and the accommodation of penetrations.
3. Heat transfer at free surface and temperature control. Liquid surface temperature and vaporization is a critical, tightly coupled problem between plasma edge and liquid free surface conditions including radiation spectrum, surface deformation, velocity and turbulent characteristics. Being a low thermally conducting medium, the Flibe surface temperature highly depends on the extent of the turbulent convection. However, the normal velocity at the free surface as well as the turbulent eddy near the surface can be greatly suppressed. A greater degradation in heat transfer (up to 50%) would be expected for the Flibe thick liquid concepts. The heat transfer at free surface issue is an even more serious concern, as the current limit on surface temperature for Flibe, as estimated by the plasma interface group, is significantly low.

Table 6
Key scientific issues for liquid walls

- Effects of liquid walls on core plasma including:
  -Discharge evolution (start-up, fueling, transport, beneficial effects of low recycling)
  -Plasma stability including beneficial effects of conducting shell and flow
- Edge Plasma–liquid surface interactions
- Free-surface heat transfer and turbulence modifications at and near free-surfaces
- MHD effects on free-surface flow for low- and high-conductivity fluids
- Hydrodynamic control of free-surface flow in complex geometries, including penetrations, submerged walls, inverted surfaces, etc.

The effects of liquid walls on the plasma core as well as edge plasma–liquid surface interactions require modeling and experiments in plasma devices. Free-surface fluid flow and heat transfer, with and without magnetic field and hydrodynamic control of free-surface flow in complex geometries require modeling and laboratory experiments. It is worth noting that a number of such important modelling and experimental R&D activities have already started as part of APEX and as part of the US Liquid Wall Research Program.

4. Thick liquid wall concepts

4.1. Introduction

The replacement of the first wall with a flowing thick liquid offers the potential advantages of high power density, high reliability and availability (due

to simplicity and low failure rates), reduced volumes of radioactive waste, and increased structure lifetime. All these advantages make the thick liquid wall approach a strong candidate in the APEX study. Specifically, neutronics analyses showed that with ~ 42 cm layer thickness, about two orders of magnitude reduction in helium and hydrogen production is achieved with either Flibe or Sn–Li. With this thickness, and a 200 DPA damage limit for structure replacement, the use of Flibe or Sn–Li can make the structure behind it a lifetime component. Furthermore, the volumes of radioactive waste from the FW/blanket system, as well as from the entire system, are substantially reduced. The emphases of the Phase I study included the exploration of design ideas, quantification of their high power density capabilities, and identification and analyses of the key feasibility issues of thick liquid wall configurations for various confinement schemes. The initial goal is to establish a viable free surface flow configuration. This involves: (1) an inlet nozzle and penetrations that pass flow without dripping or splashing; (2) a free surface flow section that allows liquid to cross temporally and spatially variable magnetic fields and provides full wall coverage; and (3) a head recovery nozzle system that accepts the flow and converts it from a free surface flow to a channel (pipe) flow without complete loss of kinetic energy.

There are three lithium-containing candidate liquids for the walls: (1) Flibe — a good neutron absorber and low electrically conducting medium of molten salt; (2) lithium — a low Z material that is more likely compatible with the plasma operation; and (3) tin–lithium — an extremely low vapor pressure fluid at elevated temperatures. Both lithium and tin–lithium are good electric conductors. Utilization of these two liquid metals will require an understanding of MHD effects, not just in the surface flows, but in supply lines and feed systems, and it also would likely require electrically insulating coatings.

4.2. Design options

Design ideas for establishing thick liquid walls were addressed for the tokamak (such as ARIES-RS) [14], spherical torus (ST), and field reverse configuration (FRC). The fact that topologies are different in different confinement schemes requires different liquid wall design approaches. For example, as compared to the ARIES-RS, the ST confinement scheme tends to be highly elongated (larger back wall radius of curvature). The centrifugal force acting on the liquid layer due to its poloidal motion is less than in the ARIES-RS. However, it uses a smaller toroidal radius as illustrated in Fig. 5. The centrifugal force acting on the flowing liquid layer in the ST configuration can be increased by utilizing swirl motion in the azimuthal (toroidal) direction. Thus, one may expect a more stable hydrodynamics condition in the ST liquid blanket. However, being highly elongated, the fluid takes more time to travel through the reactor if only one coolant stream is used. This implies that the free surface side may be overheated from a long plasma exposure time. A typical FRC reactor can be viewed as a long cylinder in which a football shaped volume of plasma lies at the center of the reactor chamber (see Fig. 6). The FRC confinement scheme appears more amenable to thick liquid walls due to its geometrical simplicity and lower strength magnetic fields.

4.3. Hydrodynamics and MHD effects

One of the most fundamental issues for the thick liquid blanket is how to form, establish, and maintain a thick liquid flow in a fusion reactor such as the ARIES-RS (as shown in Fig. 5). The simplest approach that can be conceived for a thick liquid blanket is free-flowing liquid under the effect of gravitational and inertial forces. As illustrated in Fig. 7, the thick liquid layer is injected at the top of the reactor chamber with an angle tangential to the backing structural wall. As it flows along the curved wall the fluid adheres to the structural wall by means of centrifugal and inertial forces. It then is collected and drained at the bottom of the reactor.

This Flibe approach has been modeled with a three-dimensional, time-dependent Navier–Stokes Solver that uses Reynolds Averaged Navier Stokes (RANS) equations for turbulence modeling and the volume of fluid (VOF) free surface tracking algorithm for free surface incompressible fluid flows.

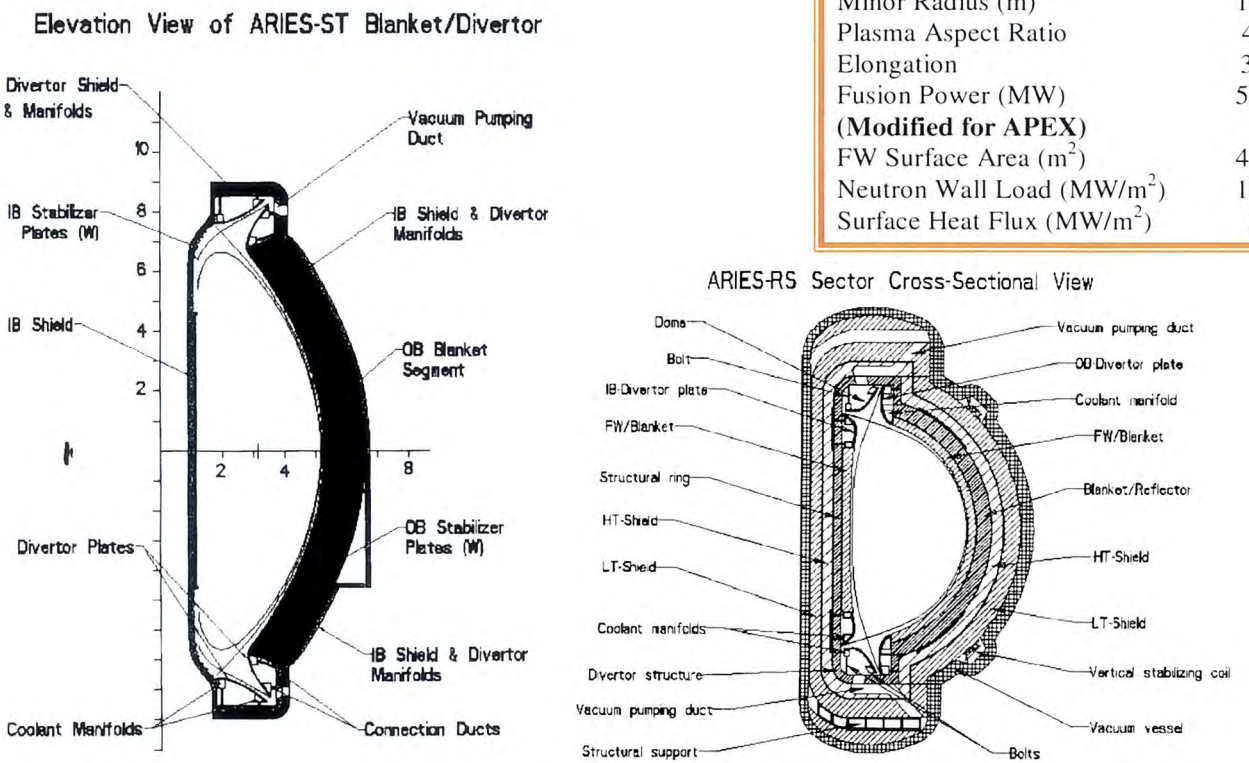

	ARIES-RS	ARIES-ST
Major Radius (m)	5.52	2.8
Minor Radius (m)	1.38	2
Plasma Aspect Ratio	4	1.4
Elongation	3.75	
Fusion Power (MW)	5480	5470
(Modified for APEX)		
FW Surface Area (m^2)	438.8	541
Neutron Wall Load (MW/m^2)	10	8.085
Surface Heat Flux (MW/m^2)	2	2

Fig. 5. Hydrodynamic configurations of thick liquid walls may be very different for ARIES-RS and ARIES-ST. Both configurations are converted to single null at the bottom of the plasma, in order to be compatible with the liquid wall configuration.

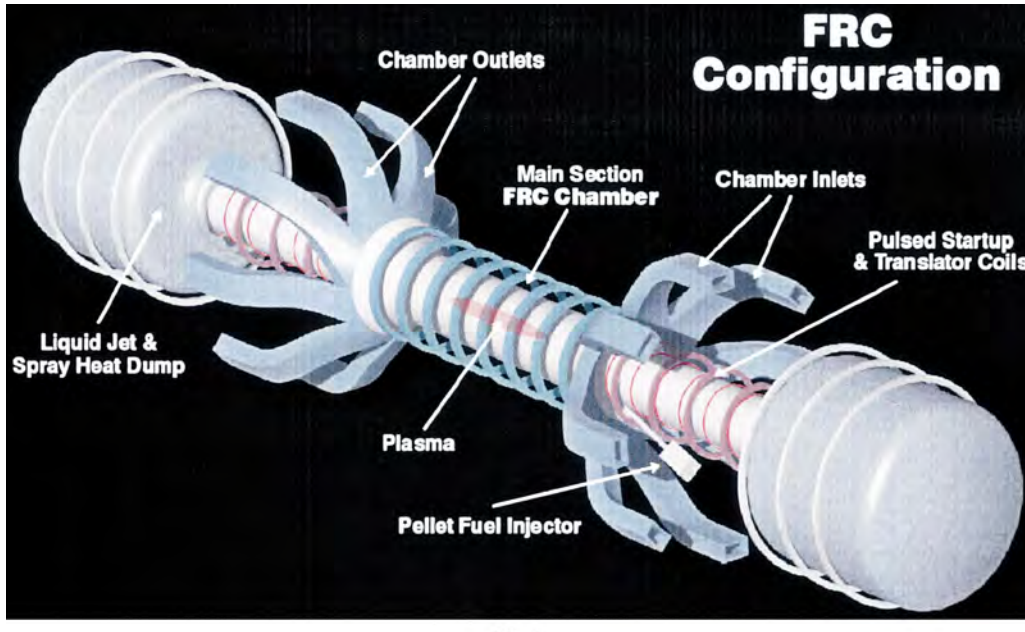

Fig. 6

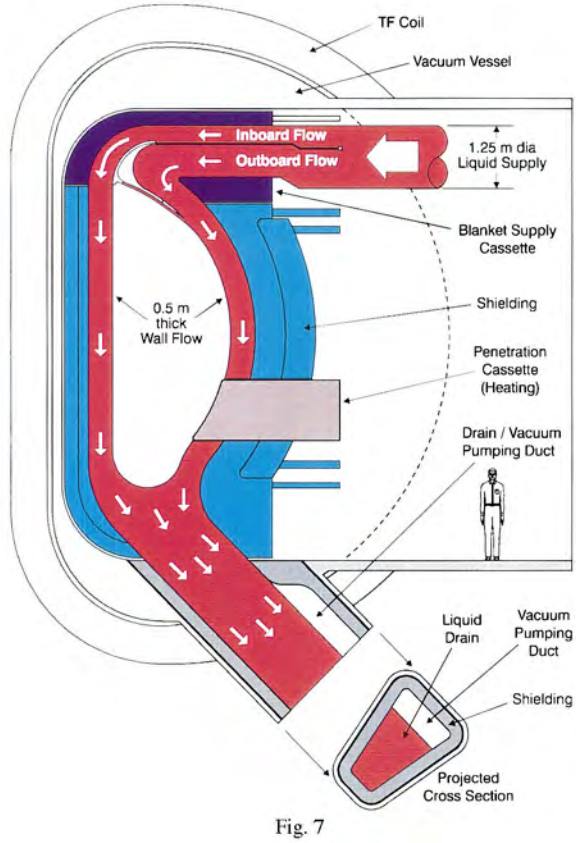

Fig. 7

Fig. 6. General layout of a FRC power plant design.
Fig. 7. A thick FW/blanket design incorporated into the ARIES-RS configuration.

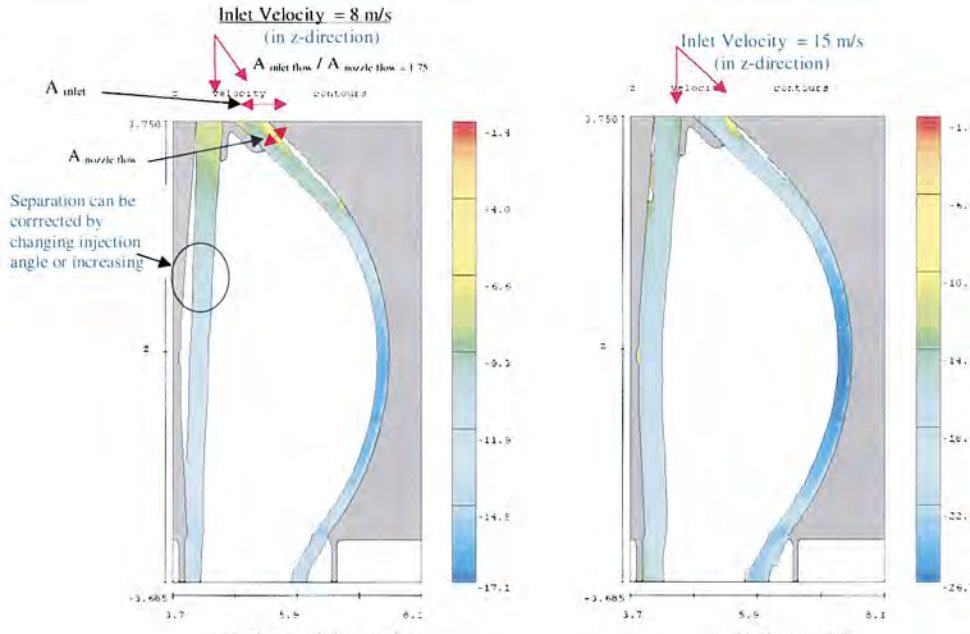

(a) t/pass = 0.9 second (b) t/pass = 0.5

Fig. 8

Parameters:
Re=4.71 x 10^6; Fr=25; Ha=3.76 x 10^5; β=0.7; χ=0.06, **2b=1.14 m**; **h_0=0.4 m**; **U_0=10 m/s**; R=6.7 m; **B_0=8 T**
Liquid: **lithium** α_0=30°; Δα=60°

$Re=U_0h_0/\nu$ $Fr=U_0^2/(gh_0)$ $Ha=B_0b[\sigma/(\rho\nu)]^{0.5}$ $\beta=h_0/b$ $\chi=h_0/R$

U_0 - mean velocity h_0 - initial thickness of the layer
B_0 - magnetic field (toroidal) R - radius of the curvature
2b - distance between two walls

ν - viscosity σ - surface tension
ρ - density g - acceleration due to gravity

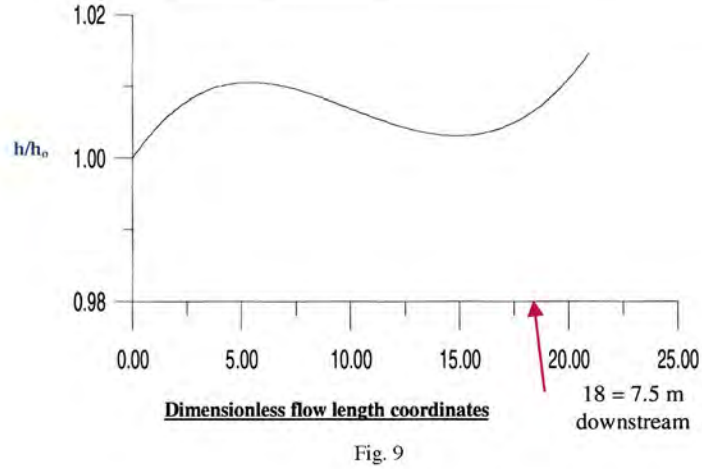

Fig. 9

Example solutions, as shown in Fig. 8, demonstrate that stable, thick fluid configurations can be established and maintained throughout a tokamak reactor configuration. Nevertheless, the flow continuity requires that some amount of thinning result from the gravitational acceleration and flow area expansions as the flow proceeds downstream. As shown, the fluid thickness is reduced by about a factor of 2 at the reactor midplane for an initial velocity of 8 m/s. This thinning reduces the liquid's potential for radiation protection of solid walls behind the liquid and creates an unfavorable situation for shielding. The jet thinning effect can be overcome by increasing the initial jet velocity; and a fairly uniform thick liquid film can be obtained throughout the plasma core if the jet is injected at velocities of 15 m/s or above (as shown in part b of Fig. 8).

The thinning effect resulting from the gravitational acceleration can be minimized by the MHD drag from the Hartmann velocity profile in a liquid metal flow. Numerical analyses were performed to determine whether or not an insulator is needed for free surface MHD flows, and to define lithium's initial velocity that enables a uniform thickness to be maintained throughout the plasma chamber in the presence of the toroidal magnetic field. The preliminary analysis shows that the MHD drag effect significantly increases the layer thickness and causes the associated reduction in the velocity. Thus, there is a need of insulators for a free liquid metal flow if a segmented toroidal liquid metal flow configuration is considered. As shown in Fig. 9, for an insulated open channel, calculations indicate that a uniform 40 cm-thick lithium layer can be maintained along the poloidal path at a velocity of 10 m/s. At this velocity, the total pressure (dynamic and static) exerted on the backplate is about 4800 N/m^2. This magnitude of pressure can be easily managed. In contrast, if the side-walls of the channel are submerged under the fluid, a fast surface layer can form naturally. The liquid near the surface, above the submerged insulated side-walls, will be unfettered by MHD drag except in areas close to penetrations, and a thin, fast layer at the surface will result (see Fig. 10).

The influence of the conducting backplate on the liquid metal flow characteristics is negligible in the presence of a purely toroidal magnetic field. However, the MHD drag can be significant if there is a radial magnetic field component — one normal to the free surface. Analyses indicate that a metallic backplate is acceptable with insulated toroidal breaks if the radial magnetic field is no more than 0.1–0.15 T. This magnitude would drop to 0.015 T for the case of toroidally continuous flow. Other MHD issues such as flow across field gradients ($1/R$ dependence of the toroidal field for example), temporal fluctuations during start-up and plasma control, have yet to be addressed adequately — ongoing work is in progress to address these important concerns.

An alternate way to form a thick liquid flow is to utilize a rotating swirl flow, where again centrifugal forces keep the liquid against the wall. The scheme appears attractive for the FRC device because of its geometric simplicity. To create a rotational flow, the liquid carries both longitudinal and azimuthal velocity components. The flow spirals while it proceeds along the flow axis as illustrated in Fig. 11. Three-dimensional numerical hydrodynamic analyses with Flibe as the working fluid show that a 0.6 m thick liquid first wall/blanket can be formed in a circular vacuum chamber of 2 m radius at an axial velocity of 7 m/s and an azimuthal rotational velocity of 10 m/s. In this design, the fluid enters the main chamber zone through a convergent nozzle and is discharged to a divergent outlet after one rotation. The velocity field along the axial direction is

Fig. 8. Some amount of thinning in liquid layer thickness was observed along the poloidal path due to gravitational acceleration and toroidal area expansion. (Z-velocity component from three-dimensional hydrodynamic computation increases due to the gravitational acceleration and it has its maximum value at the mid-plane since velocity vector has only Z component at that location.) (a) initial velocity = 8 m/s, (b) initial velocity = 15 m/s.

Fig. 9. Relative change in liquid lithium thickness as a function of distance along the flow direction for insulated open channel. The thinning effect due to gravitational acceleration can be minimized by the drag from the M-shape velocity profile (A uniform thickness of 40 cm can be established for 10 m/s lithium flow).

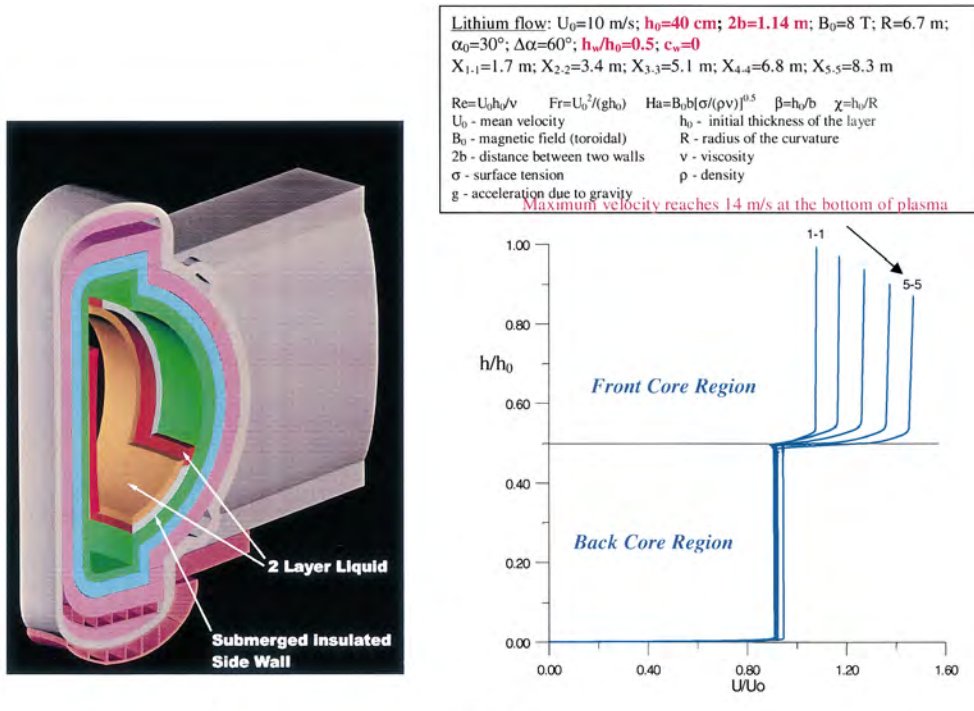

Fig. 10

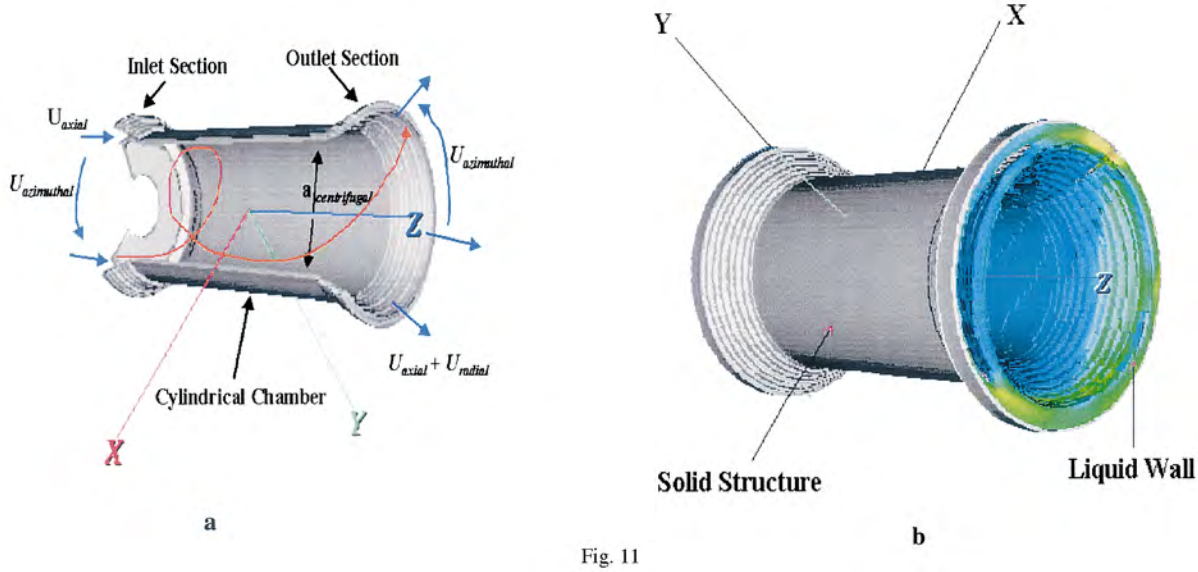

Fig. 11

Fig. 10. Two-velocity liquid metal streams can be established by having submerged sidewalls.
Fig. 11. (a) Illustration of the swirl flow mechanism in the main FRC section with converging inlet and diverging outlet sections. (b) The three-dimensional fluid distribution of FRC swirl flow. (Result of CFD simulation).

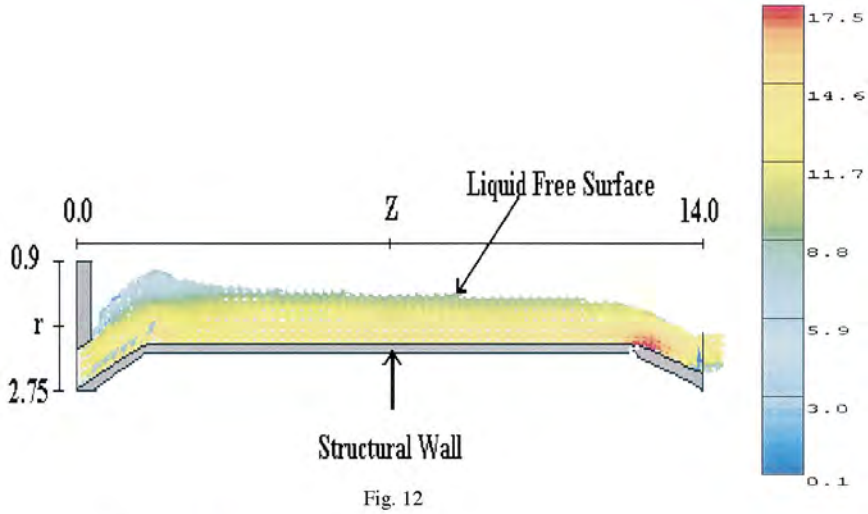

Fig. 12

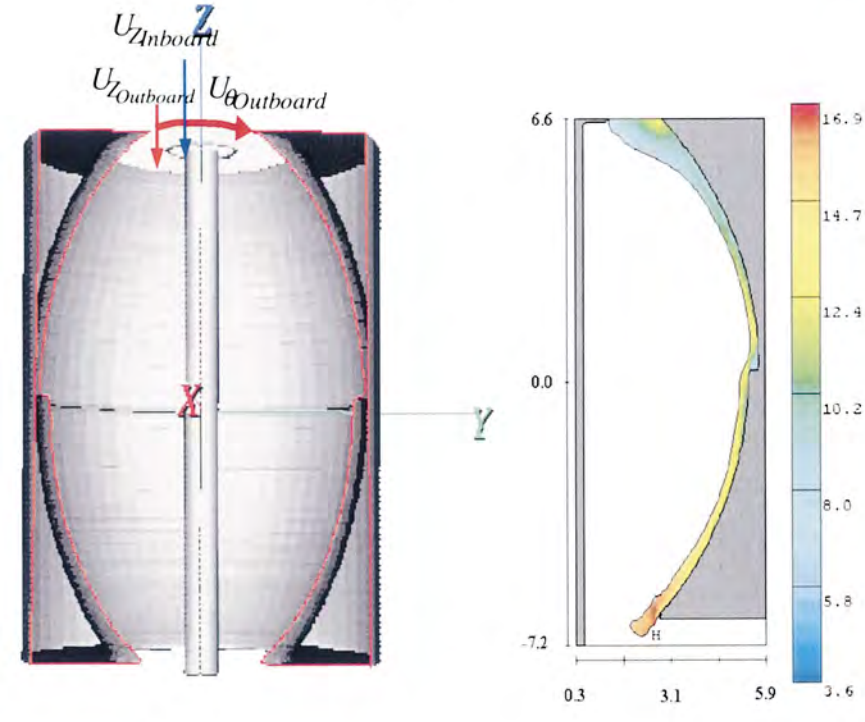

Fig. 13

Fig. 12. Two-dimensional ($r-z$) velocity distribution and liquid layer height distribution in the axial direction at an angle of 0° (where the effect of gravity on hydrodynamic behavior of the liquid layer is maximum). Inlet operating velocity: $V_\theta = 10$ m/s, $V_z = 10$ m/s.

Fig. 13. (a) The modeling of ST structural geometry including the modification in the outboard topology. (b) The liquid two-dimensional velocity magnitude contour at $r-z$ plane at the outboard and liquid layer height distribution in the z-direction at an arbitrary azimuthal angle.

shown in Fig. 12. The fluid encounters different net forces along the circumferential direction due to different relative orientations of gravity, which result in non-uniform hydrodynamics characteristics along the flow axis. Calculations indicate that an acceptable variation ($<10\%$) in liquid layer thickness in azimuthal and axial directions can be maintained for flowing Flibe with axial and azimuthal inlet velocities of 11 and 13 m/s, respectively, in a cylindrical chamber with a 2 m radius and 12 m length.

The swirl flow concept can also be applied to the ST outboard FW/blanket region. In this case, a thick liquid carrying both vertical and toroidal velocity components is injected at the top of the reactor. The centrifugal acceleration (>35 m/s^2) pushes the fluid outward and prevents the flow from deflecting into the plasma core. The axial velocity increases as the flow proceeds downstream due to the gravitational acceleration and this leads to flow thinning. The thinning effect is further manifested in the ST because of the toroidal area expansion along the flow direction (the flow area increases by a factor of 2 as the flow approaches the mid-plane). Various numerical simulations were performed to identify 'ways' to slow down the velocity and to reduce the thinning effect. Preliminary results, based on computational fluid dynamics (CFD), three-dimensional calculations, indicate that the thinning effect can be mitigated by tailoring the back wall contour and by incorporating a step along the flow direction. The calculated 'step' of about 0.2-m high, located at the reactor mid-plane, helps to maintain a liquid layer thickness greater than 0.3 m. In contrast to the rotational flow for the outboard blanket, a fast annular liquid flows along (no rotation) the central post forming the inboard FW/blanket zone, as shown in Fig. 13.

These hydrodynamics calculations (with or without the effect of magnetic field) indicate that a fairly uniform thick liquid wall can be formed in the aforementioned fusion configurations as long as the injected fluid carries an adequate inertial momentum (e.g. corresponding to a velocity of 10 m/s). Moreover, the pumping power requirement becomes less of a concern for higher power density confinement concepts (such as FRCs) as shown in Fig. 14. However, for a thick liquid wall concept to work, there remain many design issues particularly in the areas of moving liquid in and out of the reactor, of spatial and temporal MHD effects, and of accommodation of penetrations. Certainly, designs and analyses of the inlet nozzle and exit head recovery systems are needed for all the aforementioned concepts. Regarding the accommodation of penetrations (e.g. for plasma heating), simulations are performed to understand the underlying scientific phenomena and to provide design guidance. The challenges for accommodating penetrations include: flow stagnation at the front point of the penetration resulting in discharge of the fluid towards the plasma, rise of the fluid level surrounding the penetration due to the obstruction of flow path, and wake formation that persists downstream of the penetration. Different means have been proposed to avoid fluid splashing and to minimize disturbance. These involve modification of penetration shapes, introduction of guiding grooves and fins, and

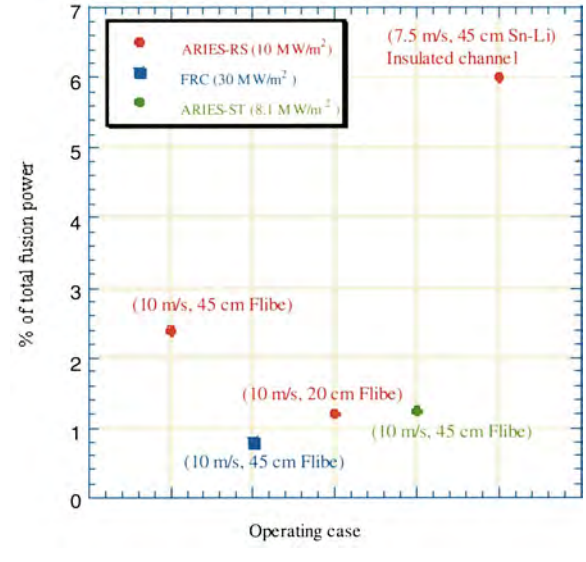

Fig. 14. The pumping power as a fraction of fusion power for various cases of liquid wall thickness and confinement configurations. Note that the pumping power is scaled from that of the HYLIFE-II design, taking into account the 50% head recovery. The effect of MHD drag will increase the calculated pumping power of a Sn–Li flowing liquid wall.

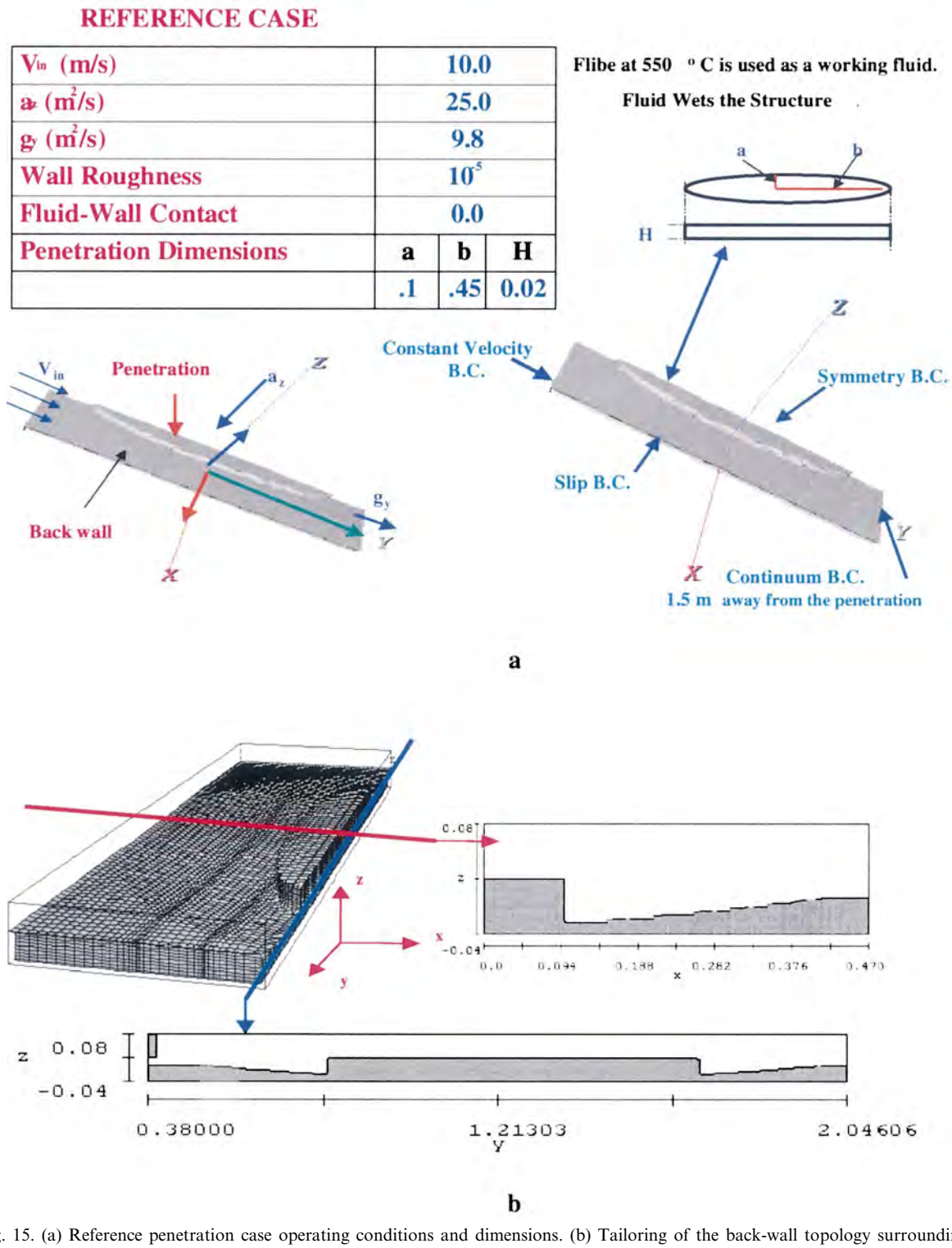

Fig. 15. (a) Reference penetration case operating conditions and dimensions. (b) Tailoring of the back-wall topology surrounding the reference penetration and related dimensions.

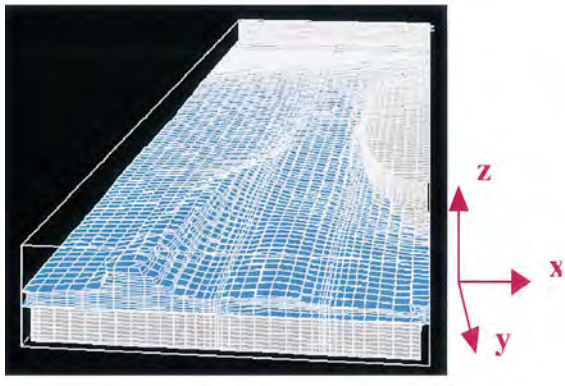

Fig. 16

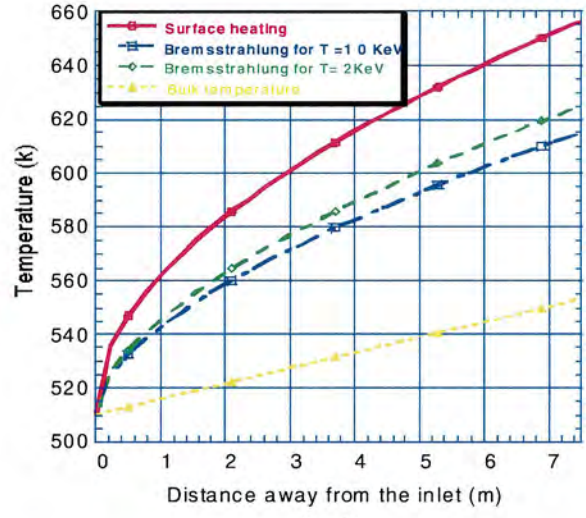

Fig. 17

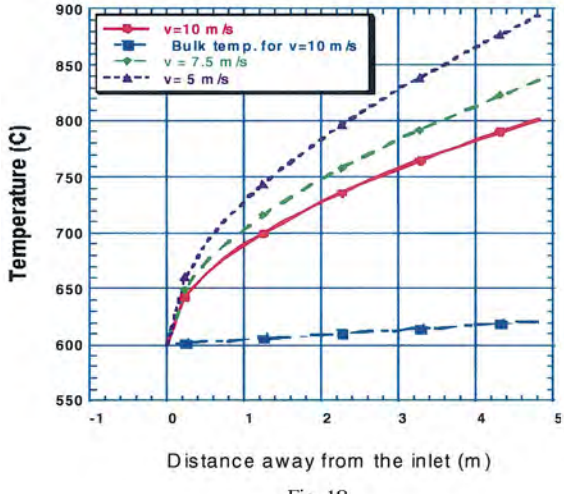

Fig. 18

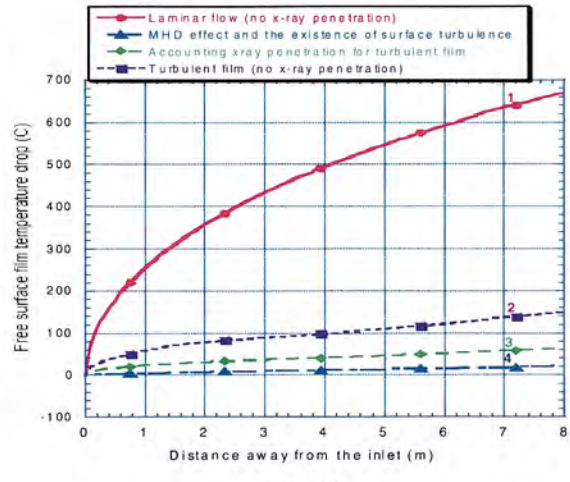

Fig. 19

Fig. 16. Three-dimensional analysis of Flibe flowing around a penetration surrounded by a tailored backwall for the case shown in Fig. 15.

Fig. 17. Temperature of free-surface liquid lithium as a function of distance along the flow path shown for various cases of treating the surface heat flux (i.e. penetration of Bremsstrahlung radiation. Also shown is the lithium bulk temperature.

Fig. 18. Sn–Li free-surface temperature increase due to surface heating as the flow proceeds downstream for different velocity magnitudes.

Fig. 19. Effect of different heat transfer mechanisms on Flibe free surface temperature (initial velocity = 10 m/s and film thickness = 2 cm; final velocity = 13.3 m/s and film thickness = 1.5 cm).

alteration of the back wall topology, such as shown in Fig. 15. Preliminary analyses for CLiFF concepts (2 cm thick convective liquid layer) confirm the effectiveness of the proposed schemes. As illustrated in Fig. 16, three-dimensional numerical simulations show a much reduced disturbance level, no splash occurring at the stagnation point, and no separation in the flow field. These results are encouraging and provide 'mechanisms' for solving penetration issues in thick liquid wall concepts (where we are dealing with a much larger volume of fluid). The problems associated with

accommodating penetrations are high priority issues for further study.

4.4. Heat transfer and free surface temperature

The power emanating from the burning plasma striking the liquid will cause its surface temperature to rise as it flows downward in the chamber. The temperature of the free liquid surface facing the plasma is the crucial parameter which governs the amount of liquid that evaporates into the plasma chamber and, therefore, is a potential source of plasma impurity. However, it can only be determined accurately if the heat transfer at the free surface/vacuum boundary is well understood as analyzed below. The allowable temperature from a plasma impurity standpoint is analyzed in the plasma edge modeling reported in Section 8.

Since a liquid metal wall will be 'laminarized' by the magnetic field, the heat transfer at the free surface wall is determined by the laminar convection and conduction. Furthermore, the lithium surface temperature is reduced because the surface heat load is deposited into the bulk due to X-ray penetration. Calculations show that, under a surface heat flux of 2 MW/m^2, the lithium free surface temperature drop can be kept below 100°C at a velocity of 20 m/s throughout the ARIES-RS reactor, taking account of X-ray penetration (see Fig. 17). This film temperature drop increases to 140°C if the lithium velocity is decreased to 10 m/s. Nevertheless, it appears that the lithium free surface temperature can be maintained below 400°C, which may be acceptable to the plasma operation. The surface temperature rise for Sn–Li as it reaches the bottom of the reactor is higher than that of lithium flowing at the same velocity. This is due to a lower thermal conductivity and a higher z. However, because of its low vapor pressure, Sn–Li can flow at lower velocities for higher surface temperatures yet not jeopardize plasma operations. However, the potential of using Sn–Li for a non-structure-thick liquid wall design is limited by its high density. As shown in Fig. 18, a velocity magnitude of about 7.5 m/s or more is needed to maintain the liquid adherence to the wall as well as the surface temperature to remain below 827°C (vapor pressure corresponding to that of lithium at 400°C). The corresponding pumping power is about 6% of a fusion power of 5480 MW for a 45 cm thick Sn–Li FW/blanket.

The molten salt Flibe, a low-conductivity, high-Prandtl fluid, is not fully laminarized by the presence of the magnetic field. The heat transfer at the Flibe free surface wall is dominated by the rapid surface renewal by the turbulent eddies generated either near the back wall or nozzle surfaces by frictional shear stress, or near the free surface due to temperature driven viscosity variations. Accurate calculations of Flibe free surface temperature require the knowledge of the turbulent structures, eddy generation and dissipation, and the degree of turbulence suppression by the magnetic field. In an attempt to calculate the Flibe free surface temperature and to examine the effects of the magnetic fields on turbulence suppressions, the so-called $\kappa-\varepsilon$ model of turbulence [1] was developed. Preliminary results based on the $\kappa-\varepsilon$ model of the turbulence, including MHD effects and various boundary conditions, predict a range of temperatures that may in some cases be beyond the plasma compatible temperatures. As shown in Fig. 19, if the Flibe flow is laminarized, the Flibe free surface can be overheated. The film temperature drop can reach 700°C at the bottom of ARIES-RS under APEX 2 MW/m^2 surface heat load (curve 1) while turbulent heat transfer considerably reduces Flibe free-surface temperature drop (curve 2). On the other hand, accounting for Bremsstrahlung radiation penetration further reduces surface temperature by about 90°C (curve 3). Furthermore, heat transfer at the vacuum/free surface interface can be significantly enhanced by the existence of surface turbulence (curve 4), while turbulence suppression due to MHD can be neglected at the current parameters of interest (curve 4). If the Flibe surface temperature is high relative to the plasma operation limit, further design modifications such as using two coolant streams may be required to accommodate this difficulty.

4.5. Power conversion and two stream flows

The challenges of the liquid wall designs go beyond achieving a low enough surface tempera-

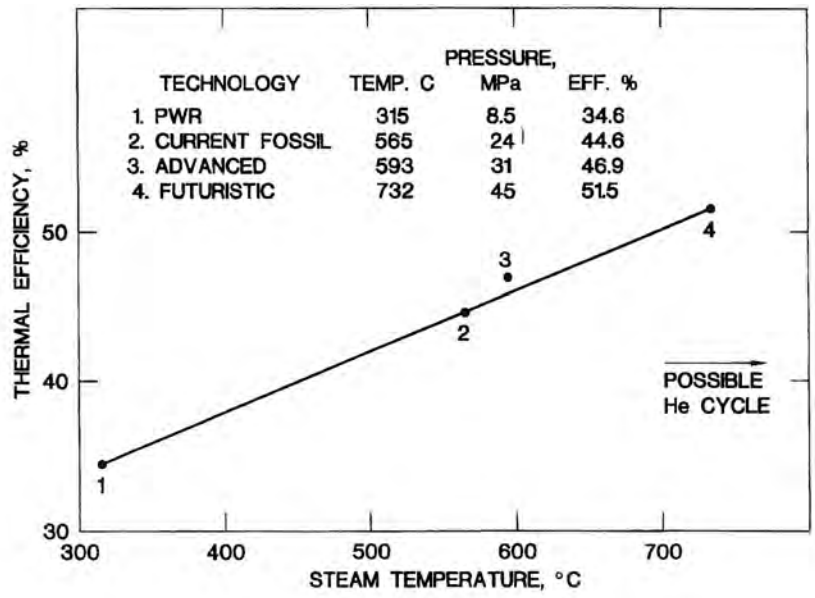

Material options for a thick liquid FW/blanket system

Material Choice	Blanket In/out Temps	η
ODFS	600/650°C	41.2%
V	600/650°C	41.2%
Nb-1Zr	650/700°C	44.6~46.9%
T-111	750/800°C	46.9~51.5%
TZM	750/800°C	46.9~ 51.5%
W	800/850°C	~51.5%

Fig. 20

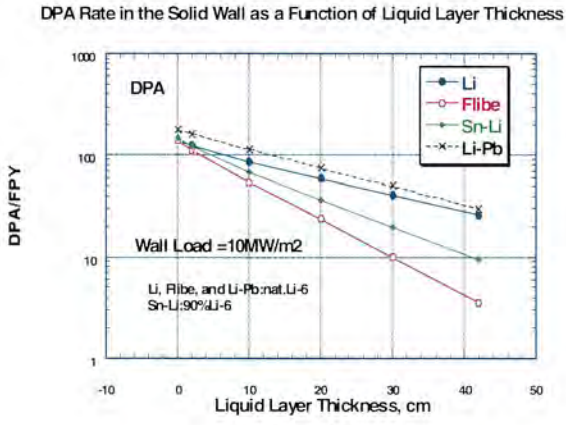

Fig. 21

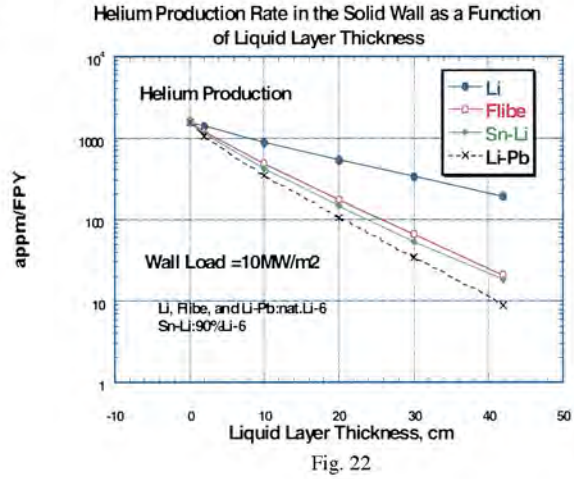

Fig. 22

Fig. 20. Thermal efficiency as a function of steam temperature in various systems. Power conversion efficiency determines material choice and bulk exit temperature.

Fig. 21. The DPA rate in the backing solid wall.

Fig. 22. The helium production rate in the backing solid wall.

ture compatible with the plasma operations, but also to maintain a mean bulk temperature of greater than 600°C for high thermal efficiency (see Fig. 20). This temperature can be higher than the maximum allowable free surface temperature. One approach to overcome this difficulty in a thick liquid wall design is to use two different coolant streams: one for surface heat removal and the other for neutronics heat deposition in order to simultaneously achieve these two conflicting temperature requirements. A power conversion system would then include two cycles: one for the conversion of the thermal power fast plasma-facing stream, and the other for conversion of the thermal power in the thick liquid behind it, which has a much higher thermal conversion potential. Since thick liquid walls will reduce both the neutron damage rate and helium transmutation rate, the choice of the structural material should be determined by the high temperature capability and liquid/structure compatibility. It appears that the use of tungsten alloys would achieve the highest thermal efficiency because of its high temperature operation capability. The oxide-dispersed ferritic steel (ODFS) can operate up to a temperature of 650°C, which provides a thermal efficiency of about 41.2%.

4.6. Effects of liquid walls on reducing activation and radiation damage

Reducing activation and radiation damage to structural materials are among the important advantages of liquid walls, particularly the 'thick' liquid wall concepts. The magnitude of these advantages is design dependent. Calculations were performed to quantify the benefits as a function of key design parameters. The results are briefly summarized in this subsection. These results were utilized to guide the choices for concept exploration discussed earlier in this section. More detailed analysis is required in the future to address flow support structures other than the backing wall that may be also needed in liquid wall designs (for example, inlet nozzles and flow dividers). The thickness of the liquid in front of these elements may be less than that protecting the backing wall. Note also that these elements are more accessible than the backing wall (or first wall in traditional concepts) and therefore faster maintenance may be possible. In particular, the key factor is the extent to which liquid walls attenuate the neutrons before they reach the structural materials. The main structural element in liquid wall designs is the backing wall. So, the thickness of the liquid wall is important in determining the reduction in activation and radiation damage in the back wall relative to the solid first wall in traditional concepts.

4.6.1. Radiation damage parameters

The effects of the liquid layer thickness on radiation damage parameters such as atomic displacement and helium production rates were studied for lithium, Flibe, Sn–Li, and Pb–Li. Figs. 21 and 22 show the rates (per full power year, FPY) of atomic displacement (DPA) and helium production (appm), respectively, in the back wall structural material as a function of the liquid layer thickness (L) protecting the back wall.

Without the liquid layer, which corresponds to a 'bare wall' case, the DPA and helium production rates in the backing solid wall are comparable in the four breeders. However, because Pb–Li exhibits larger reflection, the low-energy neutron flux is larger at the solid wall which results in larger DPA rate (occurs at all energies). This also gives smaller He-4/DPA ratio in the case of Pb–Li breeder (~ 8.7) as compared to the value with the other breeders (10–11).

As the thickness of the liquid layer increases, the reduction in these damage parameters varies among the four breeders. Lithium is the weakest material in moderating neutrons as compared to the other breeders. The reduction in DPA rate is less than an order of magnitude for $L = 42$ cm, while the reduction in helium and hydrogen production is about an order of magnitude. The attenuation characteristic of the Pb–Li breeder for the DPA rate is similar to lithium. However, the Pb–Li is superior to the other breeders in attenuating the helium and hydrogen production rate in the solid wall. This is due to its larger attenuation power to high-energy neutrons (through (n, 2n) and (n, inelastic) reactions) which is basically the main contributor to the high-

threshold helium and hydrogen reactions in the solid wall. Because of the smallest He-4 production and the largest DPA rate with the Pb–Li breeder, the ratio He-4/DPA is the smallest (~ 0.3) at $L = 42$ cm as compared to the values with the other breeders (Li: ~ 7, Flibe: ~ 6, Sn–Li: 2). The attenuation characteristics of the Flibe and Sn–Li are similar for the helium and hydrogen production. However, the Flibe gives the best attenuation to the DPA rate since it is capable of attenuating both the high- and low-energy component of the neutrons reaching the backing solid wall.

Using the damage values at the bare wall ($L = 0$ cm) and at the wall with various L thicknesses, one can estimate the tenfold thickness, L_{10}, for each breeder defined as the required thickness of the layer to reduce a particular response, R (damage parameter), by an order of magnitude. This thickness is given in Table 7 for the various damage parameters and breeders. For helium and hydrogen production rate, ~ 22 cm is required to achieve an order of magnitude reduction with Flibe and Sn–Li and smaller thickness (~ 18 cm) is required in the Pb–Li liquid layer. Twice as much thickness is required in the Li case because of its poor attenuation characteristics for helium and hydrogen production. As for the DPA rate, larger thickness is required. It is ~ 26 and ~ 36 cm for the Flibe and Sn–Li, respectively, but much larger thickness (~ 58 cm) is required in the Li and Pb–Li to reduce the DPA rate by an order of magnitude.

The DPA rate in backing solid wall is ~ 26 DPA/FPY, 3.6 DPA/FPY, 9.5 DPA/FPY, and 30 DPA/FPY, with the Li, Flibe, Sn–Li, and Pb–Li liquid layer, respectively. If the 200 DPA is considered as the limit at which the wall and shield zone require replacement, the lifetime of these components would be 7.7, 56, 21, and 7 yr, respectively. Clearly the presence of the liquid layer made these components last the lifetime of the plant (30 years) when Flibe is used as the breeder. In the case of Sn–Li, one replacement may be required after ~ 20 years. But three to four replacements may be needed in the case of Li and Pb–Li breeders.

4.6.2. Hazard and volume of radioactive waste

Another clear advantage of deploying a thick liquid wall/blanket concept is the substantial reduction in the hazard and volume of the waste generated from the activation of solid materials (including solid walls, vacuum vessels, shield and magnets themselves). It has been found [1] in comparing the liquid FW/blanket (42 cm-thick) to a conventional blanket (2 cm-thick ferritic steel, FS, FW — 40 cm-thick blanket made of 10% FS and 90% Flibe), while keeping the radial build the same (ARIES-RS radial build and materials are assumed), the specific activity (curies/cc) at shutdown in the bare FW of the conventional blanket is two orders of magnitude higher than the specific activity in the back wall of the liquid FW/blanket case. The specific biological hazard potential (BHP) has the same features. The two orders of magnitude difference continues during the first year and starts to narrow down after the first year following shutdown. The next step is to find out how this may translate into advantages from both the waste generation (dominated by long-lived nuclides) and safety hazard (dominated by short-lived and intermediate-lived nuclides) viewpoints.

An analysis comparing the waste disposal ratings and volume of waste generated in a power plant based on the two concepts was conducted.

Table 7
The tenfold thickness (in cm) of the liquid layer[a]

Parameter	Li/FS	Flibe/FS	Sn–Li/FS	Pb–Li/FS
DPA (dpa/FPY)	~58	~26	~36	~56
Helium production (appm/FPY)	~46	~22	~21	~18
Hydrogen production (appm/FPY)	~44	~22	~22	~19

[a] The thickness required to reduce a response by an order of magnitude.

Table 8
Comparison of class C waste disposal ratings using Fetter limits

Zone	FPY	Liquid blanket concept	Conventional blanket concept
Inboard FW and blanket	3	–	1.37
Inboard shield	30	0.81	0.73
Inboard VV	30	0.141	0.1
Outboard FW and blanket	3	–	1.34
Outboard shield	30	0.795	0.71
Outboard VV	30	0.087	0.06

The waste disposal ratings for the Fetter [15] and 10CFR61 [16] limits are shown in Tables 8 and 9, respectively. Results in the tables are given for compacted wastes after 1 year following shutdown. As shown in Table 8, according to Fetter limits, all components of the liquid blanket concept would qualify for disposal as class C waste after 30 FPY. All components of the conventional blanket concept, except for the first wall and blanket, also would qualify for disposal as class C waste after 30 FPY. The first wall and blanket would not qualify for disposal as class C LLW unless they were replaced every 2 FPY instead of every 3 FPY. On the other hand, the 10% steel structure in the conventional blanket provided the shield and vacuum vessel behind it with better shielding, resulting in lower waste disposal ratings in comparison to the waste disposal ratings of the shield and vacuum vessel behind the liquid blanket. Results in Table 9 show that, according to the 10CFR61 limits, all components of both blanket concepts would qualify for disposal as class C waste. The absence of contribution from ^{192m}Ir to the waste disposal ratings according to the 10CFR61 limits (10CFR61 has no limits for ^{192m}Ir) resulted in allowing for the disposal of the first wall and blanket of the conventional blanket concept as LLW after 3 FPY.

A power plant based on the conventional blanket concept will produce the equivalent of about ten blankets of additional waste during its lifetime. However, a power plant based on either the liquid or conventional blanket concepts will generate a comparable amount of waste from the shield, vacuum vessel, and magnets, whose volumes far exceed the volume of the blanket. As shown in Fig. 23, the volume of the waste generated during the life-time of a power plant (30 FPY) based on the liquid blanket concept could be a factor of six lower than the volume of waste generated during the same life-time if the plant was based on the conventional blanket concept. The factor of six is based on the assumption that the waste is non-compacted and the waste does not include the magnets. If the waste is compacted to 100% of its theoretical density, the reduction factor drops from six to two. If the waste is compacted and the magnet waste is included, a power plant based on the conventional blanket concept will generate about 35% more waste during its life-time (30 FPY) than a similar power plant based on the liquid blanket concept.

4.7. Key issues and R&D

The present state of understanding of thick liquid wall concepts does not reveal any basic flaws in the underlying scientific and technical arguments for the concepts. Yet, there remain many issues for the implementation of this concept in any magnetic fusion configuration. Near term R&D should focus on continued concept exploration as well as modeling and experiments for key feasibility issues. These include:

1. Edge-plasma and core-plasma modeling and analysis as well as experimental research in various confinement devices for plasma–liquid wall interactions.
2. Experimental data on the achievable minimum liquid surface temperatures without MHD effects for turbulent Flibe and MHD laminarized lithium/tin–lithium flow under high power density conditions.

3. Identification of practical heat transfer enhancement schemes necessary for minimizing liquid surface temperatures.
4. Experimental characteristics of small-scale liquid metal flow hydrodynamics configurations applicable to MFE confinement schemes such as $1/R$ toroidal field variation, and effects of finite radial, poloidal, and vertical field components.
5. Computer simulation of MFE relevant three-dimensional free surface liquid wall thermal and hydrodynamics performance with MHD effects. In particular, hydrodynamics characteristics near the penetrations and supply and return lines.
6. Identification of the most promising hydrodynamics configurations with respect to different MFE confinement schemes.

In addition, engineering innovations and analyses are required for the following numerous mechanical design issues including:

- How to move mass quantities of liquid metal or salt in and out of the machine reliably.
- How to provide sufficient access for supply piping and return ducts.
- How to design the piping and nozzles for reliable operation at high fluid velocity.
- How to start and stop the system safely.
- How to keep the stream attached to the inboard wall (must prevent toroidal rotation of inboard stream).
- How to provide sufficient penetrations for heating and diagnostics.
- How to account for image current effects from moving plasma.

Issues related to effects of liquid metals on the plasma core and edge-plasma liquid–surface interactions are discussed in Sections 7 and 8.

5. Thin liquid wall concepts

The thin liquid wall concept was explored in APEX for liquid metals and for Flibe. Initial designs of thin liquid walls were developed and the associated advantages and disadvantages were analyzed. Thin liquid wall concepts are called CLiFF.

The idea behind CLiFF (the Convective Liquid Flow First-Wall concept) is to eliminate the presence of a solid FW facing the plasma through which the surface heat load must conduct. This goal is accomplished by means of a fast moving (convective), thin liquid layer flowing on the FW surface (see Fig. 24). This thin layer is easier to control than a thick liquid FW/blanket, but still provides a renewable liquid surface immune to radiation damage and sputtering concerns, and largely eliminates thermal stresses and their associated problems in the first structural wall. The attractiveness potential and key issues for the CLiFF design are summarized in Table 10. The CLiFF class of liquid wall concepts is viewed as a more near-term application of liquid walls.

Details of the preliminary design, heat transfer, power balance, thermal-hydraulics, neutronics, activation and safety are included in this section. It is noted that the first several centimeters of various thick liquid FW/blanket concepts discussed in the preceding section will behave in a similar fashion to the CLiFF concept discussed

Table 9
Comparison of class C waste disposal ratings using 10CFR61 limits

Zone	FPY	Liquid blanket concept	Conventional blanket concept
Inboard FW and blanket	3	–	0.495
Inboard shield	30	0.25	0.21
Inboard VV	30	4.22×10^{-3}	2.82×10^{-3}
Outboard FW and blanket	3	–	0.473
Outboard shield	30	0.25	0.21
Outboard VV	30	2.54×10^{-3}	1.69×10^{-3}

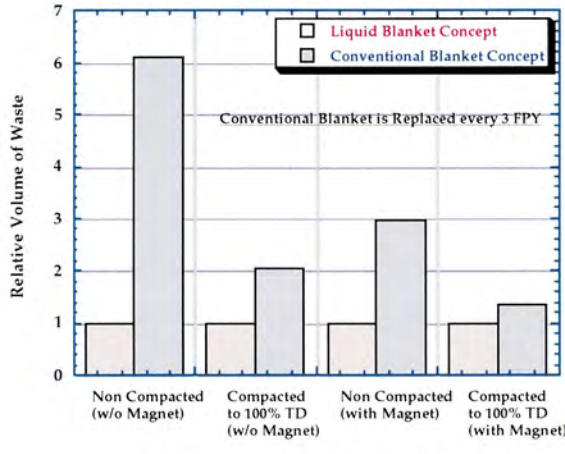

Fig. 23

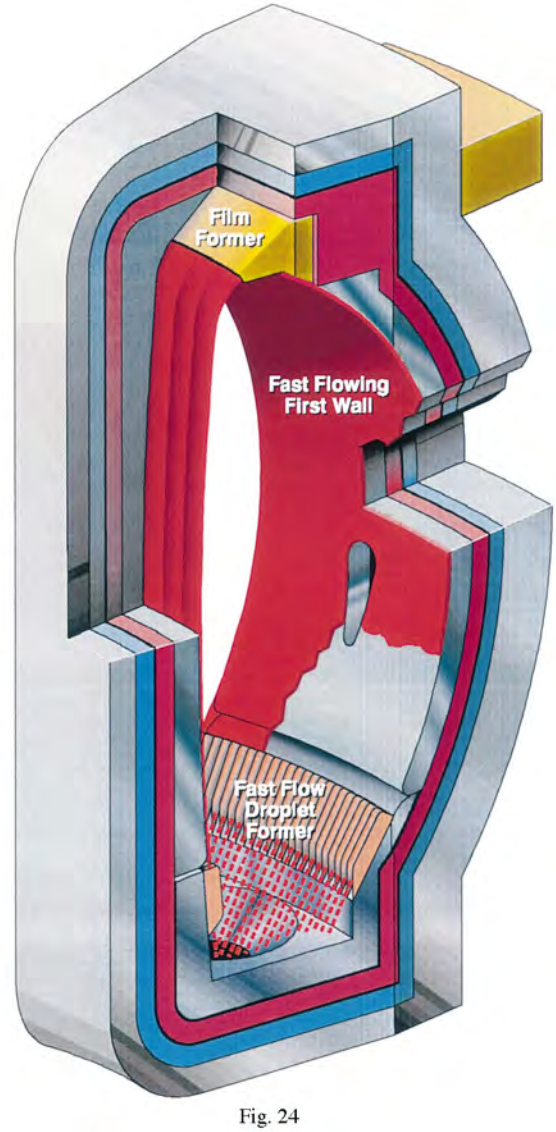

Fig. 24

Fig. 23. Comparison of total volume of waste generated in power plants based on thick liquid metal blanket and conventional blanket concepts.
Fig. 24. Conceptual sector schematic of CLiFF implementation in ARIES-RS reactor.

here, and significant overlap with those analyses is seen in what follows.

5.1. Design description

The majority of the work reported here was carried out for the tokamak. Specifically, the ARIES-RS geometry was utilized whenever possible, with modifications for the unique structures and high flowrates required for CLiFF. This means, however, that the ARIES-RS fusion power needs to be scaled-up to 4500 MW to give the 10 MW/m^2 peak neutron wall load and 2 MW/m^2 peak surface heat flux goals of the APEX study. Tokamaks present a difficult challenge for liquid walls due to the fact that the plasma cham-

ber is relatively closed with short scrape-off lengths, and so, vaporized liquid wall material must be screened by the edge plasma to keep it from penetrating to the core.

The general CLiFF design, as seen in Fig. 24, is conceptually simple in its implementation. A thin fast liquid layer is injected near the top of the plasma chamber. The layer flows down the reactor walls without excessive slowing or thinning, and is removed in some fashion from the bottom of the chamber. Layer thickness h on the order of 0.5–2 cm, and velocity U on the order 10 m/s, are considered. The curved back wall fits the plasma shape and provides an adhesion force due to the liquid's centrifugal acceleration. The criterion for continuous attachment of the liquid layer is simply $U^2/R_c > g \cos \alpha$, where g is the acceleration of gravity, R_c is the radius of curvature of the first wall section and α refers to the angle of the outward surface normal to gravity vector (so 0° is completely inverted).

The velocity range is chosen quite high both to ensure adhesion to the back-wall, but also to keep the exposure time to the plasma short, and thus keep the surface temperature low. If one desires an inlet temperature that is >300°C (for power conversion reasons), it turns out that it is this second restriction that is the more severe, based on the maximum surface temperature estimates provided by the preliminary plasma edge analysis. The high velocity requirements and the large coverage area result in volumetric flow rates in excess of 10 m^3/s compared to ARIES-RS in the 3 m^3/s range.

The conceptual CLiFF design shown in Fig. 24 has an integrated droplet-type divertor. Some means (mechanical or electrical) is used to stimulate the breakup of the FW flow into a droplet screen. It is hoped that the droplet screen will have a higher heat removal capability due to the rapid rotation and internal circulation in the droplets, but this fact remains to be proven. In

Table 10
Potential advantages and issues of CLiFF concept for APEX

Potential	Issue
Removal of surface heat loads (greater than 2 MW/m^2 possible). Local peaking and transients can be tolerated	Hydrodynamics and heat transfer involve complicated MHD interaction between flow, geometry, and the magnetic field: Suppression of turbulence and waves
FW surface protected from sputtering erosion and possibly disruption damage	LM-MHD drag thickens flow and inhibits drainage from chamber Effects of varying fields on LM surface stability and drag
Beneficial effects on confinement and stability from conducting shell and DT gettering effects	Evaporating liquid can pollute plasma, surface temperature limits unknown
Elimination of high thermal stresses in solid FW components, having a positive impact on failure rates	High flowrate requirement can result in low coolant ΔT or two coolant streams
Possible reduction of structure-to-breeder ratio in FW area, with breeder material facing virgin neutron flux	Effect of liquid choice on edge plasma gettering, tritium through-put, and tritium breeding
Integrated divertor surface possible where CLiFF flow removes all α heat	Neutron damage in structure is only slightly reduced compared to standard blankets, blanket change-out required for high power density operation
Complex tokamak D-shape and ports can likely be accommodated	

addition, for LMs, the droplet screen will be electrically isolated from the main FW flow and plasma currents will not be able to close. The liquid film can be removed from the vacuum chamber by gravity drainage or by an EM pump if the working liquid is an electrical conductor.

Supply nozzles will form the desired liquid flow at the top of the reactor. These nozzles can be designed to be protected from surface heat flux by the flowing liquids.

Note also that since these nozzles are at the top of the reactor chamber, the surface heat load and nuclear heat will be lower than the peak midplane values. Liquid removal from the plasma chamber is accomplished through a combined vacuum pumping and liquid drain port. It is envisioned that the liquid flow itself will pump a portion of the implanted plasma particles into the pumping ducts by convection, thus aiding in impurity removal.

The working liquid should be a tritium breeding material like lithium, tin–lithium or Flibe. Thus the liquid removed from the reactor can be recirculated to the blanket as the main tritium breeder and coolant. The bulk nuclear heat is added on top of the FW/divertor heat before the liquid is sent to the power conversion system. In this manner, the FW and divertor power is converted at relatively high thermal efficiency.

Penetrations for various heating, fueling and diagnostics functions will be provided as much as possible in the lower half of the outboard FW. Flow can be guided by means of submerged grooves around the penetration, and close again downstream to form a continuous surface protection as discussed in the previous section. Cooling of the penetration structures themselves will be aided by the CLiFF flow. It is likely that for LMs, the penetrations will have to be electrically isolated from the flow by means of an insulator coating. This will be true in supply lines and nozzles as well.

Off-normal plasma events like disruption can possibly induce large currents in LM CLiFF flows and cause the layer to be splashed or torn off the wall altogether. For poorly conducting Flibe, the effect of the disruption is not as clear. It is hoped that, in any case, splashing will turn out to be an allowable response, and that the liquid wall will just be restarted following the disruption. For an all-liquid wall system, this seems a reasonable assumption, except for possible damage to antennae and sensitive diagnostics. It is hoped that 'liquid tolerant' antennae could be designed that could accept the occasional splashing of liquid metal, but this certainly remains to be demonstrated.

5.2. Hydrodynamic and heat transfer analysis

Aside from plasma compatibility, one of the key issues for CLiFF is related to finding a feasible hydrodynamic configuration. A significant amount of design analysis has been done so far on CLiFF in order to answer the three basic questions: How do you form it? How do you drain it? How do you maintain it? It is noted that liquid metals and Flibe behave very differently in the magnetic environment of a tokamak. The low thermal and electrical conductivity of Flibe leads to a FW flow that will still be turbulent, and have heat transport at the free surface and flow drag at the back-wall that depend heavily upon this turbulence. For LMs the converse case occurs, where it is expected that the MHD effects will dominate the drag, and the thermal conduction dominates heat transfer.

5.2.1. Turbulent Flibe flow

Several models have been applied to predicting the flow profiles for Flibe, ranging from simple hydraulic models for the steady state equilibrium flow profile, to more complex two- and three-dimensional non-steady codes for studying phenomena like surface waves and penetrations. The 1.5 D hydraulic calculations indicate that flow depth equilibria in the range of 2 cm can be achieved for Flibe flows in the 10 m/s range (see Fig. 25). A more sophisticated, low-Reynolds number $\kappa-\varepsilon$ model of turbulence was also applied to the CLiFF flow in order to study the effect of MHD turbulence on the flow profile. In comparison to the ordinary $\kappa-\varepsilon$ model, the present one was extended to the MHD case by means of additional terms in the closure equations. Due to turbulent viscous friction, the layer thickness increases rapidly over the initial flow section (see

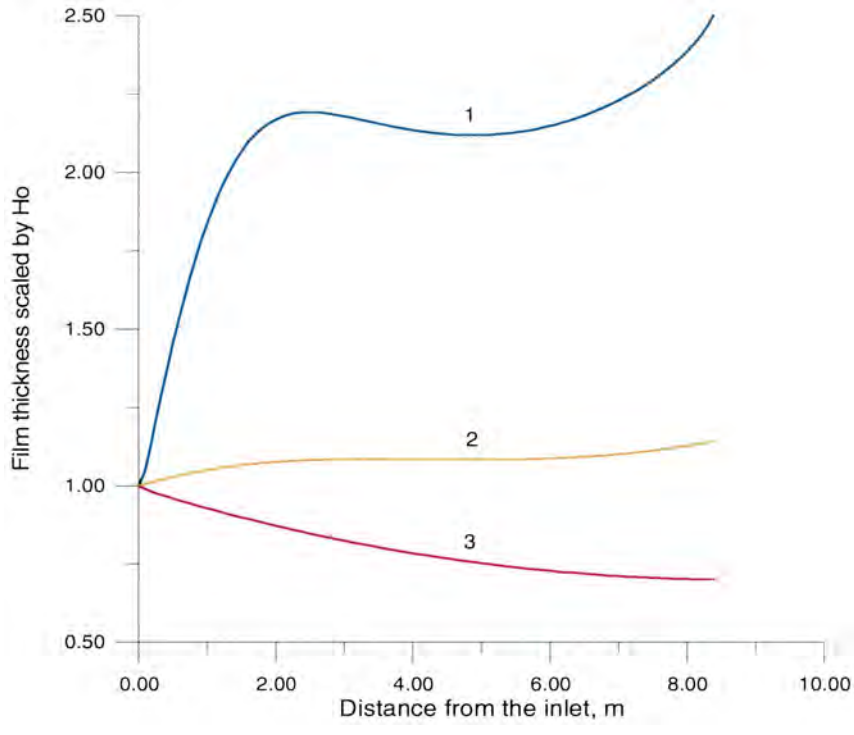

Fig. 25. Surface height predictions for Flibe with various models: Line 1: $\kappa-\varepsilon$, 2: Darcy Weisbach friction factor = 0.025, and 3: laminar.

again, Fig. 25). This is in contrast to the results presented earlier where the simple friction factor formulation predicts nearly constant flow height and velocity profiles for CLiFF. This contradictory result is cause for concern because if the layer slows down significantly, the transit time through the plasma chamber will go up, as well as the surface temperature. Attempts to benchmark the $\kappa-\varepsilon$ and friction factor against available data from the UCLA Mega-Loop Experiment [17] are inconclusive — the data splits the difference between the $\kappa-\varepsilon$ and friction factor model.

The effect of the magnetic field on the flow parameters is negligible if the Hartmann number is less than about 1000, and hence for CLiFF with Ha = 500, we conclude that there is no strong impact of MHD on the Flibe flow hydraulics.

Heat transfer calculations using this same model indicate that depending on surface turbulence assumptions, the temperature rise at the surface can be quite low. For a 10 m/s, 2 cm thick Flibe flow, the surface temperature rise is in the range of 30–160°C depending on whether optimistic or pessimistic assumptions are used. The effect of the magnetic field again appears to be small. When considering the thermal hydraulics, it is seen that the temperature window for Flibe is limited (see Flibe system diagram in Fig. 26), and so the surface heat transfer is critical for feasibility. There are, however, no experimental data, and this issue needs closer study and experimental validation.

The surface stability for Flibe CLiFF flows was also analyzed using a linear stability analysis technique for infinitesimal disturbances. For CLiFF, the results show that whenever the flow is adhered, it should be stable as well. The effect of finite size perturbations may alter this picture. The primary source of large disturbances comes from the turbulence of the flow itself. The fluid dynamic behavior of the first-wall flow system may be affected due to these eddy generating mechanisms including boundary layer relaxation near nozzles, Gortler-type instabilities, structural vibrations, etc.

Penetrations have also been analyzed for the Flibe case using a three-dimensional free surface code that allows the introduction of arbitrarily formed structures. The penetrations considered are elongated into ellipses in order to be more hydrodynamically streamlined. The specific case

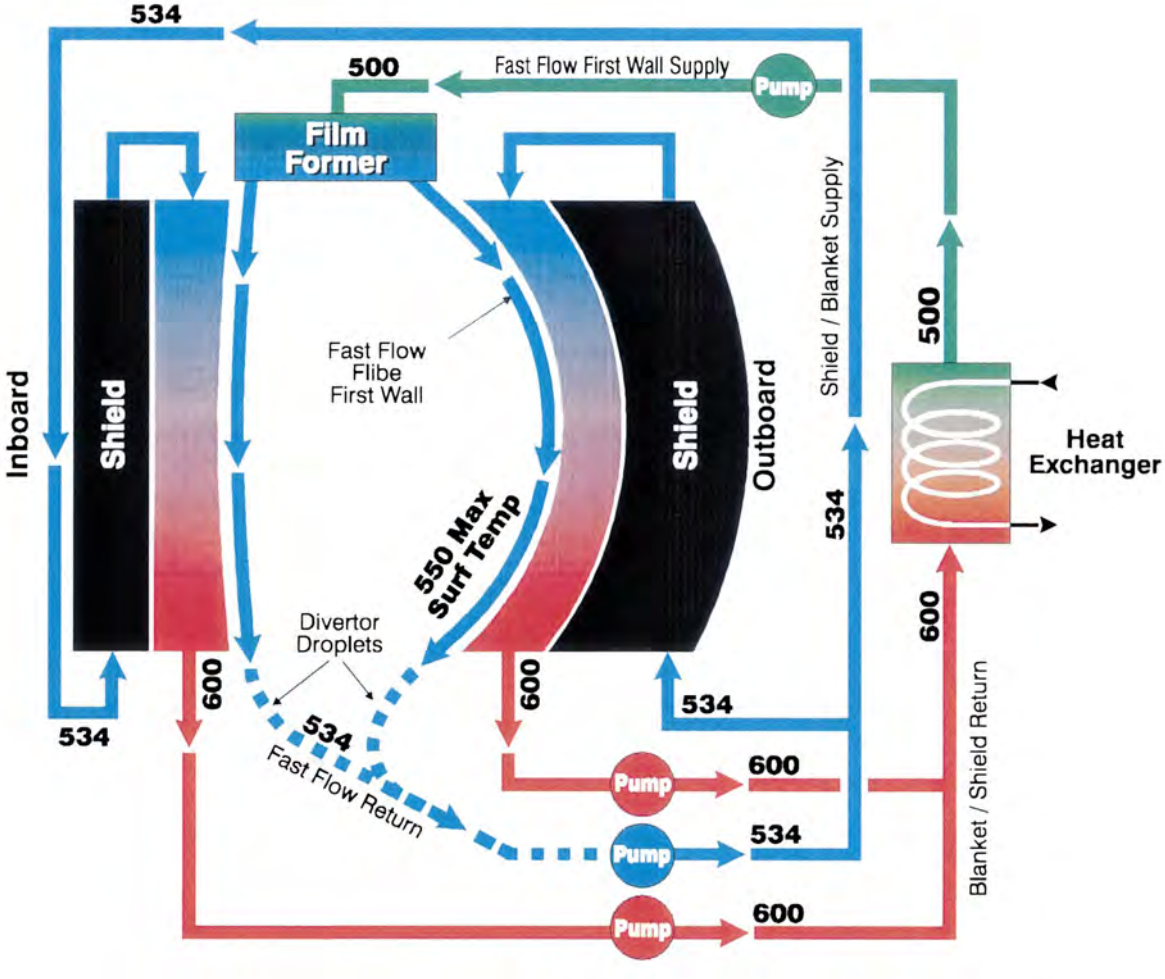

Fig. 26

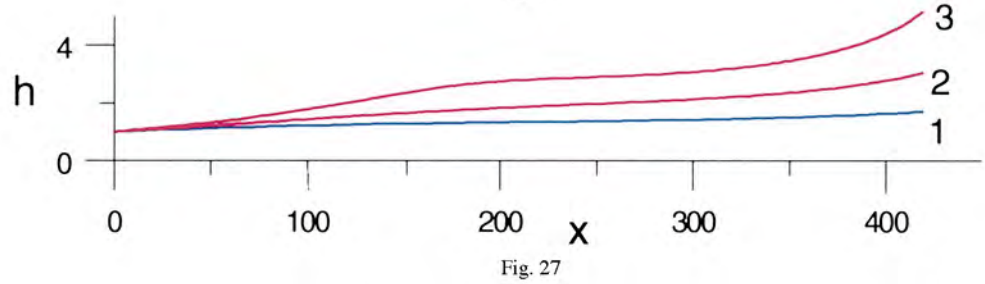

Fig. 27

Fig. 26. CLiFF — flow/temperature schematic-Flibe option.

Fig. 27. Influence of the wall conductance ratio on the layer thickness increase ($2b = 1$ m). Line 1 — $c_w = 0$; 2 — $c_w = 1.0 \times 10^{-6}$; 3 — $c_w = 2.0 \times 10^{-6}$ (Lithium).

considered has dimensions 20 cm wide and 90 cm long (in the flow direction). The back-wall in the vicinity of the penetration is tailored to guide the liquid around the penetration itself, and to aid in closing the liquid again downstream of the penetration. Results presented in the previous section of thick liquid walls show that such a design solution can successfully guide the flow around penetrations, but additional work and optimization is needed for their design.

5.2.2. Magnetohydrodynamics for lithium and Sn–Li flows

Mathematically these types of flows can be described by a set of Navier–Stokes equations for incompressible fluids and Maxwell's equations for electromagnetic phenomena. The numerical tools used to analyze this system of equations are based on two-dimensional, simplified magnetohydrodynamic equations and can be performed in practice for any values of governing parameters for ducts of various geometries. This is an extreme simplification of the physics and assumes that all currents close in their own cross-sectional plane. This type of calculation is accurate for well-behaved, nearly fully developed flows with simple geometries, but ignores significant effects near field gradients and developing regions.

It is well known that the presence of electrically conducting walls can lead to larger electrical currents in the flow domain and, as a result, to a significant increase in the MHD drag effect. In the case of free surface MHD flows, this effect manifests itself in the increase of the layer thickness with the accompanying reduction in the velocity. Ideally, if the liquid layer is assumed to be completely axi-symmetric in the toroidal direction, flow along poloidal flux surfaces with no field gradients, no MHD drag will occur. This ideal case, though, is not possible in practice and we look at two variants to gauge the relative effects of the MHD. One case is the presence of fins, side-walls, or penetrations breaking up the flow toroidally, and the other is a slight deviation of the flow path from the flux surfaces resulting in a small surface-normal field component. Figs. 27 and 28 illustrate the results for these two cases for lithium, where we assume that a doubling of the initial height represents an unacceptable result. Note that in Figs. 27 and 28, the thicknesses on the vertical axes are scaled by the initial thickness.

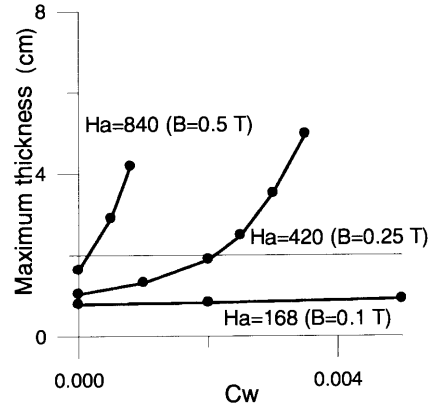

Fig. 28. Influence of the radial magnetic field and the wall conductance ratio on the maximum thickness of the lithium layer (for axi-symmetric case, $C_w = \infty$).

For the case of side-walls, it was found that electrically insulated side-walls are acceptable only if they are no closer than 1 m toroidally, and that low conductivity walls like SiC (thickness = 1 cm, assumed $\sigma = 10^3\ \Omega^{-1}\mathrm{m}^{-1}$) are acceptable provided they are no closer than 8 m. Bare metal walls (thickness = 2 mm, $\sigma = 10^6\ \Omega^{-1}\mathrm{m}^{-1}$), even if very thin, can be no closer than 110 m, and so are not feasible for CLiFF. For the case of a small radial field it was found that if the back-wall is bare metal the allowable field is only $B_r < 0.1$ T. This value goes up to $B_r < 0.5$ T if the backing wall is insulated. These calculations assume that there are insulated side-walls present at some distance to break up the toroidal electric path (but they are separated by enough distance that they do not add appreciable drag). If complete axi-symmetry is assumed, where induced currents close on themselves, the allowable radial field is $B_r < 0.015$ T! These calculations indicate that serious work is needed in the area of LM-MHD analysis and experiments to prove that passive flow schemes like CLiFF are possible.

Heat transfer at the surface is calculated for Li and Sn–Li using only conduction, but assuming some penetration of X-ray photons in the case of lithium. The conclusion is that at 10 m/s the temperature rise will be on the order of 150°C for

Li, and 300°C for Sn–Li. The thermal-hydraulic calculations utilizing these numbers result in a blanket outlet temperature around 650°C for the Sn–Li, but much lower for the lithium, possibly necessitating a two-stream approach, where only part of the Li flow is sent to the blanket.

The results of stability computations are in a good agreement with the linear stability analysis conclusions. Long wavelength initial disturbances grow very rapidly on the inverted surface under the effect of gravity and centrifugal acceleration and then propagate down with slowly decreasing amplitude. The growth rate and the maximum amplitude depend on the wavelength. The short waves (<20 cm) are suppressed rapidly by the surface tension, while the long wave disturbances (1.5–2 m) are not suppressed over the whole flow length. The most dangerous disturbances are those having the long wavelength of about 2 m, for which the amplitude can reach 40–50% of the initial flow depth, however, layer disintegration, flow separation, and/or excessive increase in the thickness do not accompany the wave propagation. Therefore, special means to suppress surface instability are not needed provided inlet fluctuations are at a level <5–10%.

Due to the complexity of the problem, no detailed work has yet been done in the area of accommodation of penetrations with liquid metals. Such penetrations represent in MHD flow both a disturbance to the hydrodynamic flow field via the physical diversion of liquid from its initial course, and also, and more significantly, a disturbance to electrical current paths that potentially can overwhelm the flow with local and global MHD drag. Preliminary conclusions, gleaned from the discussion of side-walls above, is that any penetration will require an insulator coating to isolate the structure from the free surface flow.

5.3. Nuclear heat, tritium breeding, and activation

The thin layer of liquid does not significantly alter the radial build of ARIES-RS, however, the choice of working liquid plays a big role in the neutronics. Analyses of the nuclear heating and activation have been carried out using the ARIES-RS radial build at higher power density and with different coolants. The conclusions are that waste and damage issues in the vacuum vessel, the shield and magnets are lower when Flibe and Sn–Li are used, as compared to lithium. Solid walls damage parameters are reduced by $\sim$10–15% with the 2 cm Li-layer and $\sim$20–30% with 2 cm Flibe or Sn–Li layers. Lithium coolant offers the best tritium breeding potential at natural Li-6 enrichment. Lithium and Flibe coolants have maximum tritium breeding ratio (TBR) at 25% Li-6 enrichment (local TBR $\sim$1.5 for Li and $\sim$1.2 for Flibe) whereas it keeps increasing with Li-6 enrichment in the Sn–Li coolant ($\sim$TBR $\sim$1.3 at 90% Li-6). The inclusion of beryllium drastically enhances TBR in the Flibe and Sn–Li cases (local TBR $\sim$1.7 in Flibe at 25% Li-6 and $\sim$1.4 in Sn–Li at 90% Li-6 enrichment) which indicates that the tritium self-sufficiency condition could be met with Flibe or Sn–Li breeder. With regard to power deposition however, the Sn–Li offers the largest power multiplication (PM) among the several breeders. PM is $\sim$1.4 for Sn–Li, $\sim$1.14 for Li and $\sim$1.02 for Flibe. The Sn–Li breeder therefore could offer better plant thermal output for the same fusion power.

5.4. Key issues and R&D

There are several dominant issues that go directly to the feasibility of this concept, and many more issues that weigh heavily on the ultimate attractiveness. The amount of allowable evaporation must be determined for all liquid candidates. This is both a feasibility issue and an attractiveness issue. We recognize that a fully consistent answer to this question will require a considerable amount of research in modeling and analysis of plasmas with liquid wall boundaries, as well as experimental research in various confinement devices.

In addition to the plasma compatibility, the issue of establishing a viable hydrodynamic configuration threatens feasibility. The issues in this category differ significantly for molten salts versus liquid metals. For Flibe, the main issue concerns the penetration of heat at the free surface and the availability of a robust operating

window. Other issues as to the formation and removal of the liquid flow in the plasma chamber, and the accommodation of penetrations are also serious, but in our opinion solvable via numerical modeling and scaled experiments with Flibe simulants (such as water). The heat transfer issue is a more serious unknown, as current limits on surface temperature for Flibe are estimated by the plasma interface group at about 560°C. Also a serious issue for Flibe, is the behavior in the divertor region, where direct plasma contact occurs. The amount and nature of the material sputtered and redeposited needs to be determined before accurate plasma modeling of the region can take place.

The main issue facing liquid metals is of course that of MHD interaction. The CLiFF flow itself is very sensitive to changes in drag since the only forces governing the flow are gravity and friction. Without toroidal axi-symmetry of the flow and field, reliable insulator coatings will be required on all surfaces in contact with the LM layer. MHD forces from surface normal components of magnetic field can upset this balance, even when complete axi-symmetry is assumed in the toroidal direction. Additionally, gradients in toroidal field can exert a significant drag on the free surface flow. LMs however, offer the potential for active control that is not present with the molten salt. By biasing and applying electric currents, the LM can be pumped or pushed against the back-wall in-situ — offering the chance to 'confine' the liquid wall just as we confine the plasma. All these effects need to be analyzed in greater detail, with both modeling and small-scale experimental efforts to see if a suitable flow is indeed possible in the real fields of a tokamak or other plasma confinement devices.

Apart from the free surface flow itself, MHD issues exist in the LM supply and drain lines and blanket flows as well. Insulator coatings are needed for these structures. Additionally, due to the large LM flowrates required for CLiFF, large pressure drops are expected in the entrance regions between toroidal field coil legs. These pressure drops can theoretically be overcome by in-situ LM pumping, but lead to very large pumping powers for the CLiFF designs with LMs. A clever design of inlet piping may help reduce this effect, as would a reduction in the LM flowrate as well.

Impact of liquid wall implementation on other reactor systems is another category of issues for the CLiFF concept. In particular, it will be likely that heating and diagnostic ports must be redesigned to allow flow to pass around the penetration. Pumping systems with a considerable amount of vapor from liquid evaporation will need to be modified. Tritium recovery (especially with hydrogen getters like lithium) will be even more challenging, and material selection and compatibility to help optimize liquid wall performance must be addressed. Flibe and Sn–Li database issues must be addressed for all liquid wall and blanket options as well.

6. Electromagnetically restrained lithium blanket

This section focuses on another type of thick liquid in which electromagnetic forces are utilized to restrain, or 'confine', the fluid. In this concept, called the electromagnetically restrained (EMR) lithium blanket, an approximately one meter thick shell of liquid lithium metal almost completely surrounds the tokamak's toroidal plasma discharge, absorbing plasma particles, neutrons and other radiation while breeding tritium and collecting high temperature heat for power generation. The ~ 1 m thickness is chosen based on considerations of tritium breeding, of absorbing most of the fusion power, and of minimizing activation and damage to the solid chamber walls located behind the liquid. Of the candidate liquid materials, pure lithium metal is chosen due to its high abundance, superior tritium breeding, low chemical toxicity, almost zero neutron activation, and its high conductivity resulting in low power consumption for the EMR action.

The EMR concept converts MHD difficulties introduced by the liquid metal's electrical conductivity into MHD advantages by deliberately injecting controlled electrical currents to influence liquid flow dynamics. As depicted in Fig. 29, two axi-symmetric liquid lithium streams enter the toroidal chamber's top. The two streams are electrically separated there, either by an electrical

insulator or by a non-insulating structure in which some electrical dissipation is wasted via leakage. At the top, the two streams are biased to different voltages via electrodes connected to an external power supply. Poloidal current injected via these electrodes is conducted through the streams which meet and join at the bottom of the chamber. The resulting $J \times B$ electromagnetic forces push the streams against the chamber walls and thus help hold them away from the plasma. The EMR lithium blanket concept makes use of these electromagnetic forces in conjunction with the other natural forces that exist, including centrifugal (inertial) forces, contact forces, viscosity, and surface tension. The liquid's transit time from the top to the bottom of the chamber is determined by gravity, frictional losses and chamber geometry. Since centrifugal force does not act alone in producing the liquid blanket structure, slower liquid velocities may be tolerated for the bulk liquid. Optional non-axi-symmetric solid structures could be mounted on the chamber walls to slow the lithium's rate of descent via induced eddy currents.

Conducting liquids flowing through magnetic fields can generate large MHD forces opposing their motion, if a closed path exists for electric current to flow in response to the motion-induced electric field. For flow through pipes, these MHD forces can be overcome by using high pumping pressure, but for free-surface liquid blankets, which inherently have a low pressure gradient, external pumping is not effective. The use of injected electric currents provides the possibility of compensating for some of the MHD effects in free-surface systems. However, the flow described above will need to be highly axi-symmetric to avoid large drag forces from Hartmann layers forming on non-axi-symmetric structures. In addition, the flow must conform to the shape of the poloidal flux surfaces to a large degree so that surface normal field components are avoided as well.

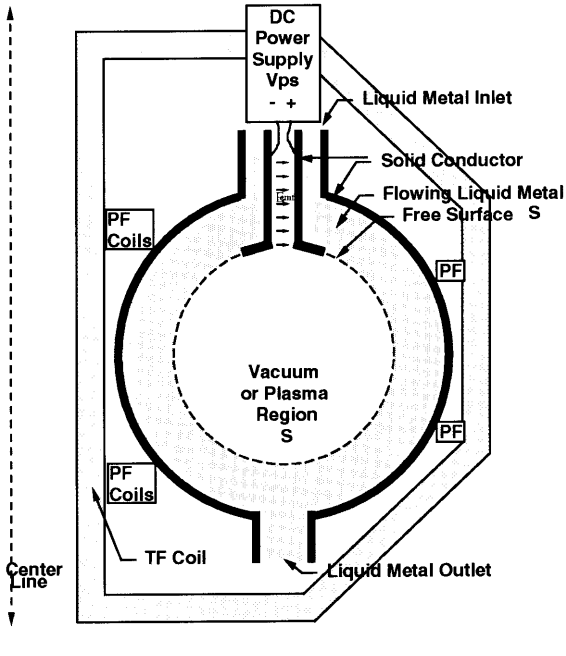

Fig. 29. Electromagnetic restraint (EMR) lithium blanket concept.

In a variation on the EMR concept, a two-pass design using hot and cold liquid sublayers may be desirable to simultaneously achieve high exit temperature of the heated lithium while keeping the maximum vapor pressure of the colder plasma-facing liquid lithium surface low. That the flow is highly laminarized by the magnetic field may be an advantage here, suppressing the mixing between the two streams and allowing them to flow directly on top of one another. Detailed analysis of this problem is being carried out in conjunction with the two-stream GMD research.

6.1. Flow phenomena with injected electric current

Significant forces can be generated in liquid lithium metal without excessive electrical power. The threshold of significance is levitation. Lithium's mass density is about half of water's, so its gravitational weight density on earth is about 5000 N/m^3. With the approximately 5 T toroidal field typical of many tokamak reactor designs, to generate a force field matching lithium's weight density requires a current density of $J = \rho g/B = 1$ kA/m^2 in the lithium, which implies an electric field of 350 $\mu V/m$ and an electric power dissipation of 0.35 W/m^3. These are modest parameters. At this 'one-gee' force-field level, a lithium EMR blanket surrounding an ITER-sized plasma would require a total current of 50 kA, implying a loop voltage of 0.01 V, and a power of 500 W. Increasing power to 1 MW would increase the lithium force field to the equivalent of 45 times gravity!

These calculations show that a relatively small current can easily overcome the effect of gravity. However, there will also be stray currents produced during operation (due to plasma motion) that could very well exceed the purposely generated currents. This fact demonstrates the importance of coupled analysis of the liquid wall and plasma MHD and the potential need for active control of the applied wall current.

6.2. Axi-symmetric LMMHD analyses

If highly conductive liquid metal were flowing in non-axi-symmetric patterns beside a tokamak plasma, MHD effects would produce non-axi-symmetric currents in the liquid. In addition to the potential to induce significant MHD drag, this could produce non-axi-symmetric magnetic fields which would perturb the plasma. Tokamaks and several other plasma confinement schemes require precisely axi-symmetric magnetic fields to maintain nested internal flux surfaces. They have very little tolerance for departures from axi-symmetry and develop 'magnetic islands' which deteriorate plasma confinement at very small levels of non-axi-symmetric magnetic field 'ripple'. A reactor blanket must therefore avoid doing harm to the plasma equilibrium, so strict axi-symmetry is an important requirement for the portions close to the plasma of a highly conductive, fast moving, liquid blanket.

Although exact three-dimensional MHD equations for an incompressible liquid are complicated, they can be simplified without any approximation for the EMR lithium blanket concept by this requirement for axi-symmetry. In deriving exact axi-symmetric LMMHD equations with independent variables (r,z,t), it is convenient to express magnetic field via the poloidal magnetic flux stream function, Ψ, and the total poloidal threading current stream function, I (including any toroidal field coil system current). Formulated in primitive hydrodynamic variables, the result is six time-dependent scalar PDEs, and an ODE-integral equation describing the effect of the power supply voltage. The full derivation of this system and associated boundary conditions are given in ref. [1].

It is important to note that boundary conditions on the surfaces of the liquid and solid metallic conductors will be required for Ψ. These time-varying boundary conditions depend on the plasma and poloidal field coil currents, which depend on the plasma scenario. For the case of no plasma or PF coil currents, the above equations are closed and are ready to be solved for specific cases. For cases including a plasma and/or PF coil current histories, additional data is needed to conduct an analysis. This magnetic coupling of the plasma/liquid wall/magnet coils set is an important feature of this formulation, and in the end will be required even for passive schemes like the GMD or CLiFF to fully described the liquid wall reaction to electromagnetic plasma events and to control field variations. It should be noted though that galvanic halo currents flowing between the plasma and the liquid conducting surface are not modeled in this system.

Although greatly simplified from the three-dimensional case, the above-described equations are not amenable to direct analytical solutions unless many approximating assumptions are made. That has not been done, but might perhaps be useful. The equations are amenable to numerical solution. No commercially available simulation code was identified capable of such a simulation, so the development of one has been undertaken. However, the code is not complete at the time of this report, so no detailed numerical studies of the EMR concept are yet available. Some important observations, though, can be made can be made directly about the equations.

- The toroidal swirl motion should remain identically zero as long as the poloidal current in the liquid metal is aligned to follow poloidal flux surfaces.
- If liquid velocity and injected current were both aligned to poloidal flux surfaces the velocity along streamlines should be unaffected by the variables magnetics (I and Ψ).

6.3. Necessary departures from axi-symmetry and key issues

It is not possible to design an entirely axi-symmetric blanket system since the flowing liquid

must cross between structural supports at some location, and in most versions of the concept need to exit and reenter the TF coil region. Analyses of these non-axi-symmetric regions will be more complex. There may be significant MHD pressure losses and pumping problems in the non-axi-symmetric regions.

The key issues with the EMR lithium blanket concept all are based on the difficulty of predicting its performance. At the present time, there are no computer tools or other methods to design such a system although several efforts have been initiated and continue this year.

7. Effects of liquid metal walls on plasma performance

The interaction of liquid walls with the plasma core is a complex topic that requires future studies. In this section, we address some potentially favorable effects of flowing liquid metal walls on tokamak plasma performance and reactor attractiveness.

Liquid metal walls have been considered in tokamaks primarily for heat flux and radiation protection, and to modify particle recycling. In addition, it is clear a priori that liquid metal walls could in principle act as a close fitting conducting shell, but the advantages of this have not been examined. Here, we describe how this can lead to higher plasma β values and improved confinement.

The stabilizing effects of the liquid metal can be either passive (merely due to the presence of a nearby conductor), or active (due to the flow of the liquid metal). The passive effects are significant because liquid metals such as lithium can be closer to a reactor plasma, as well as thicker, and thus more stabilizing. The active effects are important because they can prevent flux penetration in steady state, preventing resistive wall modes by naturally converting liquid metal kinetic energy into magnetic flux to compensate for resistive losses. It is widely recognized that resistive wall modes strongly limit performance in advanced tokamak operation, and also seriously affect reversed field pinches (RFPs) and other toroidal confinement devices. We consider both passive and active effects here.

7.1. Passive stabilization by LM walls

In reactor studies such as ARIES-RS [14], passive stabilizing conductors are placed behind the blanket. These conductors must maintain a toroidally continuous conduction path to stabilize the vertical instability. They are placed behind the blanket because structural metals compatible with the fusion environment are poor conductors, and a thickness to provide substantial conductivity would negatively affect tritium breeding if placed in front of the blanket. Also, the degradation of the conductivity of such metals due to radiation damage is a problem. In particular, radiation degradation of joints and welds may jeopardize the required toroidal continuity. The removal of the stabilizing plates by this significant distance from the plasma, substantially reduces their stabilizing effect, limiting tokamak reactor designs to an elongation κ of approximately two or less. It is well known that the maximum plasma current is a strong function of elongation, and thus, so is the attainable MHD β as well as the confinement predicted by scaling laws.

In contrast, molten lithium metal can be placed close to the plasma since it does not degrade breeding (in fact it improves it). Furthermore, the conductivity of a liquid is unaffected by the radiation environment. Liquid plasma facing designs considered by APEX have lithium much closer to the plasma. Alternatively, a liquid lithium vessel could be placed just behind a solid first wall (maintaining a toroidally continuous conduction path). Below we consider the effects of this on κ and thus on β.

An $n=0$ vertical resistive stability code has been written. It solves the perturbed Grad–Shafranov equation $\Delta*\Delta\Psi = (FF')'\Delta\Psi$ as an initial value code including inductive fields and resistive elements. The elliptic operator is inverted with vacuum boundary conditions, and includes the effects of external resistive coils, a resistive wall, and active feedback coils with voltages determined from the signals of sensor coils. Presently pressure is not included in the equi-

librium, and the toroidal current profile *FF'* is taken to be a constant. The voluminous literature on vertical stability [18] shows that plasma pressure is not a major effect (and is usually stabilizing), and hollow current profiles (as expected with high bootstrap fraction operation) are expected to be more stable than a flat current profile. Thus, the results below are more pessimistic (and thus conservative) than expected from more realistic profiles.

As examples, we consider the vertical stability of a $\kappa = 3$ plasma with aspect ratio $A = 3$ and 4, with 4 cm of lithium (a typical number for thin liquid plasma facing concepts), and the liquid at a distance $b/a = 1.2$ (i.e. a distance from the plasma of 20% of the horizontal minor radius, or about 30 cm for ARIES-RS). Liquid facing concepts usually have liquid closer than this, and would be more stabilizing. The resistive wall time is roughly 0.5 s, and the resistive vertical instability growth time is about 0.66 s. This time scale is easily within the reach of existing vertical feedback technology (which can have response times of the order of a millisecond, or slightly less). With a standard feedback geometry with the active coil above the plasma a distance which would place it behind a 1 m shield, and a sensor coil on the outboard side (though a distance which would place it inside the shield but behind the first wall), vertical stability is achieved with feedback gain about an order of magnitude larger than in the case $\kappa = 2$, and with feedback response times $\leqslant 50$ ms. This appears to be within the range of present technology. Little effort has been spent optimizing the parameters of the feedback system, and considerable improvement might be possible.

We find the consequences of this to the attainable β in advanced technology (AT) modes are large. The MHD equilibrium code TOQ [19] (used routinely by the general atomics (GA) $\sim$ MHD group) has been used, to obtain high bootstrap fraction equilibria for $A = 3$ and 4. Broad pressure profiles are used which have been used by the GA group in β optimization studies for $A = 1.4$ tokamaks. The maximum β for ballooning stability for $A = 4$ and 3 is:

$\kappa = 2$	$\beta = 5$–7%	$\beta_N = 4.5$	$S = 7.3$
$\kappa = 3$	$\beta = 20$–22%	$\beta_N = 5.7$	$S = 13.9$

As can be seen, the stable β is increased by about a factor of 3. Note β_N does not increase much, so the increased β is mainly due to increased current. The β and β_N values for $\kappa = 2$ are quite similar to those found in the ARIES-RS study ($\kappa = 1.9$, $\beta_{max} = 5.4\%$, $\beta_{N,max} = 4.8$). We do not have capabilities to examine $n = 1$ stability, so we estimate stability based on the shape factor $S = (1/aB)q_{edge}$. With wall stabilization, the maximum stable β_N is an increasing function of S and profile flatness $p(0)/\langle p \rangle$. If we extrapolate published results by Turnbull et al. [20], we infer that the much higher shape factor for $\kappa = 3$ should enable $n = 1$ stability for the modestly higher β_N value.

This has large consequences for a reactor. For a 1 GW reactor with 1 m of inboard blanket/shield and 13 T superconductors (and the same β as ARIES-RS for $\kappa = 2$):

κ	β	Major R	MW/m^2	ρ^*	H-factor (ITER89P)
1.9	4.8%	5.5	4	1/500	1.8
3	18%	3.15	9.5	1/180	1.6

As can be seen, there is a large reduction in size and therefore mass and cost. For example, the length of superconducting wire needed is reduced by about a factor of 2.5. The wall loading is in the range considered as the nominal case for APEX design evaluations of advanced wall concepts (8 MW/m^2).

Note that the ρ^* of the $\kappa = 3$ reactor is the same as JET and JT-60. Thus, this reactor is not an extrapolation in ρ^*, but rather in geometry. Since geometry is not a fundamental physics variable, we expect that extrapolations in κ from existing machines can be made with much less uncertainty than extrapolations in ρ^*.

7.2. Active stabilization of resistive wall modes

We now consider the effects of a flowing wall on the $n = 1$ resistive wall instability. We employ a self-consistent limit of the MHD equations to obtain an analytically solvable model of the β driven external kink mode. The model uses high A, reduced MHD, simplified with flat current and pressure profiles and circular plasma cross-section. We note that independently, a similar model was investigated by Betti et al. with similar results.

We obtain a β driven kink mode, which requires coupling between adjacent poloidal mode numbers m for instability. The mode can be stabilized with an ideal (perfecting conducting) wall. Finite resistivity and rotation are added numerically, using the analytic plasma response. As expected, with no rotation there is a resistive wall mode with $\gamma_{\mathrm{RWM}} \sim$ the resistive wall time. For a poloidally rotating wall (which adds a current $\eta\delta j = \mathrm{v}_0 \times \delta\ B = \mathrm{v}_0\ \delta\ B_{\mathrm{r}}$ in addition to the inductively driven current), we find stabilization when the poloidal transit time for the flow to go from the top to the bottom $1/\tau_{\mathrm{p}} = \mathrm{v}_0/\pi\ r$ is fast enough that:

$$\frac{1}{\tau_{\mathrm{p}}} \geq \gamma_{\mathrm{RWM}}.$$

This result has also been found independently by Betti. Here, we note that for 4 cm Li, this corresponds to velocity levels considered by the APEX design for liquid metal walls. Note that it is not necessary for the flow to be facing the plasma, but rather the flow could be in a cavity behind a solid first wall (but close to the plasma).

This stabilization can be interpreted as an inability of the $n = 1$ flux to penetrate if the metal flows from the top to the bottom more rapidly than the growth rate, since then the metal is always being replaced by fresh metal. Alternatively, the result can be interpreted as the dephasing of a toroidal instability which requires a particular phase relationship between different poloidal harmonics. Since each m number is Doppler shifted by a different amount, there is not rotating frame where the relative phases needed for instability can be maintained.

Note that stability requires that the conducting wall be placed somewhat closer for stability than is the case for a perfectly conducting wall. This is due to the fact that the mode can rotate with a frequency to remove wall stabilization for a single poloidal harmonic. Since only two of the three harmonics are wall stabilized, the stabilization is not as effective. However, in more realistic shaped equilibria, there is a much broader spectrum of m numbers required in the eigenfunction than in this circular model. Since only one among the large number of harmonics can escape wall stabilization, we anticipate that shaped equilibria will have rotational stabilization effectiveness more nearly equivalent to that of a perfectly conducting wall.

Stabilization of resistive wall modes would lead to several benefits. Higher β steady state equilibria could be obtained, with very hollow current profiles. Steady state operation with such profiles enables high bootstrap fractions and thus low recirculating power. Also, hollow current profiles are theoretically predicted to give $E \times B$ shearing rates larger than instability growth rates for conventional drift instabilities, leading to transport barriers and high confinement. Hollow current profiles are well correlated experimentally with such good confinement. Thus, flowing liquid walls may enable the conditions needed for high steady state confinement.

We note that the codes used to obtain the above results are being developed further to handle arbitrary equilibria output from an equilibrium MHD code. We also note that flowing liquid metals can behave differently under perturbations since they can be pushed out of the way. Analysis indicates that liquids flowing at the speeds indicated above are not greatly affected by this (though a stationary liquid would be), but inclusion of this effect is also in progress. This last point especially indicates that there is a synergism between both liquid metal walls and tokamak physics performance, both in β and confinement, as well as in the analysis of dynamics of plasma discharges and flowing wall behavior.

We recommend that this synergism be pursued vigorously through cooperation between the fusion physics and the fusion engineering communities.

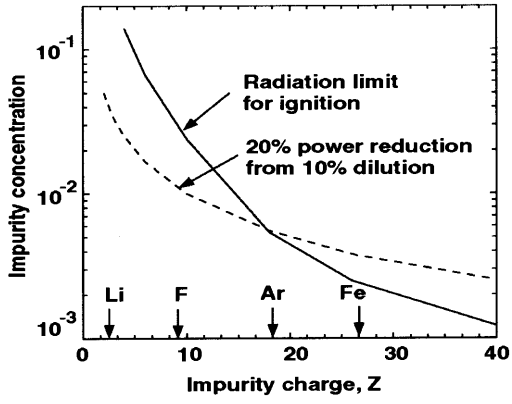

Fig. 30. Impurity concentration limits for different impurities due to radiation loss in a tokamak (solid line) and due to simple fuel dilution (dashed line).

8. Plasma–liquid surface interactions and edge modeling

The thin layer of edge plasma provides the interface between the hot-plasma core and the liquid first-walls and divertor plates. The edge-plasma properties must be accurately determined to predict the coupling between the core plasma and the wall, and the edge-plasma itself is affected by both the core plasma and the wall. Liquid surfaces can impact the edge and core plasmas by releasing impurities through sputtering, recycling, and evaporation. Such impurities degrade fusion core performance through enhanced radiation loss and fuel dilution. The tolerable levels of core impurity concentration owing to radiative energy loss [21] and to fuel dilution are shown in Fig. 30 for a tokamak. Changes in the edge plasma temperature and gradient scale-lengths can also affect the stability of the core-edge plasma, e.g. the L-H transitions, ELMs, and possibly disruptions.

The edge plasma, in turn, influences the liquid surfaces through particle bombardment and line radiation from excited ions. The bombardment leads to sputtering and recycling, and both bombardment and radiation heat the surface resulting in increased evaporation. The maximum tolerable evaporation rate determines the maximum allowable surface temperature of the liquid, and the sputtering analysis determines the required edge-plasma.

A multi-faceted, self-consistent model is required to make a complete evaluation of the interactions between the edge-plasma and the liquid walls. We have made substantial progress in developing components of this general model and in using these components for initial evaluation of some of the critical issues. The progress is summarized below and presented in more detail in Ref. [1] for the following areas: two-dimensional fluid transport simulations of properties of the hydrogenic edge plasma; two-dimensional fluid transport simulations of impurity penetration to the core region arising from evaporating Flibe and Li-based walls; one-and-a-half-dimensional kinetic and two-dimensional fluid transport calculations of evaporated and sputtered impurities from liquid divertor plates; two-dimensional simulations of intense power deposition to a lithium divertor plate during a disruption; one-and-a-half-dimensional plasma core transport modeling, beginning simulations of the behavior of small liquid samples in the PISCES plasma divertor simulator and the DIII-D tokamak.

8.1. Edge fluid transport simulations

We have used the two-dimensional UEDGE code [22] to obtain profiles of hydrogen ion density, parallel ion velocity, and separate ion and electron temperatures. The base-case is an ITER-like tokamak where the transport simulation sets boundary conditions of power and density a small distance inside the magnetic separatrix and calculates the resulting scrape-off layer (SOL) profiles. We have characterized two-dimensional plasmas profiles for both high-recycling regimes (Flibe or other non-recycling divertor) and low-recycling (lithium divertor which retains incident hydrogen). The low-recycling case results in high electron temperature at the divertor and low density, with the opposite being true for high recycling. An important consideration for the low-recycling case is the large particle flux out of the core that must be maintained by an edge particle-fueling source such as pellets.

To assess the effectiveness of the edge plasma for shielding the core from impurities, the UEDGE calculations are extended to include im-

purity gas evaporating from the liquid wall. A number of processes are included in this modeling. The impurity gas is emitted from the wall in the form of atoms at typically 1 eV, although a range of energies have been used to assess the energy of the atoms after molecular dissociation which is not yet modeled in any detail. These neutrals diffuse by elastic collisions with ions until they are ionized by the electrons of the edge plasma. Once an ion, the impurity diffuses across the magnetic field with anomalous diffusion coefficients estimated from present experimental devices. Thus, the ions can diffuse radially into the core or back to the liquid wall where they are assumed to be absorbed. In addition, the ions can flow along the magnetic field and out of the system. The electron energy lost by ionizing the impurities through all of their charge states is included, so that the impinging impurities decrease the electron temperature, especially near the liquid surface. A typical set of charge-state profiles from fluorine from a Flibe wall are shown in Fig. 31.

Similar calculations have begun for Sn–Li walls where only Li is evolved from the surface; it is assumed that evaporation of Sn is negligible. Lithium penetrates less easily to the core due, in part, to its lower first-ionization potential of 5.4 V

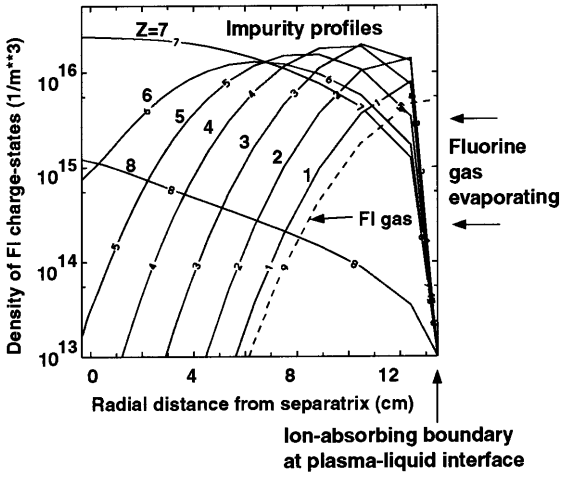

Fig. 31. Density of fluorine charge-states at the outer midplane for a gas wall flux of 8×10^{18} $m^{-2}s^{-1}$ in the standard tokamak geometry.

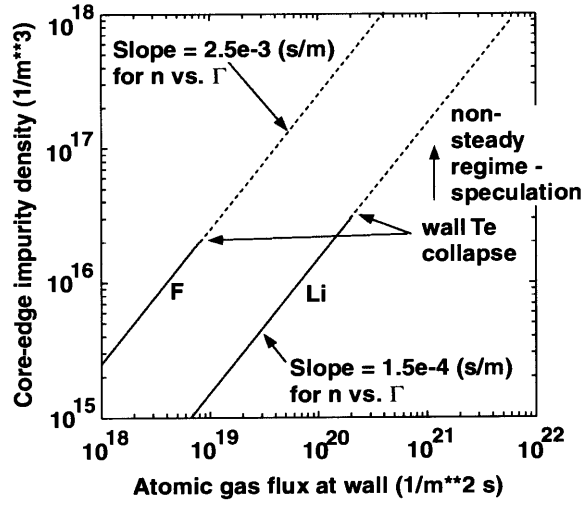

Fig. 32. Comparison of fluorine and lithium densities at the core boundary for different gas fluxes at the first wall. The dotted lines are extrapolations owing to non-steady solutions which arise with a collapse of the electron temperature just in front of the wall for larger gas fluxes.

compared to 17.3 V for fluorine from Flibe. Secondly, if one considers a Sn–Li, its evaporation rate is less than that of Flibe at a given temperature.

The comparison between the fluorine (Flibe) cases and the lithium (Li, Sn–Li) cases with respect to impurity concentration is shown in Fig. 32. This figure quantifies what core impurity core density should be expected for a given gas flux, which can be determined from known data of the evaporation rate at a given liquid surface temperature.

From Figs. 30 and 32, one can deduce that for an ITER-like tokamak with 150 MW of plasma power flowing into the scrape-off layer, impurity penetration to the core may be kept to an acceptable level if the liquid surface temperature for Flibe is 540°C or less, while for Sn–Li it is 740°C or less. However, these results are quite preliminary with one of the most important uncertainties being the fact that the transport simulations have not yet found steady state solutions at the larger gas flux regions of Fig. 32 shown by the dotted lines. These dotted line portions of the curves are just those being used to make the estimates of the maximum surface temperature quoted above.

Thus the highest priority of our present research is to better resolve and understand the non-steady solutions. Such solutions correspond to where the electron temperature near the surface abruptly drops below a few eV owing to impurity radiation and particle energy losses to the wall. This is a 'detached' type of plasma, but here the detachment is from the side wall rather than the divertor plate.

The calculations for impurity influx from side walls have been mostly performed in a tokamak geometry. More simulations are needed for alternate confinement geometries such as the field-reversed configuration (FRC), spheromak, spherical torus, and others.

8.2. Kinetic simulations of the sheath and presheath

Kinetic simulations are performed for the region near liquid divertor plates using the test-particle codes BPHI and WBC codes [23] with Monte Carlo collisions. BPHI focuses on the sheath region, including ionization within the sheath, whereas WBC uses a reduced sheath model and includes the presheath region ~ 10 cm in front the plate. Both codes begin with a hydrogen plasma from a two-dimensional fluid transport code, but then trace sputtered and evaporated impurities from the plates made of Flibe or lithium until they escape upstream or are redeposited on the plates.

For the WBC code lithium analysis, the following is observed: (1) very high near-surface lithium redeposition rate ($\sim 100\%$), (2) high redeposited average energy with highly oblique Li ion impingement. Result (1) is favorable showing low potential for plasma contamination by sputtered lithium, even for the low-collisionality, low-recycle regime. Result (2) gives rise to concerns about runaway self-sputtering although preliminary estimates using initial ALPS/APEX project data show that this will probably not occur.

WBC calculations for Flibe assessed the near-surface transport of the individual sputtered Flibe constituents of F, Li, and Be. As with the lithium surface calculations, a highly preliminary sputtering model was used. Results using a hydrogen plasma in the high-recycle regime ($T_e = 30$ eV, $n_e = 3 \times 10^{20}$ m^{-3}) show a high redeposition fraction for each element. There is a lower potential for self-sputtering runaway due to lower redeposition energies and less oblique incidence.

BPHI sheath code calculations were performed for a low-recycle plasma divertor regime with a lithium surface. Preliminary results, for one particular low-recycle regime, show that a majority of slow-moving, evaporated lithium atoms will be ionized in the sheath and will be returned to the surface due to strong sheath electric field. On the other hand, the sheath heat transmission factor will increase due to reduced sheath potential resulting from the extra electrons and ions produced by in-sheath ionization. The resulting increase in heat flux is of concern in terms of a runaway effect but this may be mitigated by the transient nature of the overheating and the fact that the lithium is flowing.

8.3. Additional on-going edge plasma simulation work

A self-consistent sputtering erosion/redeposition analysis of a lithium divertor surface is planned, using coupled UEDGE/WBC/VFTRIM (plasma SOL fluid code/Monte Carlo kinetic impurity code/vectorized fractal-TRIM sputtering code) codes. This will better compute plasma contamination potential, tritium codeposition, and self-sputtering runaway potential.

Another important question is the response of a liquid divertor plate to a tokamak disruption. A number of physical processes have been included in the HEIGHTS package [24] and simulations performed for a liquid lithium plate. The incoming power to the plate is taken as 100 GW/m^2 which is typical of what would be expected in a reactor-sized tokamak. As this high particle energy strikes the plate, material is ablated in the form of a gas vapor, which is subsequently ionized by the incoming electrons. The energy required for ionization of the vapor can decrease the incoming energy to the plate by an order of magnitude to less than 10 GW/m^2 while this partially ionized vapor cloud becomes optically thick. An additional reduction of the power to the

plate comes from the splashing of plate material into droplets due to Kelvin–Helmholtz or Rayleigh–Taylor instabilities in the vapor. The power loss in vaporizing these droplets can result in another factor of 5 reduction in power reaching the plate. The mass loss of the liquid lithium plate can likewise be reduced by about two orders of magnitude from the combined shielding of the vapor and the splash droplets. As a result, the effect of a disruption on the lithium plate is not thought to be limiting. Further assessment is needed to determine how the incoming disruption power, which is initially absorbed by the vapor and droplets but then re-radiated, affects nearby structures. Also, the vapor and splashing that result from the disruption will migrate to other surfaces in the machine. If all surfaces are moving liquids, they will self-clean; and using the same liquid for the plate and the walls will eliminate the problem altogether.

The impact of different edge-plasma conditions on the performance of the fusion core plasma is being studied with the one-and-a-half-dimensional core transport code ONETWO [25] which has been used extensively for analyzing DIII-D experimental results. As an initial case, an ITER-like tokamak is being considered with a 20 keV operating point since a lot of previous analysis has been done on this configuration which provides a good simulation benchmark. The effect of the low-recycling edge conditions using lithium plates will be contrasted with the normal high-recycling edge (which would likely arise if Flibe were used). Given this background, a similar analysis will be performed for the ARIES-RS design.

Finally, it is important to benchmark models predicting how liquid surfaces emit impurities in the presence of plasma discharges, and how the impurities transport in the plasma. At present, small samples of lithium and gallium have been used in the linear plasma device PISCES, and lithium has just been used on the DiMES probe for the DIII-D tokamak. Sputtering data is also available from particle beam measures on the University of Illinois experiment. The sputtering data from these various experiments are being tabulated and will be used as input for the fluid and Monte Carlo codes which follow the subsequent ionization and transport of the impurity ions. A challenge to impurity transport modeling for the DiMES probe is that the probe is localized to one toroidal location, so three-dimensional effects do enter which can only be estimated by the present codes. Nevertheless, these calculations begin the vital process of comparing modeling results with experimental data. Larger-scale liquid samples in experiments will improve this benchmarking. There is on-going work to use liquid divertor surfaces in other devices such as CDX-U. This type of activity is important to provide the experimental data base to validate models predicting the influence of such walls in fusion-related devices.

9. High-temperature solid wall with lithium evaporation (EVOLVE)

This section discusses a novel method to extend the capabilities of a solid wall by using a high-temperature refractory alloy with heat extraction achieved by lithium evaporation.

The desire to achieve both high power density and high power conversion efficiency leads to several required features of a first wall and blanket concept. Achieving high power density means that the coolant heat removal capability must be high and the first wall material should have attractive thermophysical properties (high thermal conductivity, low thermal expansion, etc.). Achieving high power conversion efficiency means that the first wall and blanket should operate at very high temperatures. Materials operating at very high temperatures generally have limited strength and, therefore, such a concept should operate at low primary stresses. This means that the coolant pressure should be as low as possible, and the temperatures throughout the blanket should be as uniform as possible to reduce thermal stresses.

One system that has this potential is the EVOLVE (evaporation of lithium and vapor extraction) concept. The key feature of the EVOLVE concept is the use of the heat of vaporization of lithium (about ten times higher than water) as the primary means for capturing and

removing the fusion power. A reasonable range of boiling temperatures of this alkali metal is 1200–1400°C, corresponding with a saturation pressure of 0.035–0.2 MPa. Calculations indicate that an evaporative system with Li at ~ 1200°C can remove a first wall surface heat flux of > 2 MW/m^2 with an accompanying neutron wall load of > 10 MW/m^2. The system has the following characteristics:

1. The high operating temperature translates naturally to a high power conversion efficiency.
2. The choices for structural materials are limited to high temperature refractory alloys. A tungsten alloy, e.g. W–5%Re, is the primary candidate as a structural material, with tantalum alloys as the back-up.
3. The vapor operating pressure is very low (subatmospheric), resulting in a very low primary stress in the structure.
4. The temperature variation throughout the first wall and blanket is low, resulting in low structural distortion and thermal stresses.
5. The lithium flow rate is approximately a factor of ten slower than that required for self-cooled first wall and blanket. The low velocity means that an insulator coating is not required to avoid an excessive MHD pressure drop.

The areas addressed are first wall and blanket design, tritium breeding, activation and waste, power conversion, first wall thermo-mechanical behavior, tritium extraction, and critical issues. The key features of the design are summarized in Table 11.

Table 11
Key features of the EVOLVE concept

Feature	Value
Heat capture and removal	Li vapor
Li vapor pressure	0.035 MPa
Li vapor velocity	~ 500 m/s
Structural material	Tungsten
Operating temperature	~ 1200°C
First wall heat flux	2 MW/m^2
Neutron wall load	10 MW/m^2
Tritium breeding ratio (local two-dimensional)	1.37
Power conversion efficiency	$\sim 57\%$

The cross-section design of the EVOLVE concept is illustrated in Fig. 33. In the EVOLVE concept, the first wall and primary breeding zone are combined into one unit. Behind this unit, there is as a separate component, a high temperature shield at the inboard region and a secondary breeding blanket at the outboard region. Behind the secondary breeding zone there is, as a separate component, an additional high temperature shield, required in order to meet the shielding requirements of vacuum vessel and magnets.

The first wall consists of a tube bank arranged in the toroidal direction as shown in Fig. 34. Within each tube is another tube that supplies the liquid lithium to the first wall. There are two different methods under consideration for the distribution of the liquid metal at the surface. One of them employs a large number of jets generated by nozzles in the supply tube by which the LM is distributed to the backside of the first wall. With the other one, capillary forces in a wick structure, arranged at the backside of the first wall, are employed to transport the liquid lithium from the supply tube to the entire surface of the first wall tube. This wick is connected to the supply tube via longitudinal slots in this supply tube. For a surface heat flux of 2 MW/m^2, a toroidal segment width of 3 m, and the tube dimensions given above, a boiling temperature of 1200°C (saturation pressure 0.035 MPa) results in a liquid metal velocity in the feed tube of about 1 m/s and a vapor velocity of about 500 m/s. This is about one-third of the sonic velocity and results in a tolerable pressure drop.

The blanket consists of a number of trays, stacked poloidally, containing liquid lithium. A space is left between trays to allow the Li vapor to be removed from the blanket. Each tray contains a lithium pool with a height of 10–20 cm, which is maintained constant by a system of overflow tubes. The large volume heating of the lithium leads to boiling. The vapor bubbles have to rise in the pool and separate from the liquid metal at the surface. From here the vapor flows a short distance in parallel to the surface before it enters the vertical vapor manifold. Entrained liquid metal will be separated there. Behind the trays is a manifold, approx. 20 cm thick, for collecting the

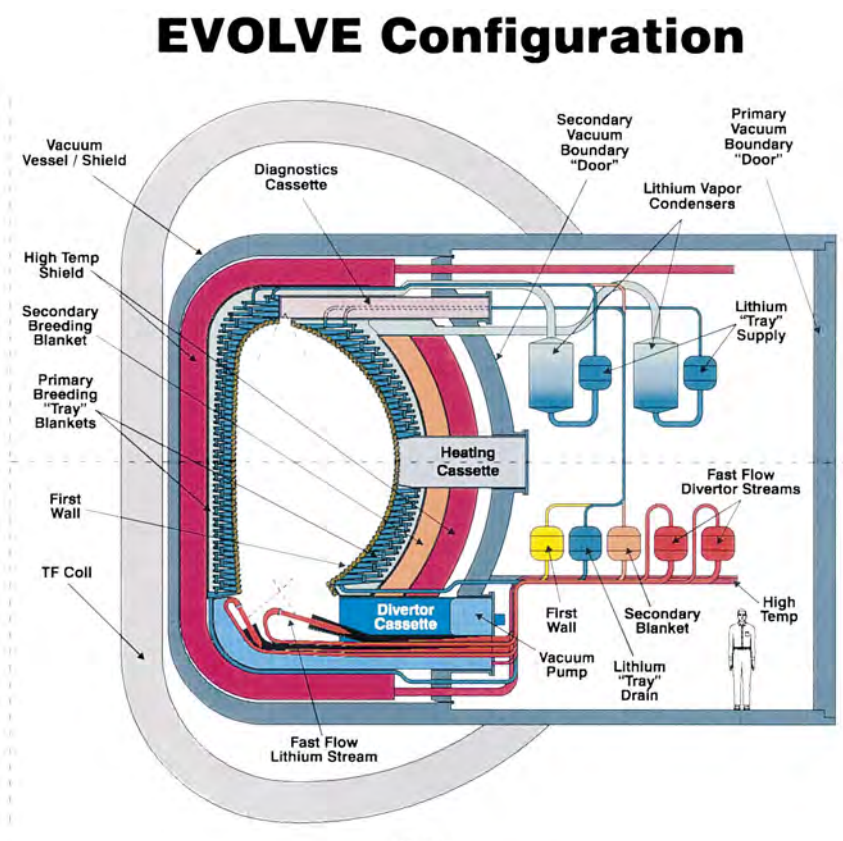

Fig. 33

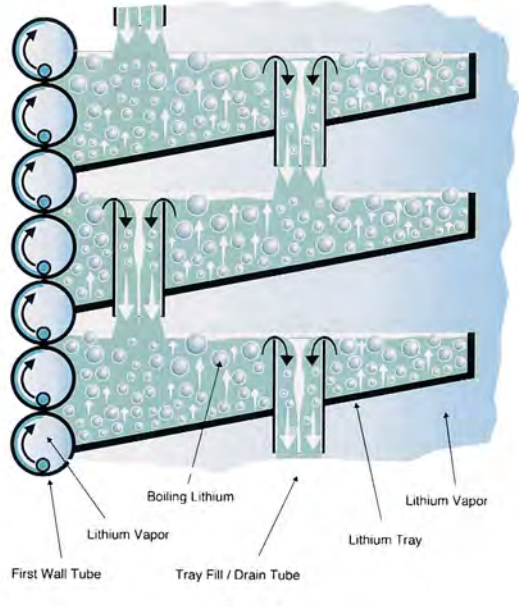

Fig. 34

Fig. 33. Cross-sectional view of the EVOLVE first wall/blanket concept.
Fig. 34. Schematic of EVOLVE first wall tubes and blanket trays containing Li.

Li vapor. The total radial thickness of the first wall and blanket is approx. 70 cm.

Two-dimensional neutronics modeling of the front evaporation cooled blanket of EVOLVE is needed to properly account for the poloidal heterogeniety and gaps between trays. The R–Z geometrical two-dimensional model used in the calculation includes the FW, trays with Li vapor manifold, secondary breeding blanket, shield, VV, and magnet in both the IB and OB regions. Both the IB and OB regions are modeled simultaneously to account for the toroidal effects. The TWODANT module of the DANTSYS 3.0 discrete ordinates particle transport code system was utilized. The overall TBR calculated for the reference design using the two-dimensional model is 1.37. It is based on the conservative assumption of no breeding in the divertor region. Tritium breeding (69.8%) occurs in the trays (57.3% OB and 12.5% IB). The OB secondary blanket contributes 27.7% of the total overall TBR (20.2% behind trays and 7.5% between trays). The contribution of the shield is only 2.5% (1% OB and 1.5% IB). Tritium breeding has a comfortable margin that allows for design flexibility.

There are two coolant streams exiting from the blanket. The front part of the blanket, including the first wall and the primary breeding zone, is cooled by boiling lithium, which carries approximately two-thirds of the total thermal power. The back part of the blanket, composed of secondary breeding zone and the high temperature (HT) shield at the outboard zone and the HT shield at the inboard zone, is a conventional self-cooled liquid lithium blanket with an exit temperature of also 1200°C, which carries the other one-third of the thermal power. The two blanket coolant streams will be fed to two heat exchangers to transfer the thermal energy to a helium loop. The reason that He is used for the secondary coolant is that a closed cycle gas turbine can be used for very efficient power conversion. The two lithium streams exit from the blanket operates in series, with the liquid lithium stream to heat up the secondary He from 700 to 800°C, while the high temperature lithium vapor super heat the same He stream from 800 to 1000°C. The He at 1000°C will enter a He turbine for power conversion. With a very high He temperature, and very high recuperator, compressor and turbine efficiencies, a very high cycle efficiency of 57.7% is calculated. This thermal efficiency includes the pumping power of the secondary He stream, but does not include the pumping power of either of the lithium streams, which is very small in any case.

Finite element thermal and stress analyses have been performed for the first wall subjected to surface heat fluxes of 1.5 and 2 MW/m^2, a coolant temperature of 1200°C, and a coolant pressure of 0.05 MPa. A single tungsten tube of radius 2 cm and wall thickness of 3 mm deforming under generalized plane strain condition is considered. The primary membrane stress in the EVOLVE first wall is so low (<1 MPa) that neither low-temperature nor high-temperature ratcheting should be a limiting criterion for the surface heat flux. The peak surface heat flux will be controlled either by creep-fatigue (which is not considered here) or possibly by brittle fracture (due to helium-embrittlement). The temperature distribution for a peak surface heat flux of 2 MW/m^2 and a heat transfer coefficient of 40 000 W/m^2/°C shows a peak temperature of 1317°C. The peak stress intensity is 158 MPa, which easily satisfies the ratcheting limits. Very little ductility is needed to maintain the allowable stress limit at a high value. For example, if the uniform elongation remains higher than 2% or the reduction in area at failure is >1%, then the allowable stress is >300 MPa. A stress of 150 MPa would be allowable even for completely embrittled tungsten at 1200°C.

The EVOLVE concept is at an early stage of evaluation. At this stage, it is important to assess the potential of the concept, identify crucial issues, and to define needed R&D work to resolve those issues. The critical issues to be addressed in the near future are:

1. Will the backside of the first wall remain wetted under all conditions?
2. Will the vapor generated in the stagnant boiling pools of the primary breeding region separate fast enough from the liquid metal?
3. Will the liquid metal overflow system work and lead to equal liquid metal pressure in each tray?

4. Is it possible to fabricate entire blanket segments of tungsten or tungsten- alloys in spite of their low ductility and their limited weldability?
5. How will the structural material behave under intense neutron irradiation?
6. Will the high after heat in tungsten cause a safety problem in case of a LOCA?

10. High-temperature solid wall with helium cooling

This section explores extending the capabilities of a solid wall using high temperature refractory alloy cooled with high-pressure helium. A primary motivation is to explore the possibility of using a high-temperature helium for high-efficiency energy conversion in a gas turbine cycle.

10.1. Material selection and compatibility

The material selection and compatibility issues are discussed in Section 12. Pure tungsten or tungsten alloyed with $\sim 5\%$ Re (to improve fabricability) appear to be suitable candidates. The unirradiated mechanical properties of tungsten are strongly dependent on thermomechanical processing conditions. The best tensile and fracture toughness properties are obtained in stress-relieved material. In order to be conservative, since data are not available on the possibility of radiation-enhanced recrystallization of W, and also to account for the presence of welds in the structure, the preliminary design is based on recrystallized mechanical properties. There are no known mechanical properties data on tungsten or tungsten alloys at irradiation and test temperatures above ~ 800°C. There are no known fracture toughness or Charpy impact data on tungsten irradiated at any temperature. Pronounced radiation hardening is observed in W and W–Re alloys irradiated at temperatures of 300–500°C to doses of ~ 1–2 dpa, which produces significant embrittlement in tensile tested specimens ($\sim 0\%$ total elongation). Simple scaling from existing data on irradiated Mo alloys suggests that the operating temperature for W should be maintained above ~ 800–900°C in order to avoid a significant increase in the ductile-to-brittle transition temperature (DBTT). The upper operating temperature limit for tungsten will be determined by thermal creep, helium embrittlement, or oxide formation issues. The thermal creep of W becomes significant at temperatures above ~ 1400°C. Helium embrittlement data are not available for tungsten; however, based on results obtained on other alloys, helium embrittlement would be expected to become significant at temperatures above ~ 1600°C (~ 0.5 melting temperature, T_M). The formation of volatile oxides is another potential problem in tungsten at temperatures above ~ 800°C especially during an air ingress event. However, if the oxygen partial pressure in the helium coolant can be maintained at or below 1 appm, then the rate of corrosion is calculated to be less than 2 μm/year for temperatures up to ~ 1400°C. In summary, the selected upper temperature limit for tungsten in the structure of the preliminary design He-cooled system is 1400°C depending on the applied stress.

10.2. He coolant impurity control

Refractory metals like W, Mo, and V are sensitive to grain boundary oxidation and embrittlement. However, if the oxygen (including H_2O, CO_2, CO, … etc.) partial pressure in the helium coolant can be maintained at or below 1 appm, then the rate of corrosion may be acceptable. With the use of Brayton cycle as the power conversion system (PCS), without the need of using high temperature water as the secondary coolant, the ingress of oxygen impurities should be much lower than the system that uses a high-temperature intermediate heat exchanger. For impurity extraction, several powder metal solid getters have been developed. Most are based on zirconium metal (ZrAl, ZrVFe, … etc.). With these materials, hydrogen can be pumped reversibly by temperature control. These solid getters will pump active gases (oxygen, oxides, N, and C_xH_y) irreversibly and have been used on the tokamak experiment TFTR. In the semi-conductor industry, getters have recently achieved the control of impurities to a level lower than 1 appb. These are

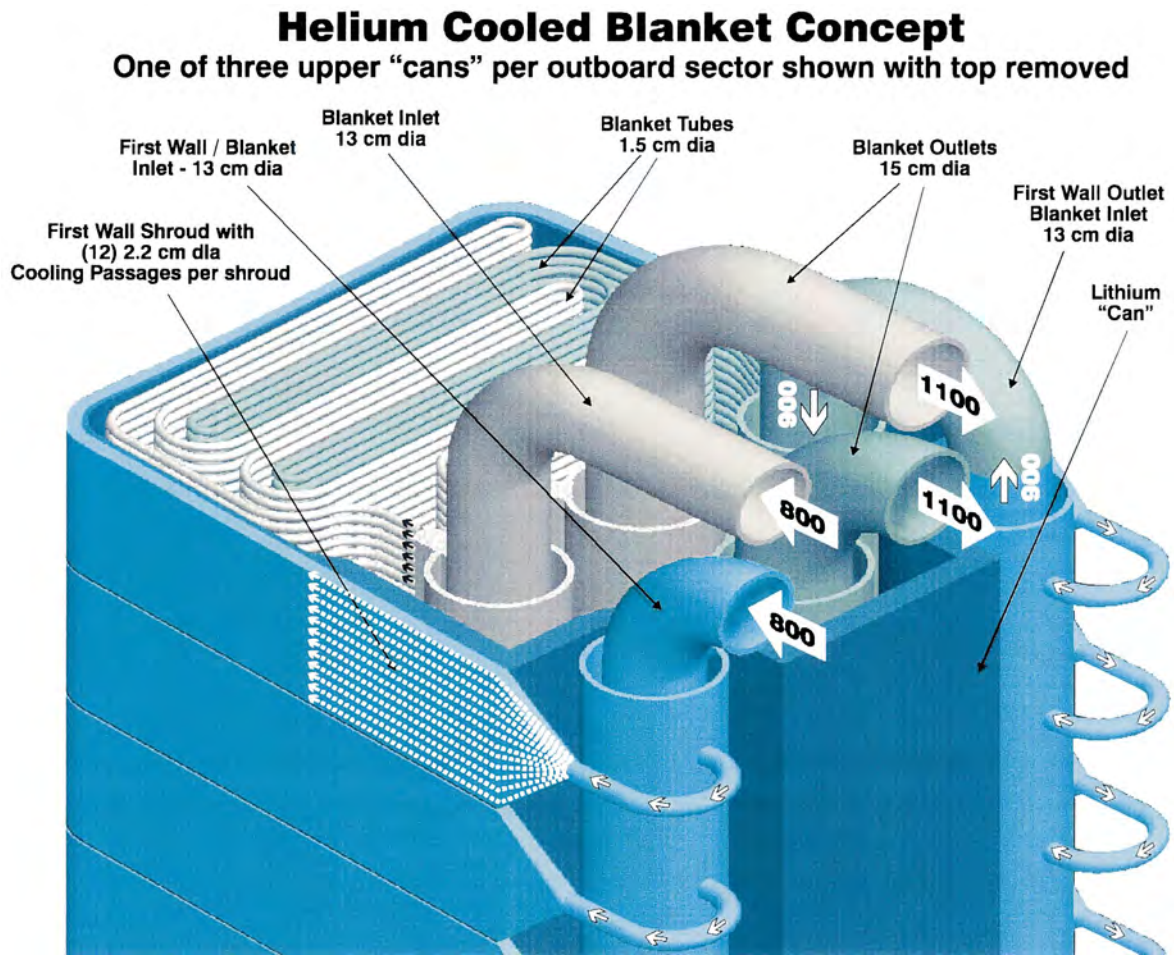

Fig. 35. Helium-cooled first wall and divertor design module.

commercial modular units with no moving parts and are self-monitoring in design.

10.3. Mechanical design and reliability

Several first wall and blanket system configurations were evaluated. The mechanical design is shown in Fig. 35. The helium-cooled refractory alloy design includes a high temperature helium-cooled first wall and a lithium bath that is also cooled with high temperature helium.

The first wall is made up of separate units which, in this case, are connected to separate cooling manifolds at the back of each module. The first wall units consist of multiple parallel passages connected through an integral manifold to round inlet and outlet connections. The large modules contain the lithium in a single volume, with pure lithium in the breeding zone and a combination of lithium and steel balls in the shielding zone. The temperature is relatively uniform, although there will be some gradients, albeit transient, between the front and back structural walls. There are two inboard and three outboard modules to each of the 16 sectors arranged in the toroidal direction. The piping is routed in two circuits. The first circuit includes the first wall and part of the interior heat exchange tubing. Helium at 800°C enters the first wall through the supply manifold and exits into the first wall outlet mani-

fold at 950°C. The helium is then routed inside the lithium can to the first supply manifold for the heat exchange tubes. The first tube circuit exits into a return manifold at 1100°C. The second tube circuit is fed at 800°C and exits at 1100°C.

One of the primary goals of the APEX study is to increase the availability of fusion reactors by increasing the mean time between failures and by decreasing the mean time to repair. To this end, we recommended the approach of sector maintenance, modular maintenance for everything and pretested modules for all components.

10.4. First wall blanket thermal-hydraulics design and analysis

10.4.1. Design inputs

With the mechanical design concept described earlier, we determined the material volume fractions and power generation from different FW/blanket zones. We performed iteration calculations between thermal hydraulics and nuclear analysis. The normalized volumetric power density for W-alloy as a function of distance x from the first wall is approximated by $\mathrm{PW}(x) = 9e^{-3x}$ W/cc per neutron wall loading in MW/m^2. The normalized volumetric power density for Li-breeder is approximated by $\mathrm{PLi}(x) = 4e^{-3x}$ W/cc. Other input parameters are:

Reactor power output	2 005 Mwe
Helium pressure	12 Mpa
Helium mass flow-rate	2 528 kg/s
Helium T_{in}/T_{out}	800°C/1 100°C
Structural material	W–5Re
Max. neutron wall loading	7.49 MW/m^2
Max. surface heat flux	2.16 MW/m^2

10.4.2. First wall design

The use of helium as a FW/blanket, divertor coolant has been proposed in various fusion design studies. To handle the high surface heat load, extended heat transfer enhancements by porous medium and swirl tape were evaluated.

10.4.3. Porous medium

A porous medium enhances heat transfer from the wall to the helium thereby reducing the film temperature drop and the absolute temperatures of the first wall. The design activity reported here was based, in part, upon development activities by two small US businesses. One of the companies, Thermacore, Inc., uses a porous medium to enhance heat transfer. Thermacore designed and built a series of helium-cooled modules that were tested at Sandia and elsewhere [26–29]. One advance in their development of a helium-cooled heat sink was the development of designs that connected open axial inlet and exhaust passages to circumferential flow passages that contained the porous medium, as shown in Fig. 36. The other company, Ultramet, Inc., has experience in fabrication of refractory materials. Ultramet has designed and built commercial products made of refractory metals for rocket nozzles and other applications in which they use a metallized foam that is integrally bonded to fully dense material [29] as shown in Fig. 37. Their experience demonstrates that a tungsten channel with integrated porous medium structure can be fabricated.

10.4.4. Swirl tape first wall design

Another method for extended surface heat transfer is to use a swirl tape insert. Swirl tape increases the heat transfer coefficient by increasing the effective flow velocity of the coolant and increasing mixing. There is a large amount of reliable data available on this method. However, the corresponding increase of coolant flow friction factor has to be accounted for.

For this calculation, the enhancement in heat transfer coefficient is given by, $h_{en} = 2.18/Y^{0.09}$, and the increase in friction factor is given by $f_{en} = 2.2/Y^{0.406}$, where Y is the twist ratio defined by pitch/2*diameter of the tube. Therefore the equivalent $h_{eq} = h^*_{en}h$ and equivalent friction factor $f_{eq} = f^*_{en}f$, where h and f are heat transfer coefficient and friction factor for a simple circular tube, respectively. In the following calculation, we used $Y = 2$.

Using a maximum neutron wall loading of 7.11 MW/m^2, and maximum surface heat flux of 2.06 MW/m^2, and the swirl-tube first wall coolant ve-

locity range of 54–62 m/s, the W-alloy maximum temperature was found to be in the range of 1073–1242°C. With simple tubes in the blanket, the W-alloy maximum temperature is 1199°C, and the lithium maximum temperature is 1228°C.

The first wall and blanket system pressure drop was also estimated. Including frictional losses, turns, contractions, expansions, and main helium inlet and outlet pipes, the total pressure drop was estimated to be 0.61 MPa, which gives a $\Delta P/P$ of 5.1%.

10.5. Thermal stress analysis of APEX first wall design

A 'ground rule' of the APEX study was that structures should be robust, and specifically, 3 mm was taken as a minimum first wall thickness (with some scientists recommending 5 mm). A

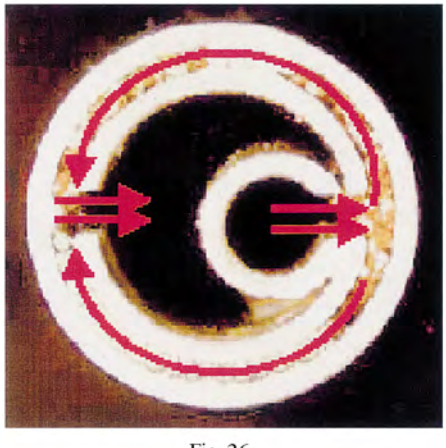

Fig. 36

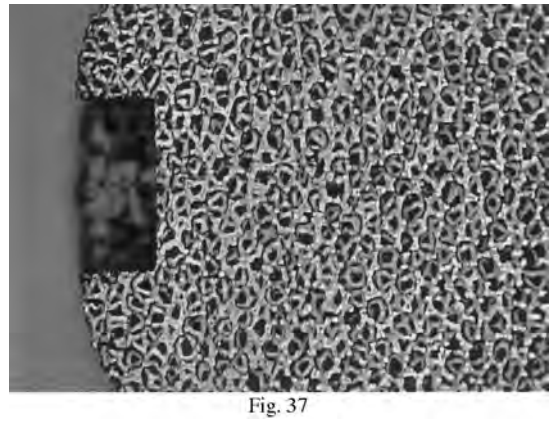

Fig. 37

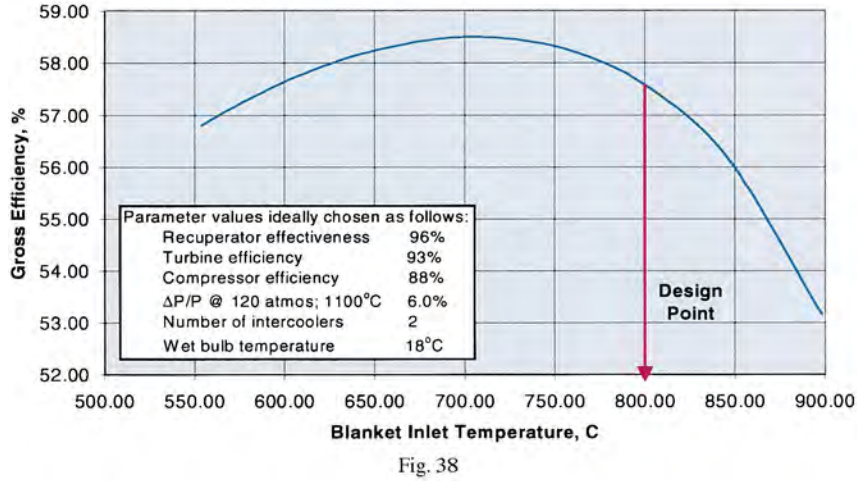

Fig. 38

Fig. 36. Thermacore circumferential flow design.
Fig. 37. Porous Ta implant, diameter is 0.75 in.
Fig. 38. Effect of FW/blanket inlet temperature on PCS gross efficiency.

central challenge in the design is to relieve the primary and secondary stresses that result from the high helium pressure, surface heat load and the related steep thermal gradient in the heated surface. The FW is permitted to flex to relieve the thermal strain (bending stresses) form the surface heat load.

A thermal analysis of a dual-channel FW structure (without the porous medium included) was performed using two-dimensional plane strain models (PATRAN/ABAQUS) for a surface heat load of 2 MW/m^2 and an internal pressure of 10 MPa; the FW was permitted to flex under the heat load. At 1000°C, the maximum von Mises stress is 80 MPa, this is well within the suggested stress limits stated below. Further iteration will be needed for the reference case of 12 MPa pressure but the result should not be significantly different. The double-tube wall design will then be incorporated into the porous medium design in the next design phase.

The thermal stress due to a prescribed temperature distribution along a single tube first wall of the APEX FW/blanket was also analyzed using the COSMOS finite element code. The structural model consisted of two-dimensional beam elements interconnected along with the defined temperature distribution. The first wall tube has an i.d. of 1.6 cm and an o.d. of 2.2 cm. The beam elements representing the lithium case are 0.2×2.2 cm for the inner case and 3.8×2.2 cm for the outer strong back case. The lithium case is supported by a guide structure attached to the vacuum vessel. It is assumed that the guide structure allows free thermal expansion of the lithium case in the vertical and radial directions. The following W–5Re alloy properties were taken at 1000°C: Young's modulus = 392 Gpa, Poisson's ratio = 0.267, and coefficient of thermal expansion = 3.96×10^{-6}/°C.

The deformed shape and maximum stress due to the prescribed assigned temperature distribution and boundary conditions were calculated. The tangential thermal growth of the first wall tube of 2.0 mm requires that the blanket modules be installed with 4.0 mm gaps in the cold condition to prevent contact with one another during operation. The radial thermal growth of the plasma facing tube is 4.4 mm. Since we projected that the irradiated W-alloy should be treated more as a brittle than ductile structural material, we proposed that the stress criteria for evaluating calculated stress intensities for tungsten materials be taken as one-half the ultimate stress (133 MPa) at 1000°C for welded joints and two-thirds the ultimate stress (177 MPa) away from joints. Adopting these criteria, the allowable stress at the weld joint due to all load combinations is 152 MPa at 1000°C. Since the proposed support structure will allow free thermal expansion of the lithium case, only the temperature difference between the first wall tube and lithium case will induce thermal stresses. The maximum thermal stress occurs in the first wall tube at its junction to the lithium case and is only 6 MPa.

Although the proposed concept for supporting the blanket induces low thermal stress, details of how to implement the support concept will certainly result in higher thermal stresses. Also, the stresses due to dead weight, pressure, and disruption loads have yet to be calculated. This will be performed in the next phase of design.

10.6. Nuclear analysis

Based on the material volume fractions generated, the reference design was determined by iteration between the thermal hydraulics task and assessed the impact of W-alloy on the nuclear heating profiles across the blanket and power multiplication (PM), and on the tritium breeding profiles and the tritium breeding ratio (TBR). The impact of Li-6 enrichment on these profiles and on TBR and PM is also assessed. In addition, we assessed the damage indices, expressed in terms of DPA, helium, and hydrogen production rates at several key locations including the vacuum vessel (VV) and TF coil case. When compared to other refractory alloys like TZM and Nb–1Zr, the best local TBR performance is with W and Li breeder. Based on a one-dimensional cylindrical base on

the outboard blanket geometry, the TBR increases with Li-6 enrichment and starts to saturate at a value of ~ 1.43 when Li-6 enrichment is $\sim 35\%$. The damage parameters, DPA rate, helium and hydrogen production rate at various locations were estimated in the W-alloy design. Compared to the liquid breeder Flibe, liquid lithium is the less effective material in attenuating the nuclear flux at the VV and TF coil by a factor of 6–10.

The radioactive waste characteristics of the different components of the machine were evaluated according to both the NRC 10CFR61 [16] and Fetter waste disposal concentration limits (WDR) [15]. According to Fetter limits, the first wall, module wall, blanket, and transitional zone would not qualify for disposal as class C waste. As a matter of fact, the W–5Re alloy produces such a high activity that the first wall would have a WDR that is more than an order of magnitude higher than the class C WDR limits. The high WDR is due to the ^{186m}Re, ^{108m}Ag, and ^{94}Nb isotopes. Only ^{186m}Re is a product of nuclear interactions with base elements in the W–5Re alloy.

10.7. Power conversion system

The major incentive for employing high-temperature refractory alloy FW/blanket with helium cooling in this design is to enable direct coupling with a CCGT (Brayton cycle) for high efficiency power conversion. This has the advantage of eliminating an intermediate high-temperature He/He heat exchanger (HX), which would be a significant technical challenge. However, the potential for tritium contamination in the power conversion system (PCS) must be addressed, and appropriate design measures must be taken to prevent further spread of contamination and to facilitate maintenance of PCS components. Fig. 38 shows the effect of FW/blanket inlet temperature variation on PCS performance for the selected outlet temperature of 1100°C. Based on this, the selected gross efficiency for the preliminary design is 57.5%.

10.8. Safety

The use of tungsten as the structural material in this concept poses some safety challenges. Tungsten is a radiologically hazardous material with high decay heat, so we must ensure that the design is such that long-term accident temperatures are low enough that unacceptably large amounts of tungsten are not mobilized during an accident. Our preliminary calculations show that design options exist that result in long-term temperatures below 800°C. Details can be found in the APEX interim report [1].

10.9. Key issues and R&D

We have completed the preliminary design of a helium-cooled refractory alloy FW/blanket design. Many development issues are identified in different areas of the design. The following is a list of key issues, grouped by areas, which will have to be addressed in order to become a viable design:

Materials	Irradiated and engineering design material properties of W-alloy.
	Design criteria for W-alloy.
	Fabrication of W-alloy components.
	Minimum cost of W-alloy components including material and fabrication.
	Compatibility between helium impurities and W-alloy.
Availability	Failure rate and maintenance.
Design	External coolant piping routing.
	Structure support to handle thermal expansion.
	High temperature piping.
	Develop robust high performance fusion power core W-alloy components.

Thermalhydraulics	Helium flow control, distribution and stability. First wall and blanket temperature management and startup.
Safety	Removal of afterheat during LOCA and LOFA.
Plasma and surface interaction	W-surface compatibility with high performance plasma.

11. Gravitational flowing Li_2O particulates

One of the concepts considered early in the APEX study attempts to eliminate the structural first wall by flowing Li_2O particulates directly exposed to the plasma. The concept is called APPLE. The Li_2O particulate flow system serves as the coolant and breeder. To be able to handle simultaneously a high neutron wall loading and high surface heat flux, the particulate material for the coolant/breeder must have good thermal conductivity and high temperature capability. The desirable material properties are:

1. Low vapor pressure at high temperature.
2. Low activation.
3. Good tritium breeding capability.
4. Low electrical conductivity.
5. High thermal conductivity.
6. Low tritium solubility.

After reviewing the potential candidates of the available coolant/breeding material, the solid breeder Li_2O was identified to have good potential to fulfill most of the requirements.

Since the coolant will be facing the plasma, the low vapor pressure requirement becomes very important. The total vapor pressure over Li_2O can be very low. At 1000°C, the combined vapor pressure of all the possible components is less than 10^{-5} torr. Therefore, the maximum allowable temperature of the Li_2O is set at 1000°C. This high allowable temperature leads to a design with high thermal conversion efficiency.

Fig. 39 shows the conceptual design of the system. The Li_2O particulate will be fed to the reactor system through a feed tube by gravitational force. After the particulate enters the reactor, it will be directed toward the inner (IB) and outer (OB) blanket by a solid baffle, made by SiC. Upon entering the IB and OB blanket module, the Li_2O will be divided into two separate streams. The stream facing the plasma will be freely dropped by gravitational force, while the flow of the stream inside the blanket will be restricted by an opening at the bottom of the blanket module to slow down the flow. It is important to reduce the flow velocity of the blanket coolant to achieve a high coolant temperature rise for optimum power conversion.

The thermal analysis of the blanket was performed, and the parameters are summarized in Table 12.

The tritium breeding and activation have been calculated. Li_2O has very high lithium density, and sufficient tritium breeding can be achieved. With the expected low structural fraction in the APEX design, the tritium breeding will not be a

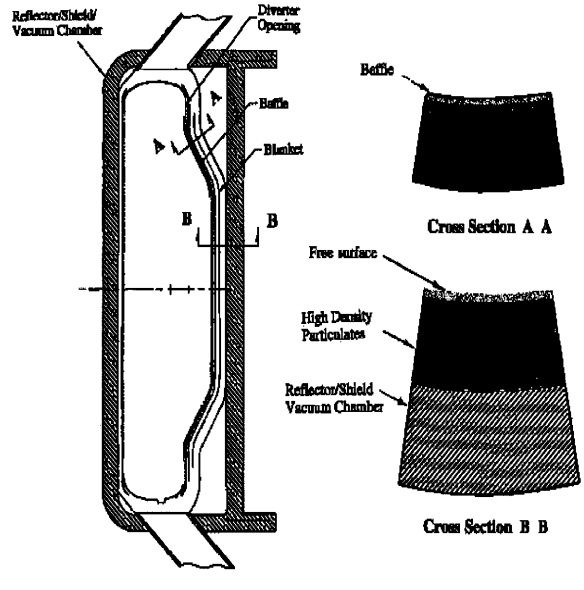

Fig. 39. APPLE configuration using baffles.

Table 12
Thermal hydraulics parameters for APPLE

Coolant/breeding material	Li_2O
Coolant inlet temperature (°C)	600
Coolant exit temperature (°C)	1 000
Coolant vapor pressure (Torr)	$<10^{-5}$
Maximum first wall coolant velocity (m/s)	5
Maximum blanket coolant velocity (m/s)	1
First wall surface heat load (MW/m^2)	2
Power conversion system	Brayton cycle
Power conversion efficiency (%)	52
Tritium inventory in the blanket (g)	5

serious issue. Both Li and O are low activation materials. The only significant activation product from pure lithium is the tritium, which is required for the fueling of the D-T plasma. The activation from oxygen is very low. The only other activation products are from the structural material inside the blanket, and from the shielding material behind the blanket. All the structural materials for this design have shown to be qualified for class C waste disposal. The summaries for the neutronics and activation analysis are summarized in Table 13.

Table 13
Summary of neutronics and activation analysis for APPLE

IB blanket thickness	40 cm
OB blanket thickness	75 cm
Li_2O density in the blanket	60%
Shield composition	80% steel 20% water
Tritium breeding ratio	1.215
Blanket energy multiplication	1.116
Peak end of life damage dpa in the shield at 30 FPY: IB	166
Peak end of life damage dpa in the shield at 30 FPY: OB	26
Shield thickness, IB	55 cm
Shield thickness, OB	40 cm
VV thickness	10 cm
End-of-life He at VV, appm	0.40
Magnet protection	Meet all the design goals
Maximum class C waste disposal rating, 10CFR61, IB shielding	0.144

One of the key concerns with the particulate flow concept is flow 'control', i.e. whether or not a particulate flow can be injected and guided without a plasma-facing wall. In contrast to liquid flow, particulate flow lacks cohesion forces. Our studies of particulate flow dynamics have not definitely confirmed, nor denied, the existence of acceptable particulate flow regimes in the complex plasma chamber geometry.

Many issues remain to be resolved for this class of particulate flow concepts. Examples of the critical issues are:

- Cooling of the solid baffle.
- Impact of oxygen contamination to the plasma.
- Material erosion and attrition issues.
- Solid material transport.
- Solid to gas heat exchanger design with the solid in vacuum.
- Particle dynamics.

12. Summary of materials considerations and database

12.1. Introduction

The list of structural materials originally considered for the APEX study includes conventional materials (e.g. austenitic stainless steel), low-activation structural materials (ferritic-martensitic steel, V–4Cr–4Ti, and SiC/SiC composites), oxide dispersion strengthened ferritic steel, conventional high temperature refractory alloys (Nb, Ta, Mo, W alloys), Ni-based super alloys, ordered intermetallics (TiAl, Fe_3Al, etc.), various composite materials (C/C, Cu-graphite and other metal–matrix composites, Ti_3SiC_2, etc.), and porous–matrix metals and ceramics (foams). In order to provide maximum flexibility in the design (and to increase the possibility for significant improvements in reactor power density), low long-term activation was not used as a defining 'litmus test' for the selection of candidate materials.

Due to limitations in resources and time, the materials analysis for APEX quickly focused on refractory alloys due to their higher thermal stress capacity and higher operating temperature capabilities compared to conventional structural materials. However, it should be emphasized that

Table 14
Costs for simple plate products (1996 prices)

Material	Cost per kg
Fe–9Cr steels	$\leq$\$5.50 (plate form)
SiC/SiC composites	>\$1 000 (CVI processing) ~\$200 (CVR processing of CFCs)
V–4Cr–4Ti	\$200 (plate form—average between 1994 and 1996 US fusion program large heats and Wah Chang 1993 'large volume' cost estimate)
Nb–1Zr	~\$100
Ta	\$300 (sheet form)
Mo	~\$80 (3 mm sheet); ~\$100 for TZM
W	~\$200 (2.3 mm sheet); higher cost for thin sheet

conventional materials may work satisfactorily in some of the APEX concepts (e.g. austenitic stainless steel located behind a thick wall of Flibe). Other promising advanced structural materials (e.g. ODS alloys, intermetallics) should be considered in future analyses.

Numerous factors must be considered in the selection of structural materials, including:

1. Unirradiated mechanical and thermophysical properties.
2. Chemical compatibility and corrosion.
3. Material availability, cost, fabricability, joining technology.
4. Radiation effects (degradation of properties).
5. Safety and waste disposal aspects (decay heat, etc.).

Work by the APEX team focused on the first four items in this list during the initial 18 months of the study, and the key findings are summarized below. More details are presented in Chap. 13 of Ref. [1].

12.1.1. Material costs and fabrication issues

The APEX materials team gathered information on the costs of many of the candidate structural materials. This raw material cost information is summarized in Table 14. The fabrication costs for producing finished products of refractory alloys (particularly W) is known to be much higher than for steels. The group V refractory metals (V, Nb, Ta) are relatively easy to fabricate into various shapes such as tubing, whereas the group VI refractory metals (Mo, W) are very difficult to fabricate. A further issue with all of the refractory metals is joining, particularly in-field repairs. Satisfactory full-penetration welds have not been developed for W, despite intensive efforts over a >25 year time span (1960–1985). The main issue associated with fusion zone welding of the group V alloys is the pickup of embrittling interstitial impurities (O, C, N, H) from the atmosphere. Experimental studies are in progress in the US to develop satisfactory fusion welds for vanadium alloys.

12.1.2. Overview of thermal stress capabilities of various alloys

The key mechanical and physical properties of high-temperature refractory alloys and low-activation structural materials are summarized in Section 13.3 of the APEX interim report [1]. A thermal stress figure of merit convenient for qualitative ranking of candidate high heat flux structural materials is given by $M = \sigma_U k_{th}(1-\nu)/(\alpha_{th}E)$, where σ_U is the ultimate strength, E is the elastic modulus, ν is Poisson's ratio, k_{th} is the thermal conductivity, and α_{th} is the mean linear coefficient of thermal expansion. In addition, temperature limits (usually determined by thermal creep considerations) can be used for additional qualitative ranking of materials. A rigorous quantitative analyses of candidate materials requires the use of advanced structural design criteria such as those outlined in Section 13.2 of Ref. [1].

The mechanical properties for recrystallized refractory alloys have been used as the reference case for purposes of APEX designs. Fig. 40 shows the ultimate tensile strength for several recrystallized refractory and high conductivity structural alloys as a function of temperature. The mechanical properties of stress-relieved (non-recrystallized) refractory alloys are superior to those of recrystallized specimens, with increases in strength of up to a factor of 2 being typical. However, the possibility of stress- or radiation-enhanced recrystallization of these alloys (along with the likely inclusion of welded joints in the structure) does not allow this strength advantage to be considered for conservative design analyses.

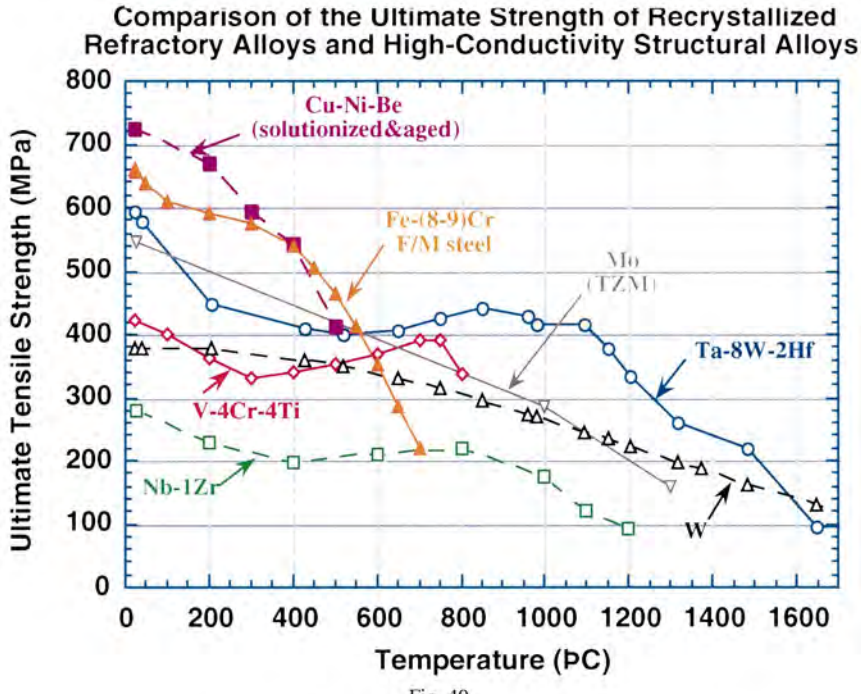

Fig. 40

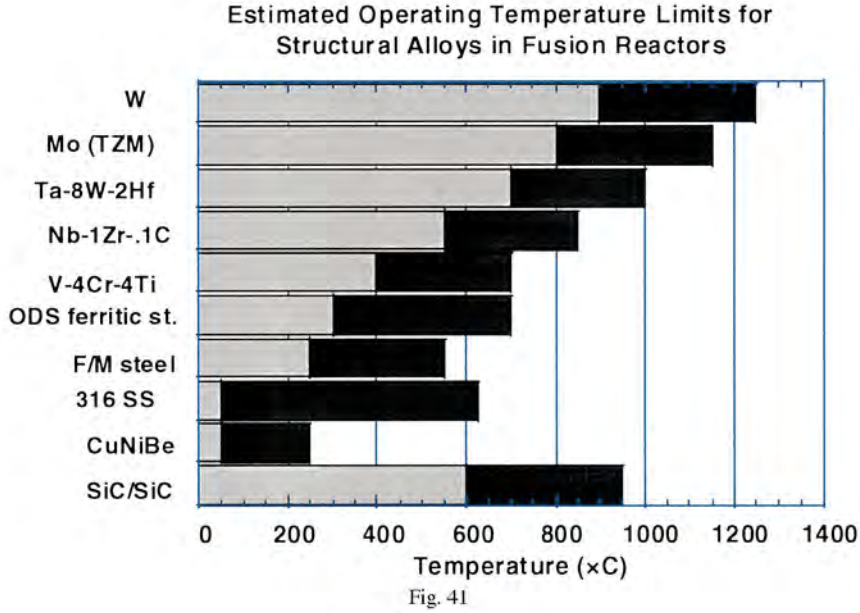

Fig. 41

Fig. 40. Temperature-dependent ultimate tensile strengths of recrystallized refractory alloys and high-conductivity structural alloys. Data from Tietz and Wilson [31], Conway [32], Buckman [33], and Zinkle et al. [34].

Fig. 41. The allowable operating temperature range for structural materials based on unirradiated/irradiated mechanical properties, void swelling and thermal conductivity degradation is denoted by the black boxes (see text). Chemical compatibility issues may cause a further restriction in the operating temperature window.

The thermal stress figures of merit vary from ~57 kW/m for a high strength, high conductivity CuNiBe alloy at 200°C [30] to ~2.0 for SiC/SiC at 800°C. Copper alloys are not attractive choices for high thermal efficiency power plants due to their high thermal creep at temperatures above 400°C. The low thermal stress resistance of SiC/SiC is mainly due to the low thermal conductivity in currently available composites (primarily due to a combination of poor quality fibers and imprecise control of the CVI deposition chemistry). The two major classes of low-activation structural alloys, V–Cr–Ti and Fe–8–9Cr martensitic steel have figures of merit of ~6.4 (450–700°C) and 5.4 (400°C), respectively. The refractory alloys offer some advantage over vanadium alloys and ferritic-martensitic steel, even in the recrystallized condition. For example, pure recrystallized tungsten has a figure of merit of $M = 11.3$ at 1000°C, and TZM (Mo–0.5Ti–0.1Zr) has a value of $M = 9.6$ at 1000°C. The alloy T-111 (Ta–8W–2Hf) has the best thermal stress figure of merit among the (non-copper) alloys considered, with a value of $M = 12.3$ at 1000°C.

12.2. Structural design criteria

Most advanced blanket design concepts require the first wall to operate in temperature regimes where thermal creep effects may be important. Therefore, in addition to the usual low-temperature design rules, high-temperature design rules may also have to be applied. We have adopted the ITER structural design criteria (ISDC) as a basis for the design rules to be used in APEX.

Since the design studies under APEX are preliminary in nature, only elastic analysis design rules are included. The design rules are divided into a high temperature section and a low temperature section, depending on whether thermal creep effects are or are not important. The low temperature rules are always applicable. High temperature rules are also applied if thermal creep may be significant. The low temperature design rules include limits associated with necking and plastic instability, plastic flow localization, ductility exhaustion, brittle fracture, ratcheting (cyclic loading), and fatigue. The high temperature design rules include limits associated with creep damage, creep-ratcheting, and creep-fatigue.

12.3. Summary of thermophysical properties (unirradiated and irradiated)

Analytical expressions for the temperature-dependent mechanical and thermophysical properties for five of the structural materials considered for APEX have been derived from least-squares fits of experimental data (Fe–8–9Cr ferritic/martensitic steel, V–4Cr–4Ti, SiC/SiC, Ta–8W–2Hf, and W–10Re) and documented in Chap. 13 of ref. [1]. Radiation-induced void swelling is not anticipated to be a lifetime-limiting issue in the refractory metals due to their BCC structure, although there are insufficient experimental studies to fully establish the void swelling behavior. Radiation hardening and associated embrittlement can have a major impact on all of the refractory alloys. The amount of radiation hardening at low temperatures ($< 0.3\ T_M$) is pronounced in all of the refractory alloys, even for damage levels as low as ~1 displacement per atom. The amount of radiation hardening typically decreases rapidly with irradiation temperature above $0.3\ T_M$, and radiation-induced increases in the ductile to brittle transition temperature (DBTT) may be anticipated to be acceptable at temperatures above $\sim 0.3\ T_M$ (although experimental verification is needed). Very little information is available on the fracture toughness of irradiated or unirradiated refractory alloys.

12.4. Coolant/structure chemical compatibility

In general, the refractory alloys have very good compatibility with the liquid metals and salts of interest for fusion applications (Li, Pb–Li, Sn–Li, Flibe). Impurity pickup (O, C, N, etc.) is the key engineering issue in most cases for refractory alloys in contact with these coolants as well as for He-cooled concepts.

Formation of volatile oxides can lead to pronounced surface erosion of group VI metals (Mo, W) at elevated temperatures. The evaporation rate increases rapidly up to ~2000 K in both Mo and W. The high-temperature oxidation of Mo and W

Table 15
Maximum allowable temperatures of structural alloys (bare walls) in contact with high-purity liquid coolants, based on a 5 μm/yr corrosion limit (Sn–Li corrosion limits are based on experimental studies conducted with liquid Sn)

	Li	Pb–17 Li	Sn–Li (Sn)	Flibe
F/M steel	550–600°C	450°C	400–500°C	700°C (304/316 stainless steel)
V alloy	~700°C	~650°C	?	?
Nb alloy	>1 300°C	>600°C(>1 000°C in Pb)	600–800°C	>800°C
Ta alloy	>1 370°C	>600°C(>1 000°C in Pb)	600–800°C?	?
Mo	>1 370°C	>600°C	<800°C?	>1 100°C?
W	>1 370°C	>600°C	~800°C	>900°C?
SiC	~550°C?	>800°C?	>760°C?	?

was analyzed using a thermodynamic model. If boundary layer scattering effects are ignored, the evaporation rate exceeds 100 μm/year at ~1500 K in both materials for 1 ppm oxygen in He at a pressure of 10 MPa. Boundary layer effects may reduce the evaporation rate by several orders of magnitude. The calculations suggest that limitations on mass transport through the boundary layer may reduce the erosion rate to less than 10 μm/year at wall temperatures up to 2600 K in both Mo and W. Although the model does not take into account many of the physical features of real wall-coolant interactions, such as roughness, bends, and temperature variations along the flow, it is reasonable to assume that the evaporation rate of W and Mo will be below a few microns per year, when operated at temperatures as high as 1200–1300°C.

Oxygen pickup in the group V metals (V, Nb, Ta) causes matrix hardening, which in turn produces an increase in the ductile-to-brittle transition temperature (DBTT). The matrix oxygen content must be kept below ~1000 wt ppm in order to keep the Charpy V-notch DBTT below room temperature. Due to the high affinity of the group V metals for oxygen, it is not realistic to avoid oxygen pickup from non-lithium coolants on the basis of thermodynamics. However, the kinetics of the oxygen pickup can be kept acceptably low either by maintaining the temperature below ~0.4 T_M or by keeping the oxygen partial pressure sufficiently low so as to prevent significant impingement of oxygen on the metal surface. A conservative analysis indicates that an oxygen partial pressure of $\sim 10^{-10}$ torr would be sufficient to keep oxygen pickup to acceptably low levels in group V metals for expected structural material lifetimes (10–50 years).

The experimental database on corrosion of structural alloys in contact with liquid metals and Flibe was reviewed. The refractory alloys have excellent compatibility with liquid lithium up to very high temperatures. The maximum operating temperatures of various alloys in Li, Pb–Li and Flibe is summarized in Table 15. There is a strong need for experimental data on the chemical compatibility of the various structural alloys with Sn–Li and Flibe although several materials appear to be compatible with these coolants at temperatures of interest for APEX. The refractory alloys do not appear to have good compatibility with Sn–Li.

12.5. Summary and conclusions

The estimated minimum and maximum temperatures for several of the structural materials considered for APEX are summarized in Fig. 41. The lower temperature limit is based on radiation hardening/fracture toughness embrittlement ($K_{1C} < 30$ MPa-m$^{0.5}$) due to low temperature irradiation. This embrittlement effect would be expected to occur for damage levels above ~1 dpa. There is a large uncertainty in the lower temperature limit for radiation embrittlement in W due to lack of mechanical properties data at irradiation temperatures above 700°C. The upper temperature limit is based on thermal creep considerations (1% creep in 1000 h for an applied stress of 150 MPa). Depending on the choice of coolant, this

upper temperature limit could be reduced due to corrosion issues. On the other hand, even higher temperatures might be conceivable for applications which have very low applied stress. The corresponding minimum and maximum temperature limits for Fe–8–9%Cr ferritic/martensitic steel are ~250 and ~550°C. The upper temperature limit could be increased by using oxide dispersion strengthened ferritic steel, which has good creep strength to temperatures in excess of 650°C. The recommended minimum and maximum temperature limits for SiC/SiC composites are ~600°C (due to radiation-induced thermal conductivity degradation effects) and ~900°C (due to void swelling concerns), although additional irradiation data are needed to firmly establish these temperature limits.

13. Safety and environment considerations and analysis

Safety and environmental issues are being considered up front in the APEX study as new ideas and designs evolve so that the goal of safety and environmental attractiveness is realized. A comprehensive safety analysis requires detailed designs [35]. Since the objective of APEX is to explore and evolve new ideas, rather than develop detailed designs, the role of safety analysis is somewhat different. Safety analysis is used in two ways: (1) for screening concepts by looking for safety issues that could be 'show stoppers', i.e. meeting safety guidelines does not look feasible, and (2) for providing guidance to the design idea developers on areas of improvements to enhance safety and environmental attractiveness.

13.1. LOCA calculations

The initial focus has been on the ability of the designs to remove decay heat. The goal here is to ensure that temperatures remain below levels at which oxidation-driven mobilization becomes unacceptable. A number of concepts were examined to determine the ability of the design to remove heat from the plasma-facing surface during an accident. If surface temperatures are low enough, mobilization of hazardous material is minimized. The CHEMCON code [36] used in these calculations was developed to analyze decay heat driven thermal transients in fusion reactors.

LOCA calculations were carried out for four different APEX concepts:

1. He-cooled, refractory alloy first wall/blanket (slowly moving liquid lithium breeder with tungsten alloy structure).
2. APPLE concept (SiC structure with flowing LiO_2 particulate breeder; total blanket thickness of ~40 cm).
3. CLiFF concept (V structure with thin, ~2 cm, liquid breeder).
4. One of the thick liquid (Pocket) concepts (a thick, ~50 cm, layer of liquid breeder flows over a ferritic steel back wall).

The decay heat distributions for the four designs analyzed are shown in Fig. 42. Note that the decay heat is shown per unit volume of the zone, including structure, voids, coolant channels, etc.

The optimal result, from a safety point of view, is when long-term accidents temperatures are adequately low without relying on active (safety-grade) cooling systems. The initial calculations for each design assumed no active cooling. If the temperatures were unacceptably high, various cooling options were then examined. Peak temperatures and the amount of time above 800°C for the APPLE, CLiFF, thick liquid wall, and He-cooled refractory alloy designs are shown in Table 16 (EVOLVE has not yet been analyzed). Because of the large amount of tungsten used in the He-cooled refractory alloy design, active cooling was necessary to keep accident temperatures to an acceptable level. Similarly, it is primarily the Tenelon in the shield that is contributing to the high decay heat in the CLiFF design. Active cooling of the vacuum vessel reduces peak temperatures to 875°C, however temperatures are above 800°C for 3.5 days.

The choice of Tenelon (which is a high manganese steel; manganese has high decay heat) in the shield behind CLiFF is independent of the idea of thin liquid wall, and thus can be easily replaced by another shielding material. Although the peak temperature during the transient for the APPLE design is above 800°C, the duration is less

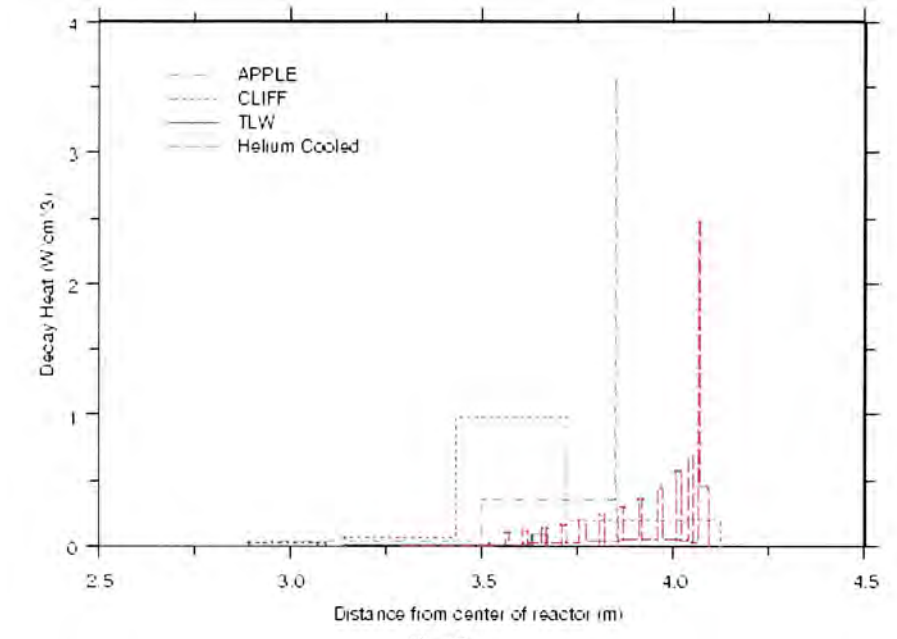

Fig. 42

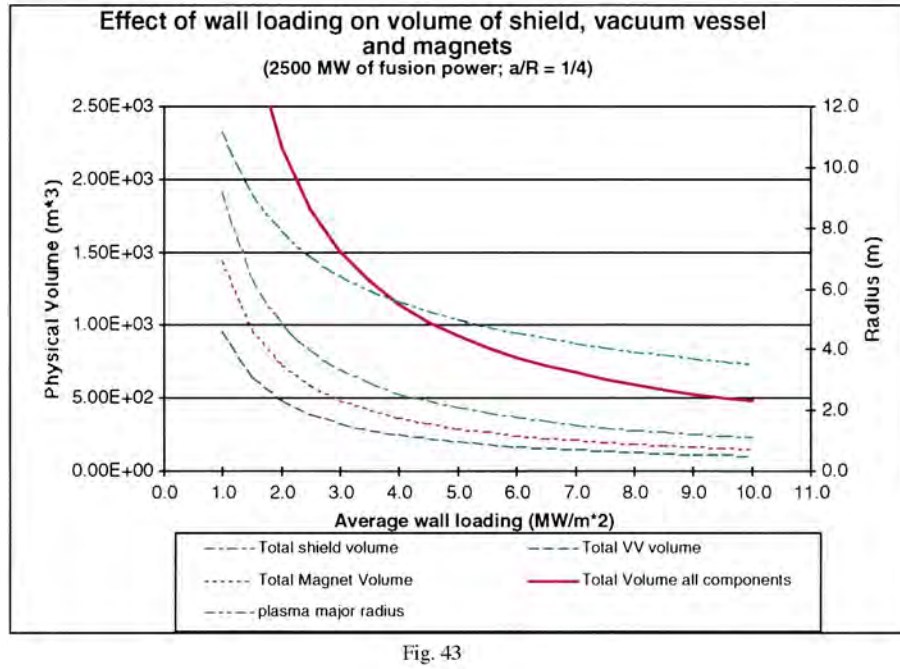

Fig. 43

Fig. 42. Decay heat distribution per unit volume for the four concepts analyzed.
Fig. 43. Volume of the shield, vacuum vessel and magnet components as a function of wall load.

Table 16
Peak temperature and time above 800°C for Apple, CLiFF, He-coded, and thick liquid designs

Concept	Peak temperature (°C)	Time above 800°C (h)
APPLE	1275	1.2
CLiFF	875[a]	84[a]
He-cooled	800[b]	<1[b]
Thick liquid	675	0

[a] See text; this is due to the shielding material, Tenelon, which can be easily replaced.
[b] With active cooling of the blanket region.

than 2 h, and the relatively low radiological hazard of SiC makes this acceptable. The temperature in the thick liquid wall design never exceeded 675°C.

Although the neutron and surface heat loads are higher in APEX designs than those in conventional fusion designs, these preliminary LOCA calculations indicate that safety criteria (and more specifically, no-evacuation guidelines) can likely be met. For the He-cooled refractory alloy design, this will likely require the use of a safety-grade system to remove decay heat during accidents. It may be necessary to avoid the use of Tenelon in the shield in designs such as CLiFF; in that case, active cooling may not be necessary. For others, such as the thick liquid concept, a safety-grade system is probably not necessary. It is desirable to make any such system passive to increase the reliability of the system.

These preliminary scoping calculations are by no means sufficient for determining whether these designs will meet safety guidelines. They are meant as a starting point, and are used to make recommendations to designers so that safety is 'built into' designs as they mature. As more design detail becomes available, further safety analyses will be needed to ensure that safety requirements are met.

13.2. Waste disposal issues

The environmental impact of waste material is determined not only by the level of activation, but also the total volume of activated material. A tokamak power plant is large, and there is a potential to generate a correspondingly large volume of activated material. The adoption of 'low activation' materials strategy, while important to reduce the radiotoxicity of the most active components, should be done as part of a broader strategy that also minimizes the volume of waste material that might be categorized as radioactive, even if low level.

There is a need to explore new and innovative concepts that can substantially reduce the activation of the large ex-vessel components that contribute significantly to the overall volume of activated material and to extend the capability of conventional conceptual fusion designs with proper optimization to achieve the same goal.

A rough order of magnitude comparison of FW/blanket waste volumes for thick liquid wall designs with ARIES-RS is shown in Table 17. Although additional study is needed to solidify these numbers, the initial indication is that thick liquid wall designs could significantly reduce this waste volume.

In addition to a reduction in the FW/blanket waste volume, higher power density designs result in a more compact machine which reduces the volume of the shield, vacuum vessel and magnet components. Fig. 43 plots the volume of these components as a function of wall load. Comparison of volume of these components at the 10 MW/m^2 value with the volume at the ARIES-RS value of 5 MW/m^2 shows a reduction in overall volume of these components by about 50%. This value assumes that all of these components are permanent lifetime components. For permanent components the volume scales inversely with the wall load. However, in ARIES-RS, part of the shield is not a lifetime component. In this case, the overall volume reduction afforded by high wall load might be reduced to about 30%.

14. Summary

The objective of the APEX study has been to identify and explore novel, possibly revolutionary, concepts for fusion chamber technology that can substantially improve the attractiveness of fusion energy systems. The first phase of the study was carried out in 1998–1999 by a multi-disciplinary

Table 17
Rough order of magnitude comparison of FW/blanket waste volumes for different concepts

Concept type	Peak wall load (MW/m^2)	FW/blanket structure fraction	Approximate structure replacement time	Reduction in waste volume of FW and blanket components for liquid wall high power density designs relative to ARIES-RS
ARIES-RS	5.5	10%	2.5 FPY	
Thick liquid walls with no structure	10	0%	n/a	infinite
Thick liquid Flibe walls with 4% structure behind walls	10	4%	40 FPY	70
Thick liquid walls with 1% structure to guide the flow	10	1%	$\sim$ 1.5 FPY	10

integrated team of scientists and engineers from 12 US organizations with participation of experts from Germany, Russia, and Japan. A set of goals for the Chamber Technology were adopted to calibrate new ideas and to measure progress. These goals include: (1) high power density capability with neutron wall load >10 MW/m^2 and surface heat flux >2 MW/m^2; (2) high power conversion efficiency ($>40\%$); (3) high availability (i.e. low failure rate and fast maintenance); and (4) simple technological and material constraints.

A number of promising ideas for new innovative concepts have already emerged from the first phase of the APEX study. While these ideas need extensive research before they can be formulated into mature design concepts, some of them offer great promise for fundamental improvements in the vision for an attractive fusion energy system. These ideas fall into two categories. The first category seeks to totally eliminate the solid 'bare' first wall. The most promising ideas in this category are in the 'concept rich' class of flowing liquid wall variations. The second category of ideas focuses on extending the capabilities, particularly the power density and temperature limits, of solid first walls. A promising example is the use of high temperature refractory alloys (e.g. tungsten) in the first wall together with an innovative heat transfer and heat transport scheme based on vaporization of lithium.

14.1. Liquid walls

The liquid wall idea evolved during the APEX study into a number of concepts that have some common features but also have widely different issues and merits. These concepts can be classified according to: (a) the type of working liquid, (b) the thickness of the liquid flow, and (c) the type of restraining force used to control the liquid flow.

14.1.1. Basic principles and concepts

The practical candidates for the working liquid are the liquid metals lithium and Sn–Li (Sn–Li was introduced into APEX because it has very low vapor pressure), and the molten salt Flibe. Many different considerations must be taken into account when assessing the performance of various liquid wall ideas. The hydrodynamics and heat transfer characteristics of high conductivity, low Prandtl Number liquid metal flows will depend heavily on the interactions with the magnetic field. In contrast, low-conductivity, high Prandtl Number Flibe flows will be dominated by turbulence considerations. The Z number and ionization potential of any vapor generated from the liquid surface will affect significantly the plasma contamination levels. The relative hydrogen solubility in the working liquid will play a significant role in the structure of the edge and the stability of the plasma discharge.

In addition, high conductivity liquid metal (LM) flows have the potential to affect the local magnetic fields and the plasma stability in a potentially positive manner. LM walls appear capable of allowing stable tokamak operation with increased elongation under reactor conditions. Modeling results indicate that the magnitude of improvement can be large with up to a factor of three improvement in stable β (from 5–7% to 20–22%) at aspect ratio 4 and 3, respectively. Flowing liquid metals can potentially stabilize resistive wall modes as well allowing higher β steady state equilibria with very hollow current profiles. Steady state operation with such profiles enables high bootstrap fractions and thus low recirculating power. Also, hollow current profiles are theoretically predicted to give $E \times B$ shearing rates larger than instability growth rates for conventional drift instabilities, leading to transport barriers and high confinement.

The selection of the thickness for the liquid wall layer flow (directly facing the plasma and in front of a solid 'backing wall') leads to different concepts that have some common issues but many unique advantages and challenges. Both thin and thick liquid walls can adequately remove high surface heat flux. A primary difference between thin and thick liquid walls is the magnitude of attenuation of neutrons in the liquid before they reach the backing wall. The 'thin' liquid wall concept is easier to attain, but 'thick' liquid wall concepts greatly reduce radiation damage and activation of the structure. Assuming a 200 DPA damage limit for structure replacement, the use of about 40 cm of Flibe or Sn–Li can make the

structure behind it a lifetime component. Furthermore, the volume of the radioactive waste from the FW/blanket system is greatly reduced.

Widely different liquid wall concepts are also obtained by applying various forces to drive the liquid flow and restrain it against a backing wall. An example is the gravity–momentum driven (GMD) concept, where the liquid is injected at the top of the chamber at an angle tangential to the curved backing wall. The fluid adheres to the backing wall by means of centrifugal force and is collected and drained at the bottom of the chamber. The criterion for the continuous attachment of the liquid layer is simply that the centrifugal force pushing the liquid layer towards the wall is greater than any destabilizing gravitational force.

Using Flibe as the working fluid, the GMD concept has been modeled with a three-dimensional, time-dependent Navier–Stokes solver that uses the Reynolds Averaged Navier Stokes (RANS) equations for turbulence modeling and the volume of fluid (VOF) free surface tracking algorithm for free surface incompressible fluid flows. Example solutions at 8 m/s inlet velocity demonstrate that a stable, thick fluid configuration can be established and maintained throughout a tokamak reactor configuration. Nevertheless, gravitational acceleration and mass continuity lead to some amount of jet thinning as it proceeds from the top to the bottom of the reactor. Jet thinning can be overcome by increasing the initial jet velocity, and a fairly uniform thick liquid film can be obtained throughout the plasma chamber if the jet is injected at 15 m/s. The thinning can also be minimized by the MHD drag from the Hartmann velocity profile in a flow with conducting toroidal breaks. More analysis of this effect is needed for Flibe.

Numerical analyses were also performed for LM flows in GMD to determine whether or not an insulator is needed for free surface MHD flows, and to define lithium's initial velocity that enables a uniform thickness to be maintained throughout the plasma chamber in the presence of the toroidal magnetic field. The preliminary analysis based on simplified magnetic field geometries with only toroidal or radial fields shows that the MHD drag effect significantly increases the layer thickness and causes the associated reduction in the velocity. Thus, there is a need of insulators for a free-surface LM flow if a toroidally segmented poloidal liquid metal flow configuration is considered (other clever options may be possible that do not need an insulator). For an insulated open channel, calculations indicate that a uniform 40 cm-thick lithium layer can be maintained along the poloidal path at a velocity of 10 m/s.

Heat transfer calculations indicate that poloidal flow options like the GMD will have a surface temperature rise in the range of 150°C for lithium, and from 25 to 150°C for Flibe (depending on turbulence assumptions) when flowing at 10 m/s. A better understanding of free surface heat transfer (including the hydrodynamics near the free surface/plasma interface) is needed to more concretely determine these values.

Variations of the GMD for the low aspect ratio spherical torus (ST) and cylindrical FRC include adding an additional azimuthal (toroidal) velocity to produce rotation. The 'swirl flow' results in a substantial increase in the centrifugal acceleration and better adherence to the backing wall, when the wall curvature in the poloidal direction is large and the toroidal curvature is comparable to the poloidal curvature.

The thin wall analog of the GMD is the convective liquid flow first-wall, or CLiFF, concept, where the goal is to eliminate the presence of a solid FW facing the plasma through which the surface heat load must conduct. This goal is accomplished by means of a fast moving (convective), thin liquid layer flowing on the plasma side of the FW. Such a thin layer is easier to control than a thick liquid system, but still provides a renewable liquid surface immune to radiation damage and sputtering concerns, and largely eliminates thermal stresses and their associated problems in the first structural wall. The CLiFF class of liquid wall concepts is viewed as a more near-term application of liquid walls, and is suitable for some currently operating plasma devices.

MHD analysis for LM-CLiFF has shown that the MHD drag can be significant if there is a radial magnetic field component — one normal to the free surface. Analyses indicate that a metallic backplate is acceptable with insulated toroidal breaks if the radial magnetic field is no more than

0.1–0.15 T. The acceptable field magnitude would drop to 0.015 T for the case of toroidally continuous flow. Other important MHD issues such as flow across field gradients ($1/R$ dependence of the toroidal field for example), temporal fluctuations during start-up and plasma control will be addressed in the next phase.

Penetrations will be required for plasma-support functions such as heating and fueling. Novel schemes for accommodating penetrations in liquid walls have been proposed. For example, modifications to the back wall topology to guide the flow around elongated penetrations are found to be effective. Computational three-dimensional fluid dynamic simulation results for the CLiFF concept with Flibe show significantly reduced liquid layer disturbance, no splash at the stagnation point, and no unwetted regions downstream the penetration. These results are encouraging and provide an excellent start for studying penetrations in thick liquid walls, where the volume of fluid is much larger.

The electromagnetically restrained (EMR), applicable only to liquid metals, is another example of liquid wall concepts. EMR utilizes a $J \times B$ force field to push the liquid against the backing wall. An injected poloidal current interacts with the main toroidal magnetic field to generate this force, resulting in liquid layer adherence to the back wall at potentially lower velocities than required for the GMD.

Other active control schemes with injected currents have been proposed as well, and will continue to be investigated with new modeling tools being developed for the task.

14.1.2. Motivation for liquid wall research

There are many attractive features of liquid walls that have motivated this research:

- High power density capability:
  - Eliminate thermal stress and wall erosion as limiting factors.
  - Smaller and lower cost components (chambers, shield, vacuum vessel, magnets).
- Improvements in plasma stability and confinement:
  - Enable high β, stable physics regimes if liquid metals are used.
- Increased potential for disruption survivability.
- Reduced volume of radioactive waste.
- Reduced radiation damage in structural materials:
  - Makes difficult structural material problems more tractable.
- Potential for higher availability.

It is not clear yet that all these advantages can be realized simultaneously in a single concept. However, the realization of only a subset of these advantages will result in remarkable progress toward attractive fusion energy systems.

14.1.3. Key issues for liquid walls

The scientific and engineering issues for liquid walls are many. Of all the potential issues, a number of them stand out as the highest priority for near-term liquid wall research.

1. Plasma–liquid interactions including both plasma–liquid surface and liquid wall–bulk plasma interactions. Plasma stability and transport may be seriously affected and potentially improved through various mechanisms including control field penetration, H/He pumping, passive stabilization, etc. More careful estimates for the allowable amount of liquid evaporation and sputtering need to be obtained and benchmarked.
2. Hydrodynamics flow feasibility in complex geometries including penetrations. The issue of establishing a viable hydrodynamic configuration threatens feasibility for all concepts, but it differs significantly for thick versus thin and for molten salts versus liquid metals. The main issue facing liquid metals is of course that of MHD interactions. Without toroidal axi-symmetry of the flow and field, reliable insulator coatings will be required on all surfaces in contact with the LM layer. Eddy current forces perpendicular to the surface can pull the LM off the surface, even when complete axi-symmetry is assumed in the toroidal direction. Additionally, gradients in toroidal field can exert a significant drag on the free surface flow. For thick liquid walls, the main issues concern the formation and removal of the liquid flow in the plasma chamber, and the accommodation of penetrations.

3. Heat transfer at free surface and temperature control. Liquid surface temperature and vaporization are tightly coupled plasma edge and free surface hydrodynamic problems that require knowledge of the radiation spectrum, surface deformation, velocity and turbulence characteristics. Being a poor thermally conducting medium, the Flibe surface temperature highly depends on the turbulent convection. However, the normal velocity at the free surface as well as the turbulent eddies near the surface can be greatly suppressed. The issue of heat transfer at free surfaces is a serious concern, especially considering that the preliminary plasma-edge modeling predicts a relatively low limit on the surface temperature for Flibe.

14.2. High-temperature solid wall concepts

APEX has also explored ideas for extending the power density and operating temperature capabilities of solid walls. Achieving high power density means that the coolant heat removal capability must be high and the first wall material must have attractive thermophysical properties. Since materials operating at very high temperatures generally have limited strength, such concepts should operate at low primary stresses. This requires that the coolant pressure be as low as possible, and the temperatures throughout the first wall and blanket be as uniform as possible to reduce thermal stress.

Analysis of materials shows that the only structural materials suitable for high-power density, high-temperature operation are refractory alloys. A tungsten alloy, e.g. W–5% Re, was selected as the primary candidate material, with tantalum alloys as the back-up. The minimum and maximum operating temperature for W and other structural materials were estimated. For W, the lower and upper operating temperature limits are about 900°C and 1250°C, respectively, depending on the choice of the coolant and the applied stress. The lower temperature limit is based on radiation hardening/fracture toughness embrittlement due to low temperature irradiation. There is a large uncertainty in the lower temperature limit for radiation embrittlement in W due to lack of mechanical property data at irradiation temperatures above 700°C. The upper temperature limit is based on thermal creep considerations and, depending on the coolant, could be further reduced due to corrosion issues.

Two coolant schemes were evaluated. The first uses helium with the motivation to explore the possibility of using high temperature helium for high-efficiency energy conversion in a gas turbine cycle. The key difficulties with helium cooling are the very high pressure (~ 12 MPa) and large temperature rise, which push the requirements on the refractory alloy structural material to the range of uncertainty in available data.

A more promising idea is an innovative cooling scheme based on the use of the heat of vaporization of lithium (about 10 times higher than water) as the primary means for heat removal. This idea, called EVOLVE (evaporation of lithium and vapor extraction) was explored in APEX in some detail and will continue to be investigated.

Calculations indicate that an evaporative system with Li at ~ 1200°C can remove a first wall surface heat flux of > 2 MW/m^2 with an accompanying neutron wall load of > 10 MW/m^2. The system has the following characteristics:

1. The high operating temperature leads to a high power conversion efficiency.
2. The choices for structural materials are limited to high temperature refractory alloys.
3. The vapor operating pressure is very low (subatmospheric), resulting in a very low primary stress in the structure.
4. The temperature variation throughout the first wall and blanket is low, resulting in low structural distortion and thermal stresses.
5. The lithium flow rate is approximately a factor of ten slower than that required for self-cooled first wall and blanket. The low velocity means that an insulator coating is not required to avoid an excessive MHD pressure drop.

A preliminary conceptual design was developed and analyzed for EVOLVE. Key issues that need to be addressed in the future in order to assess the potential of the concept include: (1) three-dimensional heat transfer and transport modeling and analyses for the two-phase flow including MHD

effects; (2) feasibility of fabricating entire blanket segments of W alloys; (3) effect of neutron irradiation on W alloys; and (4) analysis of safety issues associated with the high afterheat in tungsten in case of a LOCA.

14.3. Future work

The APEX team has already initiated its efforts for the next phase, which will focus on more detailed exploration of liquid walls and EVOLVE. The effort will include modeling, analysis, laboratory experiments, as well as collaborating with the physics community to conduct liquid wall relevant experiments in existing plasma physics devices.

Acknowledgements

This work was supported by the Department of Energy, Office of Fusion Energy Sciences, through various research grants, and involved the hard work and creativity of many fusion researchers at the participating organizations. Special thanks to Sam Berk (US-DOE), whose deep understanding of fusion technology issues was instrumental in initiating the present study. Many thanks also to Charles Baker, Kenzo Miya, Tomoaki Kunugi and Grant Logan for their continued guidance and valuable advice in support of the APEX study. The APEX team is grateful to many members of the fusion community for their encouragement, support, and contributions.

References

[1] M.A. Abdou, et. al., On the exploration of innovative concepts for fusion chamber technology: APEX interim report. UCLA-ENG-99-206, University of California-Los Angeles, November, 1999.
[2] M.A. Abdou, The APEX Team, Exploring novel high power density concepts for attractive fusion systems, Fus. Eng. Des. 45 (1999) 145–167.
[3] N.C. Christofilos, A design for a high power density ASTRON reactor. Lawrence Livermore National Laboratory, Livermore, CA, UCID-15731 . Also issued in revised form as UCRL-72957 (1971) for submittal to Nuclear Fusion but never published in that journal. Ralph Moir published this paper for Christofilos in:, J. Fus. Energy 8 (1989) (1970) 97.
[4] A.E. Robson, in: B. Bruneli, G.G. Leotta (Eds.), The LINUS Concept, Unconventional Approach for Fusion, Plenum, New York, 1982.
[5] R.W. Moir, Mirror plasma apparatus. US Patent 4.260.455, 7 April, 1981.
[6] R.W. Moir, Rotating liquid blanket for a toroidal fusion reactor, Fus. Eng. Des. 5 (1987) 269.
[7] R.W. Moir, Liquid first walls for magnetic fusion energy configurations, Nucl. Fus. 37 (1997) 557–566.
[8] A.P. Fraas, The BLASCON—An exploding pellet fusion reactor. Oak Ridge National Laboratory, Oak Ridge, TN, TM-3231, 1971.
[9] W.R. Meier, J. Maniscalco, Reactor concepts for laser fusion. UCRL-79694, Lawrence Livermore National Laboratory, Livermore, CA, 1977.
[10] M. Monsler, J. Maniscalco, J. Blink, J. Hovingh, W. Meier, P. Walker, Electric power from laser fusion: The HYLIFE concept. Proceedings of IECEC Conference, San Diego, CA, August, 1978, p. 264. See also, J.A. Blink et. al., The high yield lithium injection fusion energy (HYLIFE-I) reactor. Lawrence Livermore National Laboratory, Livermore, CA, UCID-53559, 1985.
[11] V.A. Evtikhin et al., Liquid lithium tokamak reactor. 16th IAEA Fusion Energy Conference, Montreal, Canada, October, 1996.
[12] R.W. Moir, HYLIFE-II inertial confinement fusion reactor design, Fus. Tech. 19 (1991) 617.
[13] L. Zakharov et al., Magnetic propulsion of conducting fluid and the theory of controlled tokomak fusion reactors. Meeting on liquid lithium controlled tokomak fusion reactors & MHD. International Sherwood Fusion/Plasma Conference, Atlanta, GA, 21 March, 1999.
[14] F. Najmabadi and the ARIES Team, Overview of the ARIES-RS reversed-shear tokamak power plant study, Fusion Engineering and Design 38 (1997) 3–25.
[15] S. Fetter, E. Cheng, F. Mann, Long term radioactive waste from fusion reactors, Fus. Eng. Des. 13 (1990) 239.
[16] Nuclear Regulatory Commission, 10CFR part 61, Licensing requirements for land disposal of radioactive waste. Federal Register FR 47, 57446, 1982.
[17] N. Morley, et al., Initial liquid metal magnetohydrodynamic thin film flow experiments in the MeGA-loop facility at UCLA, Fus. Eng. Des. 27 (1995) 725–730.
[18] See for example, S.W. Haney, J.P. Freidberg, Physical Fluids B1 (1989) 1637.
[19] R.L. Miller, J.W. Van Dam, Nucl. Fus. 28 (1987) 2101.
[20] A. Turnbell, et al., Nucl. Fus. 38 (1998) 1467.
[21] H.P. Summers, M.v. Hellermann, in: R. Janev, H. Darwin (Eds.), Atomic and Plasma–Material Interaction Processes in Controlled Thermonuclear Fusion, Elsevier, Amsterdam, 1993, pp. 87–118.
[22] T.D. Rognlien, J.L. Milovich, M.E. Rensink, G.D. Porter, J. Nucl. Mat. 196–198 (1992) 347.
[23] J.N. Brooks, Physical Fluids B2 (1990) 1858; T.Q. Hua, J.N. Brooks, Physical Plasmas 11 (1994) 3607.
[24] A. Hassanein, Fus. Tech. 30 (1996) 713.

[25] H. St. John, T.S. Taylor, Y.R. Lin-lui, A.D. Turnbull, Proceedings of the 15th IAEA Conference, 26 September–1 October 1994, Seville, Spain, IAEA-CN-60/D-P22, p. 603.
[26] M.T. North, J.H. Rosenfeld, Test results from a helium gas-cooled porous metal heat exchanger, in: Khonsary (Ed.), High Heat Flux Engineering III, vol. 2855, 1996.
[27] D.L. Youchison, J.M. McDonald, Thermal performance and flow instabilities in a multi-channel, helium-cooled, porous metal divertor module. To be published in Proceedings of International Symposium on Fusion Technology, 19–24 September, 1999, Rome, Italy.
[28] D.L. Youchison, M.G. Izenson, C.B. Baxi, J.H. Rosenfeld, High heat flux testing of helium-cooled heat exchangers for fusion applications, Fus. Tech. 29 (1996) 559.
[29] H. Kurishita, et al., Effect of neutron-irradiation on low temperature toughness of TiC-dispersed molybdenum alloys, J. Nucl. Mat. 239 (1996) 253.
[30] B.L. Cox, F.W. Wiffen, J. Nucl. Mat. 85–86 (1973) 901.
[31] T.E. Tietz, J.W. Wilson, Behavior and Properties of Refractory Metals, Stanford University Press, Stanford, CA, 1965.
[32] J.B. Conway, in: R.H. Cooper, Jr., E.E. Hoffman (Eds.), Proceedings on Refractory Alloy Technology for Space Nuclear Power Applications, CONF-83008130, Oak Ridge National Laboratory, Oak Ridge, TN, 1984, p. 252.
[33] R.W. Buckman, Jr., in: C.L. Briant et al. (Eds.), High Temperature Silicides and Refractory Alloys, MRS Symposium Proceedings, vol. 322, Materials Research Society, Pittsburgh, PA, 1994, p. 329.
[34] S.J. Zinkle et al, in: Fusion Materials Semi-Annual Progress Report (for period ending 31 December, 1997), DOE/ER-313/23, Oak Ridge National Laboratory, Oak Ridge, TN, 1997, p. 99.
[35] D.A. Petti, K.A. McCarthy, ITER safety: lessons learned for the future, Fusion Technology 34 (3, part 2) (1998).
[36] M.J. Gaeta, B.J. Merrill, CHEMCON User's Manual Version 3.1. INEL-95/0145, September 1995.